An Investigation into the Cellular Mechanisms Underlying Photodynamic Rejuvenation in Human Skin

by

Student: Victoria Louise Van Kets

Student number: VKTVIC001

SUBMITTED TO THE UNIVERSITY OF CAPE TOWN

In fulfilment of the requirements for the degree

M.Sc in Medicine

Faculty of Health Sciences
UNIVERSITY OF CAPE TOWN

Date of submission: 11 July 2012
Supervisor: Dr Lester Davids

Department of Human Biology
Faculty of Health Sciences

Declaration

I, ……., hereby declare that the work on which this dissertation/thesis is based is my original work (except where acknowledgements indicate otherwise) and that neither the whole work nor any part of it has been, is being, or is to be submitted for another degree in this or any other university.

I empower the university to reproduce for the purpose of research either the whole or any portion of the contents in any manner whatsoever.

Signature: ……

Date: ……..

Acknowledgements

First and foremost I would like to thank my supervisor Dr Lester Davids for all his guidance, support and patience over the past two and half years. Your ability to calm me down in panicked states and give me direction when I felt lost and overwhelmed was greatly appreciated. I thank you for giving me the opportunity to discover this work and giving me the freedom to explore my ideas.

I would like to thank my funders in supporting me personally for the last two years: NRF DOL Scarce Skills Scholarship, Marion Beatrice Waddle Bursary, Siri Johnson Bursary, Stella and Paul Lowenstein Charitable Trust Scholarship, KW Johnston Bequest. In addition the funders who supported this project: NRF Thuthuka and the National Laser Centre (CSIR, Pretoria).

I would like to make special mentions for the following people at the National Laser Centre who gave their time to teach me the essence of my work (laser physics): Aletta Karsten, Kaminee Maduray, Ivy Ndhundhuma in the Biphotonics unit; the Post grad students at the NLC, Malcolm, Darryl Attie, Yaseera and Nicolene for making my month away from home a fantastic experience; the staff at the NLC who were so helpful, Thomas, Johan and Henk, your advice was always valued. To Ingrid Baumgarten, thank you for the donation of the fibroblasts used in the initial work of this project. They were undoubtedly invaluable.

I would also like to thank my "lab mom" Toni Wiggins for, firstly, culturing the primary fibroblasts essential to this project. Secondly, for always having time to listen to the trials and tribulations of this post grad student and offering helpful and insightful advice and thirdly, for keeping me in line when I started to deviate from the work plan.

This project would not have been as successful or fun without the "Redox Labsters". Britta, we have spent many weekends, late nights and early mornings in the lab together through thick and thin times. Your support in and out of lab has been invaluable and I'm sure we'll have our friendship for life. Emma, you were there from the beginning and I always tried to work as hard as you did. Thanks for always keeping in entertained with your stories during the long waits between time points in experiments. I look forward to more in the future. To Ayesha, Rosa (for being awesome in bearing the brunt of my Friday post-PBL session), Morea, Ana, Krishna, Tyrone, Maureen, Mariba, Khwezi and Karusha, thank you for all the good times and feedback on my work, I always appreciated it.

I would like to thank: Stem Cell lab with Dr Robea Ballo, Mubeen, Anita, Yolande and Dennis and the T-box lab with Prof Sharon Prince, Amaal, Deeya, Sabina, Aretha, Shannagh, Jarrod and Saeb for being fantastic people and helping out whenever a hand was needed.

Special thanks to the Confocal Unit in our department, under the leadership of Prof Dirk Lang and Susan Cooper, for their excellent advice and guidance which produced the amazing images seen in this project.

In the Department of Human Biology I would like to thank: Ray and Charles for being willing to assist, Amod for all his advice on DCF-DA and Nazeem for coming to the rescue with any computer problems.

Thanks to the following laboratories for the use of their equipment during this project: Sturrock ACE laboratory (fluorimeter), Brombacher laboratory (ELISA plate reader), SATVI unit with Ronnie Dreyer (FACS machine).

Last but not least, to my parents (Rik and Lou) for being wonderful and supportive during the tough times and long nights. To my amazing boyfriend, Dan, who has kept calm and focused to the end and who has been everything to me during these last few years. To my friends, new and old, thanks for keeping me sane and balanced during this time. Thank you for listening to my rants and being patient when my life was ruled by experiments.

Table of Contents

List of Abbreviations

µg	microgram
µl	microliter
ALA	Aminolevulinic Acid
AP	Activator protein
ATP	Adenosine triphosphate
BCA	Bicinchoninic acid assay
BSA	Bovine Serum Albumin
cm	centimetre
DCF-DA	5(6)-Carboxy-2′,7′-dichlorofluorescein diacetate
Dept	Department
DiOC5	3,3-dipentyloxacarbo- cyanine iodide
DMEM	Dulbecco's modified eagles medium
DMSO	dimethyl sulfoxide
DNA	deoxyribonucleic acid
ECM	Extracellular matrix
ELISA	enzyme linked immunosorbant assay
em	Emission
ER	Endoplasmic reticulum
ex	Excitation
FACS	fluorescent activated cell sorting
GAG	Glycoaminoglycans
GFP	Green fluorescent protein
h	hours
HAS	Human Serum Albumin
IHC	immunohistochemistry
IL	interleukin
IPL	Intense Pulsed Light
J	Joule
LED	light emitting diodes
MAL	Methyl aminolevulinate
MEF	murine embryonic fibroblasts
MMP	Matrix Metalloproteinase
NaCl	Sodium Chloride
nm	nanometre
PDL	Pulsed dye laser

PDR	Photodynamic Rejuvenation
PDT	Photodynamic Therapy
PS	Photosensitizer
RIPA	radioimmunoprecipitation
RT-PCR	Reverse Transcriptase Polymerase chain reaction
TGF-β	transforming growth factor - beta
TIMP	Tissue Inhibitor of Metalloproteinase
TNF-α	Tumour necrosis factor - alpha
USA	United States of America
UV	Ultraviolet
W	Watt
YFP	Yellow fluorescent protein

List of Figures

Chapter 1

Chapter 2

Chapter 3

Chapter 5

Appendix A

List of Tables

Chapter 1

Chapter 2

Chapter 3

Abstract

Photodynamic Rejuvenation (PDR) is a novel therapy used to treat the signs of skin ageing. It is a promising dermatological therapy due to its less severe side effects and superior results when compared to other chemical treatments. This therapy involves the topical application of a photosensitizing drug (PS) which is activated by a specific wavelength of light to react with oxygen and generate reactive oxygen species (ROS) in the skin. At low levels ROS are able to alter cell signalling and are thought to be the key mediators that reverse the signs of ageing. Dermatologists use this therapy to treat various characteristics of skin ageing such as fine/coarse wrinkles, mottled pigmentation, skin roughness and telangiectasia (small broken blood vessels near the surface of the skin). Initial clinical reports showed success; however, inconsistencies in patient outcomes provide impetus to improve characteristics of current treatment regimes including the PS, light sources, fluences and irradiances.

As very little is known about the actual biological mechanism of PDR in human skin cells, the aim of this investigation was to first optimise a protocol using the PS, hypericin, activated with 3 different light sources. Hypericin, an extract from St Johns Wort, is a second generation PS that has many benefits such as low dark cytotoxicity, no carcinogenicity/mutagenicity, high quantum yield and can be activated by several wavelengths of light. We chose three light sources that emitted light within hypericin's absorbance spectra: two lasers emitted light at 561nm and 632nm and lamps in a UVA transilluminator emitted a light range with a peak at 365nm. Cultured primary human fibroblasts were chosen as the cell model as they are an ideal representation of the dermal layer of the skin.

Our results showed that low hypericin concentrations (0.25-0.5μM) at all three wavelengths caused an increase in cell viability. When this increase was investigated in relation to growth or cellular activity, growth curves showed that PDR with all 3 wavelengths had no effect on the cell proliferation rate. To confirm whether ROS was indeed occurring after the therapy, a ROS assay was performed. The yellow laser and UVA transilluminator, which emit light maximally absorbed by hypericin, were used. UVA served as the upper limit for ROS generation as this range of wavelengths is known to cause intracellular ROS. Yellow laser-activated hypericin resulted in a non-significant increase in intracellular ROS which was less than the levels in fibroblasts with UVA activated hypericin. This confirms that PDR using hypericin does generate ROS. As migration is considered inverse to collagen production and increased collagen is a main objective of skin rejuvenation, we studied fibroblast migration after PDR. To assess fibroblast migration in response to yellow laser light activation of

hypericin, a scratch assay was used. This PDR protocol showed that migration was significantly slowed after treatment. Our proposal is that our PDR protocol with yellow laser light decreases migration diverting energy to producing collagen.

The subcellular location of hypericin closely relates to its mechanism of action in PDR. This study showed that hypericin localises to the perinuclear region of the fibroblast and colocalizes within the Golgi apparatus with partial colocalization in the mitochondria and hardly any with the endoplasmic reticulum. This has not been shown before and gives clues as to how hypericin interacts in the cell with our protocol.

These results characterise the initial cellular response of an optimised PDR protocol using the PS hypericin with different wavelengths of light. Future work will involve determining the expression levels of several dermal and signalling proteins known to be modulated during skin rejuvenation.

Note: The first part of this work has recently been published (Lasers in medical science epub May 12 2012, DOI: 10.1007/s10103-012-1115-2) and the second is currently being prepared for submission.

1. Chapter 1: Literature Review

1.1. Introduction

The skin is the largest organ of the body and its main function is to provide protection from the environment. The skin is divided into three layers: the epidermis, dermis and hypodermis. The epidermis is the outer most layer and is the first line of defence against any insult. The dermis provides the structure of the skin through a framework of interconnected proteins known as the extracellular matrix (ECM). The hypodermis is the deepest layer and mainly comprises of fat-containing cells. As one ages, characteristics of the skin change resulting in - thinning of the epidermis, fine wrinkle development, increased dryness, decreased elasticity and overall slower cellular turnover (Gilchrest, 1996). Furthermore, there are certain environmental factors that accelerate the ageing process. The most prominent factor being chronic UV exposure from sunlight. This type of ageing is also known as extrinsic or photoageing (Farage *et al.*, 2008; Gilchrest, 1996).

Photoageing, in addition to the characteristics of natural ageing, has further distinct hallmarks - irregular pigmentation, increased skin roughness, coarse wrinkle development and increased small blood vessels near the surface of the skin (telangiectasia) (Avram *et al.*, 2006; Farage *et al.*, 2008; Gilchrest, 1996). Chronic UV exposure to the skin causes several signalling irregularities in the skin that result in these changes (Pillai *et al.*, 2005; Rittié & Fisher, 2002). The skin layer most affected by this altered signalling is the dermis. During UV exposure, the dermis has an upregulation of ECM degrading enzymes, known as matrix metalloproteinases (MMP), and a down regulation of collagen synthesis (Brennan *et al.*, 2003; Fisher *et al.*, 1996, 1997, 2002, 2008; Pillai *et al.*, 2005; Rittié & Fisher, 2002; Talwar *et al.*, 1995). Collagen type I is the main protein in the ECM accounting for 80% of its dry weight (Schultz *et al.*, 2005). The damage caused by MMP and the inability to generate new collagen results in a broken, structurally comprised ECM of the dermis leading to wrinkle formation. The fibroblasts are mechanosensing cells, therefore, decrease tension caused by the broken ECM leads to a slowing of cellular metabolism (Varani *et al.*, 2001, 2006). In addition, repeated exposure of UV to fibroblasts in this already compromised situation further exacerbates the signalling changes (Fisher *et al.*, 2009; Varani *et al.*, 2004). Overall, the changes result in wrinkle formation among other cellular changes. Coarse wrinkles are the most clinically evident sign of chronic UV exposure (Avram *et al.*, 2006).

There are many treatments available to reverse these signs of skin ageing. Many have shown increased collagen synthesis as well as a downregulation of the MMP (Fisher *et al.*, 1996). In addition, improvement in skin texture, irregular pigmentation and telangiectasia has also been demonstrated (Avram *et al.*, 2006). One such treatment is laser therapy. This therapy

uses the ability of certain compound in the skin to absorb light energy. There are many of these endogenous compounds, known as chromophores, in the skin that capture light (Peng et al. 2008; Waibel 2009). In the case of irregular pigmentation, the pigment melanin is targeted and destroyed. Haemoglobin is targeted to destroy small blood vessels thereby resolving telangiectasia. This type of therapy has been very successful and its use is wide spread (Avram *et al.*, 2006). Stemming from this therapy is a treatment called photodynamic rejuvenation (PDR).

PDR is a relatively new dermatological therapy that has shown great results in reversing the signs of skin ageing. It has shown promise as an anti-ageing therapy and numerous *in vivo* studies have shown its positive effects on all signs of photoageing (Bjerring *et al.*, 2009; Bruscino *et al.*, 2010; Buggiani *et al.*, 2008; Christiansen *et al.*, 2007; Clementoni *et al.*, 2010; Dover *et al.*, 2005; Haddad *et al.*, 2011; Kosaka *et al.*, 2010; Orringer *et al.*, 2005; Ruiz-Rodriguez & López-Rodriguez, 2006; Ruiz-Rodriguez *et al.*, 2002; Ruiz-Rodríguez *et al.*, 2008; Xi *et al.*, 2011; Zane *et al.*, 2007). PDR involves the topical application of a photosensitizing drug, or photosensitizer (PS), to the skin and its subsequent activation with a specific wavelength of light. A PS has a specific absorbance spectrum that indicates the wavelengths of light it maximally absorbs. The wavelength with a highest absorbance will result in maximum energy being trapped by the PS causing it to enter a higher energy state or become activated. In its activated state it undergoes photochemical reactions and transfers its energy to surrounding molecules such as oxygen. Reactive oxygen species (ROS) are the most common product (Agostinis *et al.*, 2011; Kiesslich *et al.*, 2006). As mentioned previously, ROS can change cellular signalling. The exact molecular mechanism of PDR remains largely unknown except for a few preliminary studies (Almeida Issa *et al.*, 2009; Choi *et al.*, 2010; Issa *et al.*, 2010; Karrer *et al.*, 2003; Marmur *et al.*, 2005; Orringer *et al.*, 2005; Park *et al.*, 2010). This led to the purpose of this study to investigate hypericin mediated PDR and characterise its *in vitro* effects on human dermal fibroblasts.

1.2. Skin

The skin is the largest organ in the body and has a number of functions of which protection of the body and its internal organs is the most important. The skin is primarily made up of three layers viz. the air-facing epidermis, the lower dermis and deep, fat-containing, hypodermis.

The epidermis is a stratified squamous epithelium layer consisting of several cell types and is, itself, divided into several strata. The keratinocytes make up the major cell type of this epithelium and its proliferative component resides on the basement membrane in a layer called the stratum basale. The layers immediately above, called the stratum spinosum and granulosum, contain differentiating cells and cells undergoing cell cycle arrest, respectively. The uppermost layer comprises of dead cells filled with keratin called the stratum corneum. In the stratum basale, there are a small number of other epidermal cells that intersperse the keratinocytes such as the pigment-producing melanocytes, immune-responsive Langerhans cells and pressure-sensing Merkel cells (Kierszenbaum, 2002a; Young & Heath, 2000). Despite the basement membrane originally being touted as an almost "impregnable layer" delineating the epidermis from the dermis, we now know that the epidermis and the dermis are not distinct independent entities but interact and communicate through paracrine mechanisms (Fagot *et al.*, 2002; Ghaffari *et al.*, 2009; Karrer *et al.*, 2004; Maas-Szabowski *et al.*, 1999).

Below the epidermis is the dermis. The main cellular component of this layer is the fibroblast. This cell type is important as it produces the majority of the matrix proteins in this part of the skin. Together, these proteins provide the structural function of the dermis. The framework of this layer, known as the ECM, is composed of several different proteins summarised in Table 1.2.1. The dermis provides support for nerves, blood vessels, lymphatic vessels and skin appendages such as the hair follicle.

Components	Proteins	Functions
Collagen	• Several different types found in the dermis • Collagen type I is the most prominent in the dermis (80-85%) with collagen type III (8-11%) also being present	• Rigidity • Scaffolding for dermal structures • Tensile strength
Elastic Fibres	• Elastin proteins are at the core of the elastin fibres • Fibrillin protein surround the core of elastic protein and are essential for the integrity of the elastic fibres	• Elasticity • Resilience • Recoil
Glycosaminoglycan (GAGs)	• Polysaccharide chains with amino sugars • e.g. Hyaluronic Acid	• Strongly hydrophilic • Trap water molecules • Molecule becomes swollen • Enables the dermis to withstand compression forces
Proteoglycans	• Core protein with GAGs attached • e.g. Heparan Sulphate Decorin Perlecan	• Retain water • Allow for movement of nutrients, hormones and ions • Play a role in signalling molecules and their presentation to the cell membrane receptors
Fibronectin	• Glycoprotein	• Involved with the interaction between the ECM proteins and cell membrane receptors e.g. integrins • Link different ECM proteins • Involved in wound healing
Laminin	• Large protein with 3 polypeptide chain • Cross-shaped molecule	• The ends of this protein bind collagen type IV, proteoglycans and integrin receptors • It is a bridge between ECM proteins and the basement membrane

Table 1.2.1 The different dermal proteins that are present in the extracellular matrix (adapted from Schultz et al. 2005)

The fibroblasts attach to the ECM, via integrin receptors, to create tension across the cell. This tension in the cell's cytoskeleton plays an important role in the functioning of the fibroblast and is responsible for its classical spindle shape. The integrin receptors are the

tethering points for the fibroblasts (Varani *et al.*, 2004; Welch *et al.*, 1990). The receptors form part of signalling cascades by communicating extracellular signals into the cell. Changes to the tension across the cell, therefore changes to integrin receptors, stimulate signalling cascades and ultimately result in altered gene and protein expression (Varani *et al.*, 2004). The fibroblasts constantly remodel the proteins of the ECM in response to various signals and stimuli through their attachment to the matrix (Fisher *et al.*, 2008; Varani *et al.*, 2004). Collagen type I is the most abundant protein in the ECM and is secreted by the fibroblasts. Collagen type I is integral to the structural integrity of the skin.

1.2.1. Collagen Type I

Collagen type I makes up 80% of the dermis' dry weight (Jenkins, 2002; Schultz *et al.*, 2005). However, other collagen types are also present in the dermis but to lesser extents. The upper papillary dermis consists of fine collagen type I and III fibres whereas the lower reticular dermis has thicker bundles of collagen type I as seen in Figure 1.2.1

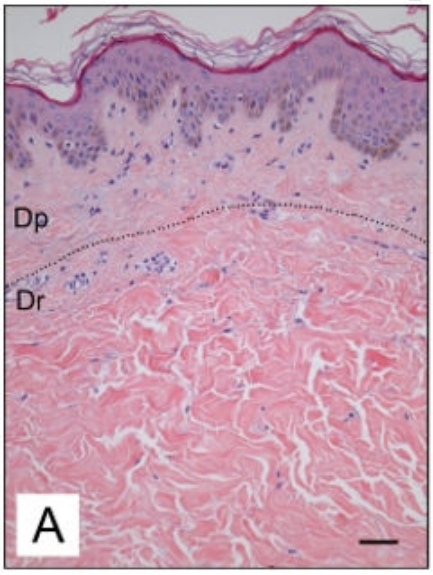

Figure 1.2.1 A histological section of the skin stained with haematoxylin and eosin demonstrating the fine fibres of the papillary dermis (Dp) and the dense bundles of the reticular dermis (Dr) (taken from Mine *et al*)

Collagen type I is part of a wider family of 16 collagen proteins. A collagen type I fibre consists of three protein chains which are bound together by covalent forces. Collagen type I is first transcribed from the COL1A1 and COL1A2 genes which produce α1 and α2 peptide chains, respectively (Alberts *et al.*, 2002; Kierszenbaum, 2002b). As each collagen protein consists of three peptide chains bound together, the individual α chain mRNA transcripts are transcribed in various ratios and are specific for the type of collagen protein being produced (Alberts et al. 2002).

The pre-procollagen peptide chains are translated from the mRNA transcripts by the ribosomes and deposited into the endoplasmic reticulum (ER). They have an amino acid repeat motif of X-Y-glycine, where X and Y are usually proline and lysine. These amino acids are hydroxylated in the ER creating a zipper effect which stabilises a helix formation between 3 prepropeptide chains (Lodish et al. 2003; Alberts et al. 2002). This triple helical propeptide, is then transported to the Golgi apparatus where it is further processed and secreted from the cell into the extracellular space (Figure 1.2.2). The protein, now known as procollagen, has its non-helical N and C terminals extracellularly cleaved, resulting in tropocollagen (Kierszenbaum, 2002b). Cleavage of these end terminals result in spontaneous assembly into collagen fibrils. Cleaved tropocollagens are arranged in a staggered manner creating a collagen fibril (Figure 1.2.2) (Alberts et al. 2002).

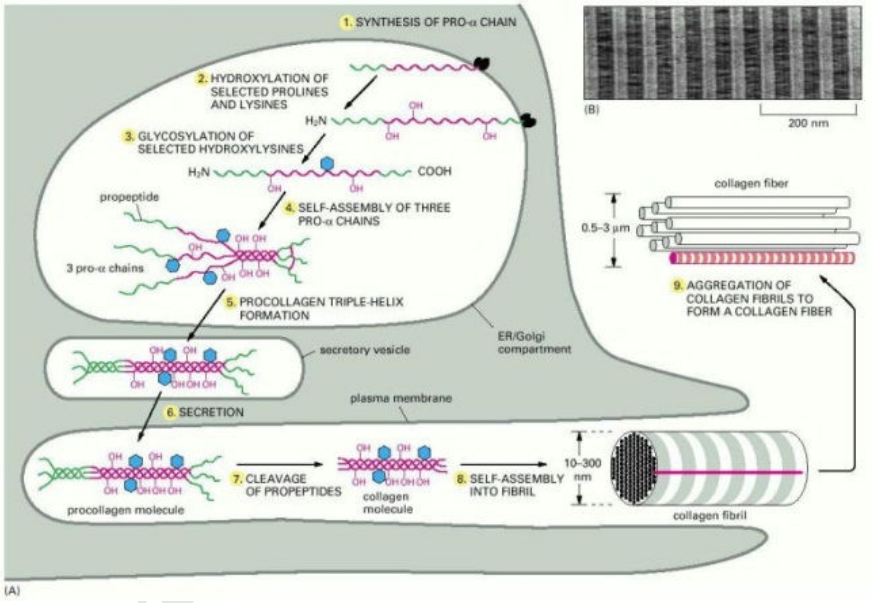

Figure 1.2.2 A diagram demonstrating collagen gene transcription and protein translation in the cell (taken from Alberts et al. 2002)

The rate of collagen synthesis is determined by fibroblasts in response to various signalling molecules, as well as their interaction with the extracellular matrix (Fisher *et al.*, 2008, 2009; Kierszenbaum, 2002b; Lodish *et al.*, 2003; Varani *et al.*, 2004). This synergy between extracellular signals and the environment are what define the metabolism and protein synthesis of fibroblasts. The fibroblasts initiate various signalling cascades from their mechanosensing interactions with the ECM which control collagen protein synthesis. A compromise, therefore, in the structure of collagen fibres, often seen during ageing, will result in decreased contact thus decreased fibroblast activity (Varani *et al.*, 2004). As the half-life of collagen is 16 years, accumulation of broken fibres over time result in the structure of the dermis weakening thus leading to one of the most common signs of ageing, wrinkles.

1.3. Skin Ageing

Two types of ageing exist - intrinsic and extrinsic ageing. Intrinsic ageing is non-pathological, natural process of the skin where changes are not detrimental to the functioning of the skin. In contrast, extrinsic ageing is thought to, not only accelerate the natural ageing process, but lead to other symptoms such a deep wrinkles, mottled pigmentation and the development of small blood vessel near the surface of the skin (known as telangiectasia).

Changes in the skin during ageing occur in both the epidermis and dermis. The dermis has the most dramatic changes during both types of ageing. The ECM undergoes severe changes resulting in the collapse of the framework thereby compromising the overall structural integrity of the skin (Avram *et al.*, 2006; Fisher & Voorhees, 1998; Fisher *et al.*, 2008; Gilchrest, 2006; Jenkins, 2002).

1.3.1. Intrinsic Ageing

During intrinsic ageing, the skin's appearance is finely wrinkled, smooth to the touch and dry with a loss of elasticity. The overall thickness of the papillary and reticular dermis is thinner as it undergoes atrophy. Dermal thinning leading to symptoms of decreased resistance and the inability to rebound after tension is applied. The epidermal-dermal ridges are also smoother with decreased cellularity which affects wound healing (Farage *et al.*, 2008; Gilchrest, 1996, 2006). The collagen fibres degenerate, thus, their structure and stability within the dermis leads to a comprise resulting in laxity, droopiness and fine wrinkles (Farage *et al.*, 2008; Gilchrest, 1996). The inability of the fibroblasts to attach to an intact ECM leads to decreased biosynthetic capacity resulting in slower rate of remodelling by the fibroblasts in response to stimuli (Varani *et al.*, 2004). Together these events affect the skin with regard to mechanical strength, appearance and wound healing.

1.3.2. Extrinsic Ageing/Photoageing

Extrinsic ageing is seen as accelerated ageing from exposure to environmental factors – the chief being ultraviolet (UV) radiation from sun exposure - this type of ageing is also referred to as photoageing. Although it shares many characteristics with intrinsic ageing, other symptoms can occur. These signs are often superimposed on intrinsic ageing and determining the differences between "normal" intrinsic ageing and "externally-induced" extrinsic ageing is very difficult (Gilchrest, 2006; Rittié & Fisher, 2002).

Photoageing has been attributed to 90% of cosmetic problems relating to skin ageing (Avram *et al.*, 2006). A table describing symptoms of photoageing and associated dermatological conditions are shown below in Table 1.3.1. Photoaged skin can have a thickened epidermis with possible cellular atypia that may manifest as actinic keratosis as well as irregular, mottled pigmentation. Interestingly, the dermis does have distinct extrinsic ageing characteristics that set it apart from intrinsically aged skin (Farage *et al.*, 2008; Gilchrest, 1996). These characteristics arise from molecular changes caused by UV radiation (Callaghan & Wilhelm, 2008; Fisher *et al.*, 2008; Jenkins, 2002; Pillai *et al.*, 2005; Rittié & Fisher, 2002).

A

Photoageing Characteristics
Wrinkling
Coarseness
Dryness
Mottled pigmentation
Loss of elasticity
Easy bruising
Telangiectasia
Benign, pre-malignant or malignant growths

B

Conditions Associated with Photoageing
Localized hypomelanism
Localized hypermalanism
Seborrheic keratoses
Senile keratoses
Senile lentigines
Freckles
Acne rosacea
Spider nevi
Varicose veins
Dry skin
Wrinkled skin
Ptergygia
Arcus senilis

Table 1.3.1 Characteristics (A)and associated conditions (B) most often seen in photoaged skin (adapted from Gold *et al.*, 2006)**.**

A major histological hallmark of sun exposed skin is the presence of an amorphous mass of elastin fibres in the papillary dermis known as solar elastosis. This is caused by UV irradiation increasing elastin gene transcription. The skin then appears with a slightly thicker looking epidermis and has a yellowish appearance illustrating elastotic degenerative changes (Nishimori *et al.*, 1998).

The upper papillary dermis presents with a severely broken collagen fibre network in photoaged skin. These broken fibres are as a result of exposure to UV which led to an increase in collagen degrading enzymes (Figure 1.3.1) (Brennan *et al.*, 2003; Brenneisen *et al.*, 2002; Callaghan & Wilhelm, 2008; Dong *et al.*, 2008; Fagot *et al.*, 2002; Fisher *et al.*, 1996, 1997; Jenkins, 2002; Petersen *et al.*, 1992).

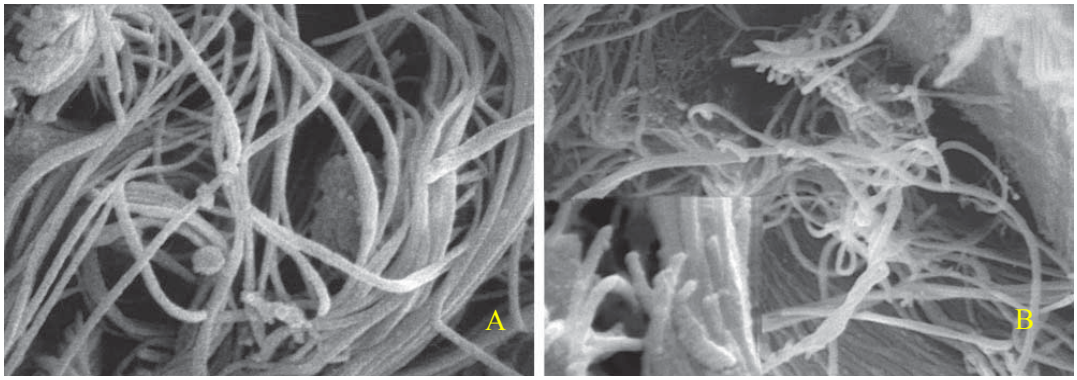

Figure 1.3.1 Ultrastructural images of collagen fibres in the dermis. (A) undamaged skin with intact collagen fibres (B) represented photoaged skin with broken fibres (taken from Fisher *et al.*, 2008)**.**

These enzymes, matrix metalloproteinases (MMP), are a class of zinc coordinate enzymes that have specific substrates in the ECM (Page-McCaw *et al.*, 2007). They are present at very low levels under normal physiological circumstances, and are only upregulated during wound healing (Quan *et al.*, 2009). Table 1.3.2 represents MMP found in the skin and their substrates. MMP activity is regulated at three levels: synthesis (primarily transcription), activation of the zymogen through cleavage of its prodomain, and inhibition of proteolytic activity by tissue inhibitor of metalloproteinases (TIMP) (Page-McCaw *et al.*, 2007).

MMP	Substrate	Alternate name
MMP-1	Interstitial collagens (types I, II, and III)	Collagenase-1, interstitial collagenase
MMP-2	Type IV collagen	Gelatinase A
MMP-3	Fibronectin, Laminin, collagens III, IV, IX, and X, and cartilage proteoglycans	Stromelysin 1, Progelatinase
MMP-8	Type I, II and III collagens	Neutrophil Elastase
MMP-9	Type IV and V collagens	Gelatinase B
MMP-10	Proteoglycans and Fibronectin	Stromelysin 2
MMP-13	Type II collagen and to a lesser extent, types I and III	Collagenase 3
MMP-14	Latent MMP-2 protein	Membrane-inserted MMP

Table 1.3.2 Summary of matrix metalloproteinases (MMPs) and theirs functions (derived from Gene Entrez, 2011)**.**

MMP-1 and MMP-3 are increased in the dermis after UV irradiation through signalling proteins as described later (Brennan *et al.*, 2003; Fisher *et al.*, 1997; Pillai *et al.*, 2005). The breaks that result in the collagen fibres are at random locations (Figure 1.3.1) which block the regular enzymatic sites and stop clearance of these damaged fibres through regular enzymatic methods. UV also causes a decrease in collagen synthesis therefore, if the broken fibres are removed, they are not replaced with new fibres (Fisher *et al.*, 2000; Imokawa, 2009). The collagen fibres are weakened and due to the slow turnover of collagen in the

dermis result in a compromised framework and can be referred to as a "Solar scar". Over time the constant weakening will result in wrinkle development (Figure 1.3.2) (Fisher *et al.*, 1996, 1997, 2008; Imokawa, 2009; Jenkins, 2002).

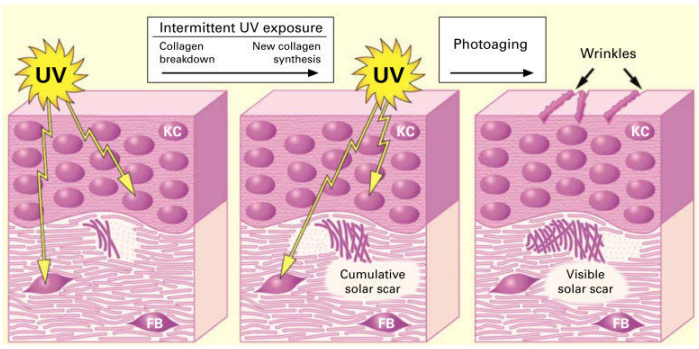

Figure 1.3.2 Chronic UV exposure to the skin results in the imperfect repair of collagen fibres. These fibres cause structural collapse of the skin which is seen as wrinkles (taken from Fisher *et al.*, 1997)

At the cellular level the broken fibres result in the fibroblasts losing their shape and gaining a stellate appearance due to the loss in tension (Varani *et al.*, 2001; Welch *et al.*, 1990). As mentioned previously (Section 1.2.1), this environment leads to cells decreasing their collagen production and increasing MMP production. This highlights the ECM's influence on fibroblast metabolism and that it is not solely dependent on extracellular signals (Fisher *et al.*, 2009; Varani *et al.*, 2001, 2004). UV exposure to the skin results in alterations in the normal signalling within the fibroblasts and surrounding cells. These changes in the molecular pathways, and thus the overall functioning of the cell, result in a situation where photoageing signs are exacerbated.

1.3.3. Signalling Pathways of Extrinsic Ageing

Photoaged skin has different molecular characteristics compared to intrinsic aged skin (B. A Gilchrest 1996; Farage et al. 2008). Photoaged aged skin has reduced levels of antioxidant enzymes, high levels of inflammatory cytokines and presence of neutrophils (Pillai *et al.*, 2005). These changes, both histologically and molecularly, are caused by the skin's exposure to UV radiation from sunlight.

UV exposure results in an increase in reactive oxygen species (ROS). ROS are known to be initiators in normal cell signalling (Thannickal & Fanburg, 2000). However, ROS are believed to be the initiators in the signalling cascades that ultimately result in photodamaged skin (Brenneisen *et al.*, 1998; Pillai *et al.*, 2005; Rittié & Fisher, 2002). In addition to eliciting a signalling response, high levels of ROS can cause damage by oxidising biomolecules in the cell i.e. DNA, protein and lipids (Halliwell & Gutteridge, 2007a). Most cells have an antioxidant system to protect against ROS by neutralizing their reactive nature

(Bickers & Athar, 2006; Rhie *et al.*, 2001). In case of high UV radiation the antioxidant system is overwhelmed and ROS drive the signalling response in the skin (Bickers & Athar, 2006; Brenneisen *et al.*, 1998; Rittié & Fisher, 2002).

UV exposure to the skin has several effects as summarised in Figure 1.3.3. Immediately after the initial ROS, there is an increase in inflammatory cytokines and immune cells. Inflammatory proteins and cytokines such as nuclear factor kappa beta (NF-κβ), tumour necrosis alpha (TNF-α) and interleukin 1 (IL-1) from activated macrophages and monocytes propagate the cell signalling (Meier *et al.*, 1989; Pillai *et al.*, 2005; Wlaschek *et al.*, 1997).

This results in Mitogen Activated Protein Kinase (MAPK) pathways being activated resulting in increased level of c-jun in the epidermal and dermal cells. Together with c-fos, c jun forms part of Activator Protein-1 (AP-1) (Fisher & Voorhees, 1998; Fisher *et al.*, 1998, 2000; Mauviel *et al.*, 1996; Quan *et al.*, 2002, 2010; Verrecchia *et al.*, 2001). This increase of AP-1 has two effects on the fibroblasts. The first is an increase in the transcription and translation of MMP proteins and the second an inhibition of transforming growth factor-β (TGF-β) (Fisher *et al.*, 1998, 2000; Quan *et al.*, 2002) (Figure 1.3.3).

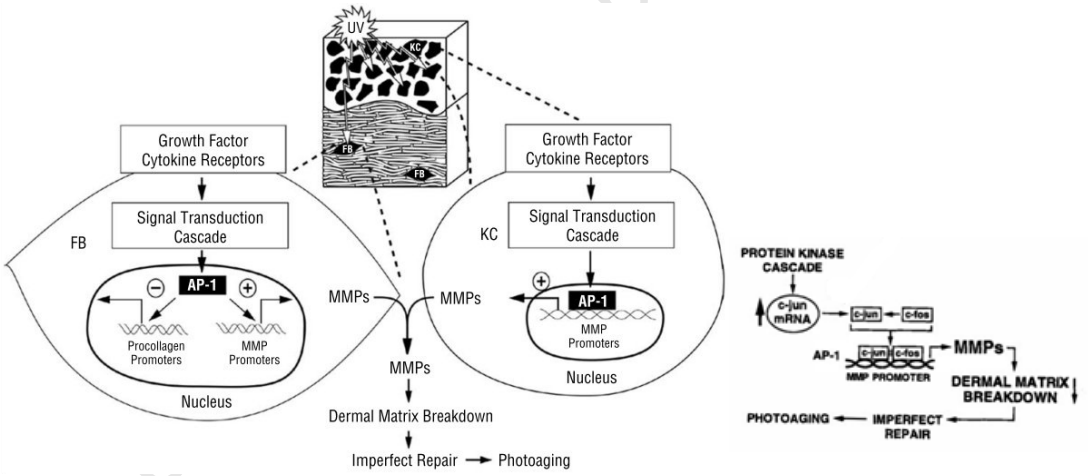

Figure 1.3.3 Signalling mechanism for photoageing with chronic UV exposure insert expanded view of AP-1 induction (adapted from Fisher & Voorhees, 1998; Fisher *et al.*, 2008)**.**

TGF-β is a cytokine that is integral in regulating the proliferation and collagen synthesis in fibroblasts (Grotendorst *et al.*, 2004; Ignotz & Massagué, 1986; Leask & Abraham, 2004; Varga *et al.*, 1987). TGF-β has been shown to inhibit proteolytic enzyme, such as the MMP (Quan *et al.*, 2002). TGF-β, therefore, is associated with maintaining the homeostasis of the ECM. UV-induced AP-1 blocks TGF-β and reduces the number of TGF-β receptors on the cell resulting in decreased collagen synthesis and increased collagen breakdown resulting in a damaged and a structural compromised ECM (Figure 1.3.3) (Chung *et al.*, 1996; Quan *et al.*, 2002; Verrecchia *et al.*, 2001).

The damage caused by UV exposure over several years, and these processes being upregulated time and time again, result in a compromised skin structure. This occurs due to an accumulation of MMP-damaged collagen fibres and by the suppression of collagen synthesis through the broken ECM environment and activated signalling pathways. Over time, these molecular changes result in clinically evident characteristics (as presented in Table 1.3.1). To alleviate these often unsightly symptoms, several therapies are used to, not only rectify the irregular signalling, but to stimulate the fibroblasts to remove damaged fibres and replace it with new collagen proteins.

1.4. Treatments for Skin Ageing

There are many regimes and therapies on the market to treat the signs of skin ageing. These treatments can be invasive, involving surgery and chemical peels, or non-invasive such as topical creams and laser therapies. Invasive methods are used to remove the unsightly skin generating a healing response to cause rejuvenation in the skin. Invasive therapies are common as the results are generally satisfactory but complications are more severe than the non-invasive methods. As individuals heal uniquely, side effects include prolonged inflammation, excessive scarring or hyper/hypopigmentation of the specific area (Avram *et al.*, 2006). The non-invasive methods are increasing in popularity. Although the outcomes are more subtle and usually more than one treatment is needed, these therapies have shown to have a comparable effect to invasive therapies (Dierickx & Anderson, 2005; Nestor *et al.*, 2000). In addition, the benefits tend to be longer-lasting with less associated side-effects. One treatment that is popular in society nowadays is laser therapy (Avram *et al.*, 2006; Waibel, 2009).

1.4.1. Laser Therapy

Techniques such as laser therapy can be both invasive and non-invasive and treat most of signs of photoageing. Invasive, or ablative, laser therapy has the same complications as surgery and chemical peels. Non-invasive laser therapy can treat a wide range of skin conditions such as wrinkles, mottled pigmentation, telangiectasia, purpura, rosacea and rough skin texture (Avram *et al.*, 2006; Rinaldi, 2008; Waibel, 2009). This therapy involves the use of a laser emitting a specific wavelength of light targeting various compounds or cells in the skin (Peng *et al.*, 2008).

Recent advancements in photonics and optics allowed for the manufacturing of lasers emitting numerous wavelengths across the light spectrum. This evolution was to target specific organelles and compounds in the cell, such as the mitochondria and porphyrin rings in haemoglobin. These compounds capture specific wavelengths of light thereby absorbing

their energy. These lasers deliver high levels of energy to either destroy a cell at a specific location, as in the case of removing varicose veins, or ablate certain compounds, as is the case with the removal of irregular pigmentation. This results in the targeted compound alone being destroyed and leaving the surrounding tissue relatively unharmed (Peng *et al.*, 2008; Rinaldi, 2008; Waibel, 2009).

Low doses of light energy to the cells can be stimulated to reduce the signs of ageing and resolve other dermatological problems (Dierickx & Anderson, 2005; Rinaldi, 2008; Waibel, 2009). A threshold between destroying and stimulating cells is a matter of energy, in the form of photons, delivered to the skin. If the amount is too high, the energy will scatter throughout the tissue causing thermal damage whereas too small an amount will not lead to stimulation.

1.4.1.1. Principle workings of a laser

Irradiation using a laser is dependent on 3 main variables: energy, power and irradiation time. Energy is defined as the ability to cause work and is represented by the unit, Joule (J). The energy density or energy per unit area is represented as Joules per square centimetre (J/cm^2). It is also known as fluence, and is the most reported variable when using a laser on the skin (Armstrong, 1992). A high dose of energy can lead to side-effects such as purpura (red and purple discolouration of the skin), erythema (redness of the skin due to inflammation) and oedema (fluid accumulation in the skin) (Waibel, 2009). Indirect damage through the generation of high levels of ROS may occur, potentially leading to more serious effects (Bickers & Athar, 2006; Mbene *et al.*, 2009).

Relative to the energy density is the power. It is defined as the rate at which energy is delivered and is represented as Watts (W). Power density, otherwise known as irradiance, refers to the power in a given area (W/cm^2) (Armstrong, 1992; Pryor *et al.*, 2011). High levels of power or power density have the same effect on cells as high doses of energy. These two variables are dependent on one another and involve the time of exposure as seen in the equation below (Armstrong, 1992).

$$Time = \frac{Dose\ (J/cm^2))}{Power\ Density\ (W/cm^2)}$$

Equation 1.4.1 Equation used to determine, energy and power density and exposure time.

Thus, these three variables are important when using laser therapy and vary greatly when treating different skin conditions. In addition, when it is used for the skin, a process known as photorejuvenation, there is significant variability in protocols depending on the skin condition being treated (Da Silva *et al.*, 2010; Waibel, 2009).

1.4.2. Photorejuvenation

Photorejuvenation is a light therapy used to treat the signs of skin ageing. It changes cell signalling pathways to cause an overall rejuvenation effect (Dierickx & Anderson, 2005; Lubart *et al.*, 2007). Specific changes are seen such as increased synthesis of collagen and upregulation of cytokines that promote repair and maintain ECM homeostasis (Gu *et al.*, 2011; Huang *et al.*, 2011; Wong *et al.*, 2009). Different light sources and types of light are used to stimulate the fibroblasts located in the dermis. There are several different types of light sources used in photorejuvenation (Dierickx & Anderson, 2005).

One of the most common light sources utilized is intense pulsed light (IPL). IPL is a non-laser, non-coherent, filtered flashlamp emitting high intensity, pulsed, broad bandwidth (500 nm – 1200 nm) light (Goldman *et al.*, 2005). IPL is one of the most common light sources used to treat photodamaged skin due to its relative inexpensiveness and easy application (Goldman *et al.*, 2005). The precise molecular mechanisms of IPL photorejuvenation are not known and results vary between patients. An increase of TGF-β and collagen type III mRNA and protein were found in fibroblasts irradiated with IPL with a 570nm cut-off filter with a dose of 75J/cm², highlighting a possible mechanism of rejuvenation through TGF-β (Wong *et al.*, 2009). Another article showed that modulation of both MMP-1 and TGF-β1 in fibroblasts through MAPKs was light dose dependent when using IPL (Huang *et al.*, 2011).

In recent years the use of a laser for photorejuvenation has become popular due to the specificity one gets in manipulating certain variables, such the energy and power density and the light beam itself. The table below (Table 1.4.1) summarises lasers that are used in photorejuvenation and their emitted wavelengths The wavelengths are related to the targeted compound or tissue being treated (Dierickx & Anderson, 2005; Waibel, 2009).

Type of Laser	Emitted Wavelength
CO_2	10μm
Nd:YAG	1μm
Er:YAG	2.5μm
Diode	variable
PDL	595nm
IPL	400-1200nm
KTP	532nm

Table 1.4.1 Lasers used in photorejuvenation and the wavelengths of light emitted. CO2 , Carbon dioxide; Nd:YAG, Neodymium: Yttrium-aluminium garnet; Er:YAG, erbium: Yttrium-aluminium garnet; Alexandrite, alexandrite crystal; PDL, pulsed dye laser; IPL, intense pulse laser; KTP, potassium titanyl phosphate (adapted from Waibel 2009).

In practice, low level laser irradiation of cells involves using low energy densities by laser light to cause changes in the collagen matrix through the stimulation of the resident cells, with few side effects (Frigo *et al.*, 2010; Lubart *et al.*, 2007). It is proposed the biostimulatory effect of energy delivered by a laser altered the cellular activity. In wound healing, red laser light at low fluences resulted in an increase in fibroblasts proliferation and an acceleration of wound healing (Hawkins & Abrahamse, 2006; Houreld & Abrahamse, 2007; Peplow, Chung, & Baxter, 2012a; Rodrigo *et al.*, 2009; Whelan *et al.*, 2001). Due to the increase in wavelengths available, photodynamic rejuvenation (PDR) has gained momentum as a rejuvenative skin tool as it has been reported to be more effective than photorejuvenation alone (Nootheti & Goldman, 2006).

1.5. Photodynamic Rejuvenation (PDR)

PDR is a new therapy which involves the use of a topically applied photosensitizer (PS) that is activated by a specific wavelength of light in the presence of oxygen to cause alterations in cellular metabolism and signalling. It was developed from a therapy of the same principle called photodynamic therapy (PDT). PDT was discovered in the 1970s where crude extracts of blood containing PS compounds were found to give the skin sensitivity (Allison & Sibata, 2010). There has been an incredible amount of research in the last few decades for its use in the field of dermatology (Kohl *et al.*, 2010; Steinbauer *et al.*, 2010). One of the observations noted when using PS to treat benign sun-induced skin lesions, actinic keratoses, was the overall improved appearance of the skin (Alexiades-Armenakas & Geronemus, 2003; Bruscino *et al.*, 2010; MacGregor & Dover, 2010; Szeimies *et al.*, 2009). This led to the development of PDR for the sole use of treating photoaged skin. There are two main variables when using PDR: the PS and the activating light source. Both are equally important and relate to the efficacy of the treatment.

PS are integral parts in the efficacy of this treatment. Upon light activation the PS is excited from the ground state, S0, to the first excited singlet state, S1, which may be followed by fluorescence emission, heat dissipation or yield a triplet state (Kiesslich *et al.*, 2006). Once the PS is in the triplet state, it undergoes photochemical reactions where energy is transferred to nearby molecules such as oxygen or becomes a free radical itself (Figure 1.5.1). One of the products of these reactions are ROS (Agostinis *et al.*, 2011; Lubart *et al.*, 2007) (as described in Figure 1.5.1). ROS are able to alter signalling pathways in the cell and cause a release of factors that change the cell's functionality (Lubart *et al.*, 2007).

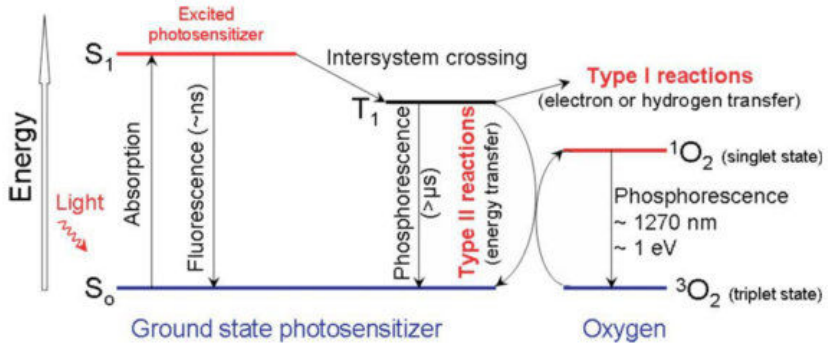

Figure 1.5.1 Photosensitization process of a PS activated by light. The excited PS moves from the ground singlet state (S0) to an excited singlet state (S1). The molecule in S1 may undergo intersystem crossing to an excited triplet state (T1) and then either form radicals via type I reactions or singlet oxygen from type II reactions. ns indicates nanoseconds; µs, microseconds; nm, nanometres; eV, electron volts (taken from Agostinis *et al.*, 2011)**.**

PS can be divided into two major groups: porphyrins and non-porphyrin photosensitizers (O'Connor *et al.*, 2009). Porphyrin molecules possess a highly conjugated, heterocyclic macrocycle and may contain a central metallic atom such as iron or magnesium (O'Connor et al. 2009). The most common porphyrin PS available today are aminolevulinic acid (ALA) and its methyl ester methyl aminolevulinate (MAL). They are precursors in the haem-biosynthesis pathway and are converted to protoporphyrin IX by ferrochetalase inside the cell. ALA itself is not a PS but when converted; its porphyrin product is photoreactive. Non-porphyrin PS include toluidine blue, methylene blue and hypericin. These compounds do not possess a porphyrin ring, but in a similar manner, capture light and can undergo photochemical reactions. Each PS has a specific absorbance spectrum which illustrates the wavelengths of light captured by this compound resulting in activation. In some cases, the PS can be activated by several wavelengths making it a versatile tool when developing a therapy to treat specific skin conditions. For example, according to ALA's absorbance spectra, blue light is maximally absorbed. Researchers have found that red light could be used for PDR with ALA and was superior to red light alone (Bjerring *et al.*, 2009; Gold *et al.*, 2006; Kosaka *et al.*, 2010; Xi *et al.*, 2011). Various light sources are used to activate PS and many are similar to those used in photorejuvenation. These include IPL, lasers, normal halogen lamps generating white light, and light emitting diode (LED) lamps emitting a variety of wavelengths. The light sources chosen depend on the absorbance spectra of the PS. A PS might have more than one peak in its absorbance spectra indicating that it can be activated by several wavelengths of light.

Most of the basic science research is in the absorption, distribution, metabolism and excretion (ADME) of a PS compound. All of these characteristics play a major part in the mechanism of the therapy and its safety. The quantum yield of the PS will indicate the amount of energy it can capture and transfer to the surrounding molecules. The higher the

quantum yield, the less PS will be needed to generate ROS and other reactive species. This leads to fewer side-effects occurring from phototoxic reactions.

There have been numerous clinical studies showing the range of cosmetic improvements that can be achieved with PDR. Various PS, light sources and activating wavelengths were used; all show an improvement in an aspect of skin rejuvenation. These reports were summarised in Table 1.5.1 and Table 1.5.2.

1.5.1. Summary of Clinical Reports using PDR

Table 1.5.1 was compiled to illustrate the variety of clinical data in the literature regarding study design, applications, outcomes and side effects of photodynamic rejuvenation.

The sample sizes in the clinical studies varied in range from 7 to 37 subjects and were generally quite small. Overall patient group size had a mean of 26 per study.

The patients were in the 5th to 7th decade of life for over half the studies. This is in line with the development of photoageing being in the later years of life. Most studies were conducted on patients who had lighter skin tones and were grouped in Fitzpatrick's scale I-III. This correlates with lighter skin types being more prone to develop skin ageing characteristics therefore in need of intervention (Farage *et al.*, 2008; Rawlings, 2006).

The longer wavelengths of light were chosen as they can penetrate deep into the dermal layer and potentially activate the PS within that area. There was a trend of 37J/cm^2 energy density used for these *in vivo* studies. Although, a range of energy densities (4-96J/cm^2) were used. The high energy densities resulted in an increased severity of adverse side-effects such as erythema, oedema and crusting. It was common that authors did not mention the power density.

IPL is the most common light source used in PDR. IPL emits a wide range of wavelengths (550nm-1200nm) and is often used with a cut-off filter which limits the range mainly to the red light spectrum. Red light is also emitted from LED. The IPL and LED systems are commonly used in dermatological clinics for photorejuvenation; therefore, their use with PDR makes them a viable and cost effective option.

The most common PS used in PDR are ALA and MAL. This is due to their easy availability as licenced drugs in both the United States of America and Europe. ALA is provided as a 20% solution, however researchers used lower concentrations. Kosaka *et al*, for example, investigated the differences in fluorescence in skin using different concentration of ALA (Kosaka *et al.*, 2010). They found that 5% ALA concentration had a similar fluorescence to the higher concentrations. ALA is prescribed to be applied 14-18h before light activation

according to the manufacturer's instructions. Shorter incubation times were employed in some studies and resulted in similar outcomes compared to the longer incubation periods, and with less severe side effects (Bjerring *et al.*, 2009; Christiansen *et al.*, 2007). In the majority of the cases a 3 hour incubation of the PS was used. Another aspect was to investigate improving the manner in which a PS was applied to the face and suggested microneedling, tape stripping and dermabrasion in order to increase its penetration and thereby increasing its efficacy (Clementoni *et al.*, 2010; Lowe & Lowe, 2005).

Another interesting variable were the number of treatments applied and intervals between them. The number of treatments did not exceed three and in most cases these were separated by 30 days intervals. One study debated whether more treatments with lower concentration of PS and shorter incubation times and lower energy densities gains superior results as opposed to one treatment with higher concentrations, longer incubations times and increased energy densities (Xi *et al.*, 2011). A high PS concentration and energy density is a harsh PDR protocol that may result in severe reactions and more pronounced side effects. In contrast a "softer" protocol, using low concentrations of PS and energy densities, would result in a subtle and gradual improvement in the signs of skin ageing (Xi *et al.*, 2011).

In performing this therapy, the PS was either applied to the entire face or only half the face, known as a split-faced study. The split-faced studies determined if the light alone had an effect on the skin. In some cases, actinic keratoses were specifically investigated as a sign of photodamage and the PS was only applied to the lesional area. However, in these studies, the authors retrospectively commented on the overall good cosmetic appearance of the skin after treatment (Alexiades-Armenakas & Geronemus, 2003; Bruscino *et al.*, 2010)(Ruiz-Rodriguez *et al.*, 2002). The follow up period for the studies was generally between 1 and 6 months after the last treatment. One or two follow up consultations took place where the investigator either took photographs or biopsies.

Various methods were used to assess the efficacy of PDR. The most commonly used were photographs taken before the start of the study and at follow ups. These photographs were either analysed by the investigator or by an independent clinician. In a large portion of studies, each individual characteristic of photoageing was assessed and graded. In most cases a point scale system was used to investigate mottled pigmentation, sallowness, telangiectasia, roughness, fine lines/wrinkles, deep wrinkles and global photoageing. Fine lines or wrinkles, mottled pigmentation, sallowness and tactile roughness of the skin were often improved. Interestingly, telangiectasia and coarse lines/wrinkles were often not improved with PDR treatment. In split-faced studies, the PDR treated side had better results than the light only control (Bjerring *et al.*, 2009; Gold *et al.*, 2006; Kosaka *et al.*, 2010;

Nootheti & Goldman, 2006; Xi *et al.*, 2011). In studies which took into account the patient's observations, a high patient satisfaction was noted.

Interestingly, the information gleaned from Table 1.5.1 indicates that no clear "gold standard" protocol exists for using PDR. Variables include different ethnic populations, different outcomes, patient education and skin tone. In addition, the disparity between protocols and assessment methods makes it difficult to effectively compare these studies (MacGregor & Dover, 2010). However, a cross comparison such as this has not been attempted before and sheds valuable light on the field of PDR.

Overall, the outcome of PDR on the photoageing was satisfactory for both the patients and clinicians. Although the studies were generally quite small, the rejuvenative power of PDR was seen throughout. The phototoxic reactions that occurred when using PDR were temporary and side effects were resolved within 7 days with no further complications experienced. Interestingly, the inconsistencies in outcomes seen in Table 1.5.1 were possibly due to the different patients, the type and application of the PS, light sources, irradiation protocol, and the individual patient's response to the therapy. However, this therapy was never detrimental to the health of the patient and the appearance of the skin never worsened because of it. Some pain management was needed during the treatment but overall it was well tolerated. This therapy has shown great promise in treating photoageing especially in the categories of mottled pigmentation, skin roughness and fine wrinkles.

1.5.2. Summary of Molecular Reports using PDR

The molecular mechanisms behind PDR have only recently been investigated and are presented in Table 1.5.2. Researchers, using pathways established from other anti-ageing therapies, investigated certain downstream effectors and determined their modulation after PDR.

In a variety of studies, the models used to determine the molecular mechanism of PDR were human, mice and single cultured cell types. These models allowed the researchers to examine several effects of PDR under controlled conditions. For examples, primary fibroblasts and keratinocytes were used in most cases as they are the two main skin cell types affected and they communicate extensively with one another (Fagot *et al.*, 2002; Ghaffari *et al.*, 2009; Karrer *et al.*, 2004; Maas-Szabowski *et al.*, 1999). The researchers investigated the specific reactions of these cells after treatment. ALA and MAL were used in the majority of the molecular studies. The concentration and incubation times of the PS differed between experimental models. For example, *in vitro* experiments using primary

fibroblasts were treated for 24h compared to the *in vivo* studies using humans and mice where the incubation time was 3h (Karrer *et al.*, 2003) (Table 1.5.1).

IPL, PDL and lamps were the most common light sources used and the most common wavelengths were in the red range. The energy densities delivered from these light sources range from very low (7.5J/cm^2) to very high values (100J/cm^2). The power density was kept in the low range of 35-100mW/cm^2.

Interestingly, a single PDR treatment was used on primary cells whereas patients were treated several times in accordance with previous clinical protocols (Table 1.5.1). Accordingly, follow up times varied as many studies focused more on immediate changes whereas patient-driven studies were days or weeks after PDR treatment.

The outcomes of PDR were analysed by investigating changes in mRNA and protein expression levels and enzyme activity. Various assays were employed for these analyses: RT-PCR for gene expression analysis; western blot analysis, ELISA and immunohistochemistry for protein expression; and zymography for enzyme activity.

The effect of PDR treatment on collagen type I expression seemed to be time dependent (Choi *et al.*, 2010; Orringer *et al.*, 2005) (Table 1.5.2). Using RT-PCR, Karrer *et al* found collagen type I mRNA to be decreased 24h after treatment returning to basal levels after 72h (Karrer *et al.*, 2003). Analyses of later time points in different studies, showed collagen mRNA and protein levels increased after 16 days (mice) and from 1 to 6 months (humans). Overall, it appears that collagen synthesis is initially decreased by PDR and increases at later time points.

MMP are enzymes that selectively breakdown the ECM. It is thought that an increase in MMP levels in PDR remove the damaged collagen fibres thereby stimulating collagen synthesis in the fibroblasts. A variety of MMP enzymes were investigated. MMP levels showed an inverse correlation to collagen levels, where there was an early increase in all the experimental models used. MMP-1 mRNA and protein consistently displayed an immediate increase post-PDR treatment. Other MMP's in the family, such as MMP-3, MMP-2 and MMP-9, in both *in vivo* and *in vitro* studies, had a similar response as MMP-1 and all returned to basal levels a few days later.

TGF-β is a major regulator of collagen homeostasis (Section 1.3.3). However, there have been limited studies investigating TGF-β after PDR. Park *et al* found that TGF-β and its receptor were increased in the epidermis one month after treatment (Park *et al.*, 2010). Choi *et al* found that TGF-β1 mRNA increased 2 days after PDR in mice (Choi *et al.*, 2010). However, from this data we cannot draw a conclusion as on PDR's effect on TGF-β.

The overall picture after analyses and summary of these two tables demonstrate a lack of consistency and information regarding PDR treatment. However, these tables illustrate the data available and represent the information contributed to this field and that which still needs to be discovered. The overview from the reported results indicates that PDR is a useful tool for the treatment of photoaged skin although an optimised protocol still needs to be established. As such, the aim of this project was to develop a PDR protocol using a PS from the extract of the *Hypericum perforatum* plant, commonly known as St Johns Wort. We used this PS in a novel way in its development for PDR and determined its effects on primary human dermal fibroblasts.

Reference	No. of Patients	PS & concentration	PS incubation period	Wavelength of Light	Light Source	Energy/ Energy Density	Power/ Power Density	No. of Follow up	Follow up time	No. of treat-ments	Intervals between treat-ments	Application	Assessment method	Comment	Side Effects
(Ruiz-Rodriguez *et al.*, 2002)	17	20% ALA	4h	Non-coherent light filtered - 590 to 1200 nm	IPL	40 J/cm^2	N/A	Full-face	1 and 3 months	2	1 month	AK lesional area treated	Author commentary	Cosmetic appearance improved drastically	Erythema, oedema, crusting
(Alexiades-Armenakas & Geronemus, 2003)	41 (Mean age 70 years)	20% ALA	3h under occlusion or 4-18h not occluded	595nm (pulsed light)	PDL	4-7.5J/cm^2	N/A	5	10 days, 2, 4, 6 and 8 months	1	0	Full face application	Biopsies and photographs were taken	No difference between the 3h and 14-18h incubation times regarding efficacy. PDL light only had no effect on AK lesions after 1 month. Excellent post treatment cosmesis was noted and was seen as a major advantage of this treatment over other treatments for AKs.	including stinging, burning, erythema, and pain were recorded
(Touma *et al.*, 2004)	18 (Ages 41 - 76 years)	ALA	1,2 and 3h	Blue	Fluo-rescent tubes	10J/cm^2	N/A	0	1 day, 1 week and 1 month, 10 patients for 6 month follow up	1	0	Full face ALA treatment with split faced for creams applied before the ALA treatment (vehicle vs. 40% urea cream)	8-point Griffiths score index and patient and investigator evaluations.	Great improvement with regard to sallowness and fine lines and mild improvement on mottled pigmentation. Patient satisfaction was high with 76% of patients noting a good response to the treatment. Neither ALA incubation time had no effect nor did 40% urea cream pre-treatment result in significant differences regarding photoageing or side effects.	Erythema and oedema were noted to be moderate to severe 1 day after treatment. At 1 month after treatment most of the side effects has resolved. Most patients had no crusting.
(Lowe & Lowe, 2005)	6 patients	5% ALA	30 min	633nm	LED	96 J/cm^2	105 mW/cm^2	1	Only before and 4 weeks after treatment were reported for photoageing.	1	0	Stripping with tape	Clinical assessment using photographs and a grading system. Grading was done according to the Glogau grading scale. (Glogau, 1996)	Significant improvement in the periorbital region with a reduction in fine lines in 67% of the patients.	Treatment was tolerated well and no adverse side effects were noted,

Reference	No. of Patients	PS & concentration	PS incubation period	Wavelength of Light	Light Source	Energy/ Energy Density	Power/ Power Density	No. of Follow up	Follow up time	No. of treat-ments	Intervals between treat-ments	Application	Assessment method	Comment	Side Effects
(Dover *et al.*, 2005)	20 (White, mean age: 55 years)	ALA	30-60min	515-1200nm	IPL	23-28J/cm^2	N/A	Full-face	4 weeks	5	3 weeks	3 ALA-IPL treatments and 2 IPL alone treatments	Independent investigator who assessed fine lines, mottled pigmentation, tactile roughness, sallowness, and a global score for photoageing using a 5 point scale system.	The greatest results were in mottled hyperpigmentation and global photoageing, and to a slightly lesser extent, in fine lines over IPL irradiation only. However, areas like sallowness and tactile roughness did not show any improvement. The authors comment on the possible accelerated improvements when the skin was pretreated with ALA.	Erythema, scaling, dryness and oedema but were reported to be minimal
(Gold *et al.*, 2006)	16	ALA	30-60min	515-1200nm with 550nm cut-off filter	IPL	34J/cm^2	N/A	2	1 and 3 months	3	1 month	Split-faced	Blinded independent investigator assed tactile roughness, crow's feet appearance, mottled pigmentation, facial telangiectasia, and facial AKs via a graded scale.	In all areas -Crow's feet, tactile skin roughness, mottled hyperpigmentation, telangiectasia and actinic keratoses improvement was greater in the ALA pretreated side compared to the IPL only treated	Erythema and oedema were seen in fewer than 10% of the treatments and were noted on both sides of the face.
(Ruiz-Rodriguez & López-Rodriguez, 2006)	10	MAL	1 and 3h	630nm	LED	37J/cm^2	N?A	1	2 weeks	3	N/A	Split-faced	Reported by the author	3hr incubation showed superior results to 1hr incubation. Skin quality and fine wrinkles ad improved but not telangiectasia or mottled pigmentation. Compared different light sources in PDR.	3hr incubation had more severe erythema, oedema and crusting
(Zane *et al.*, 2007)	20 (White; Mean age of 68.9 years)	ALA	3h	Red	LED	37J/cm^2	N?A	2	At second treatment and 2 months after last treatment	2	1 month	Full face	Photoageing was quantified using a five point scale. A global score was recorded in addition: fine periocular lines, mottled pigmentation, sallowness, and tactile roughness.	Significant improvement in the following signs of photoageing: global ageing, fine lines, mottled pigmentation, sallowness and roughness. Deep wrinkles, telangiectasia, facial erythema, and sebaceous gland hypertrophy did not show any improvement. Most patients were very satisfied with the treatment (12/18 patients).	erythema and oedema which only lasted for 3 days

Reference	No. of Patients	PS & concentration	PS incubation period	Wavelength of Light	Light Source	Energy/ Energy Density	Power/ Power Density	No. of Follow up	Follow up time	No. of treat-ments	Intervals between treat-ments	Application	Assessment method	Comment	Side Effects
(Buggiani *et al.*, 2008)	25	5% ALA	3h	636nm	Lamp	N/A	N/A	2	2 weeks after first treatment, at the end of the last treatment.	3	I month	Prepared the skin with glycolic acid or pirutic acid. Full face application	Observation from investigator and OCT	Observed improvements in mottled pigmentation and skin texture but not in wrinkles or telangiectasia. Using OCT the epido-dermal junction became undulating from a relatively straight junction. At the end of the last treatment 70% had improvement regarding skin texture.	N/A
(Ruiz-Rodríguez *et al.*, 2008)	10 (White, mean age: 55 years)	MAL	1 and 3h	630nm	LED	37J/cm^2	N/A	1	2 months	3	2 weeks	Split-faced	Blinded independent investigator	Improvement in the skin was only seen with the 3 hour incubation in the categories of skin tightness and fine wrinkles. None of the other signs showed the improvement that was seen in early studies.	3hr incubation had more severe erythema, oedema and crusting
(Szeimies *et al.*, 2009)	131	160mg/g MAL	3h	630nm	LED	37J/cm^2	56-83mW/cm^2	2	2 weeks and 3 months	2	1 week	Full face	Independent clinician noted the resolution of AK lesions	AK were significantly decreased at 3 months along with excellent cosmetic results. Authors suggest PDR when cosmesis is a high priority when treated AK, i.e. when AK are present on the face.	Pain, burning and erythema were common and were resolved within several days
(Kosaka *et al.*, 2010)	5 (Japanese, mean age: 36 years)	5% ALA	2h	515-1200nm	IPL	23–30 J/cm^2	N/A	2	1 and 3 months	3	1 month	Split-faced	Independent investigator using a 5 point scale assessment for mottled pigmentation, crow's feet appearance, fine lines, tactile roughness and sallowness were evaluated as indexes of photodamage.	Improvement in all areas but it was found that there was no significant difference between IPL using ALA and IPL alone however; IPL using ALA was tending to has superior effects.	The authors suggest that due to the darker skin type of the patients the side-effects were more pronounced and last longer.

Reference	No. of Patients	PS & concentration	PS incubation period	Wavelength of Light	Light Source	Energy/ Energy Density	Power/ Power Density	No. of Follow up	Follow up time	No. of treat-ments	Intervals between treat-ments	Application	Assessment method	Comment	Side Effects
(Clementoni *et al.*, 2010)	21 patients (White; Mean age: 56 years)	ALA	1h	(1) 550nm-1200nm; 560nmcut-off filter; (2) 630nm	(1) IPL; (2) LED	19–22 J/cm^2	N/A	2	3-6 months	1	0	Microneedling followed by ALA. Full faced. Treatment with LED after IPL.	Three physicians used the 5-point scale for the categories: fine lines, mottled pigmentation, sallow complexion, tactile rough-ness, telangiectasia, and coarse wrinkles	A statistical difference was present between 3 and 6 months for global score, fine lines, sallowness and tactile roughness. No statistical differences were seen between 3 and 6 months after the treatment for mottled hyperpigmentation and telangiectasia. At 3 and 6 months after the treatment, coarse wrinkles showed no statistical significance compared to the baseline.	Erythema, oedema and crusting were noted 1 day after the treatment and were resolved by day 7. No pain management was necessary.
(Bruscino *et al.*, 2010)	1 (Italian female 88 years old)	160mg/g MAL	3h	632nm	Lamp	37J/cm^2	70-100mW/ cm^2	1	1 month	1	0	Applied to lesional area	Photography and 3D-profilometry	Significant reduction in wrinkle depth one month after treatment through 3D profilometry	Burning, crusting and pain 7 days after treatment
(Sanclemente *et al.*, 2011)	48 females. Mean age: 51.5 year	0.5g MAL	3h	Red	N/A	37J/cm^2	N/A	2	1 month after 2 treatment and 1 month after the last treatment	4	2-3 weeks	Split-faced where one side was treated with PDT and the other had light only.	Independent, blind investigator	Improvement in the MAL activated by light in the following areas: global photoageing signs, fine and coarse lines, mottled pigmentation, tactile roughness and sallowness	The PDT treated side experienced: more pain and desquamation vs. placebo, erythema was frequent, oozing was noted. Pigmentation occurred and was resolved within a few days.
(Haddad *et al.*, 2011)	21	ALA	2h	500 to 1200nm with a 515-nm filter	IPL	20, 25, 40, and 50 J/cm^2	N/A	2	5–7 days and 8 weeks	1	0	Full face	Photodamage severity was determined by the 9-point photonumeric Griffiths scale.	Increasing fluence did not significantly change the results regarding resolution of photoageing signs. However, the majority of patients did note an improvement overall and ALA pretreatment had superior results compared to IPL alone.	Erythema, oedema, crusts and erosion, and pain occurred. Graded on a 5-point scale. The higher the fluence resulted in more severe side effects.

Reference	No. of Patients	PS & conc	PS incubation period	Wavelength of Light	Light Source	Energy/ Energy Density	Power/ Power Density	No. of Follow up	Follow up time	No. of treat-ments	Intervals between treat-ments	Application	Assessment method	Comment	Side Effects
(Rossi, 2011)	25 (Female)	ALA	N/A	632nm	Lamp	37J/cm^{2}`	70-100mW/ cm^{2}	1	3 months	3	1 month	Full face	Investigator observations and optical coherence tomography (OTC)	Saw improvement in mottled pigmentation and skin roughness. Improvement in the epido-dermal junction ridges from baseline readings.	N/A
(Xi *et al.*, 2011)	24 patients; mean age: 48 year, Dark skin tone	5-10% ALA	1h	550nm-1200nm (590nm cut-off filter)	IPL	14-21J/cm^{2}	N/A	2	1 and 2 months	3	1 month	Split-face	An independent investigator monitored and graded global photoageing, tactile skin roughness, fine lines, coarse wrinkles, and mottled hyperpigmentation	PDR results in global photoageing score, fine lines, and coarse wrinkles showed superior improvement compared to IPL alone treatment.	Side effects were more severe in the ALA pretreated side regarding erythema and oedema. Post inflammatory hyperpigmentation occurred transiently and faded within 2 month.

Table 1.5.1 Sumamry of clinical studies that used PDR. AK: Actinic Keratosis/Keratoses; IPL: intense pulsed light, N/A: information not available; conc: concentration

Reference	No. of Patients	PS & conc	PS incubation period	Wavelength of Light	Light Source	Energy/ Energy Density	Power/ Power Density	No. of Follow up	Follow up time	No. of treatments	Intervals between treatments	Application	Assessment method	Comment	Side Effects
(Karrer *et al.*, 2003)	Normal and scleroderma primary human fibroblasts	ALA	24h	580nm-740nm	Halogen Lamp	24J/cm^2	40mW/ cm^2	Dependent on assay used	0, 4, 6, 12, 24, 48, and 72 h	1	0	Collagen lattice with fibroblasts were treated with medium containing ALA	XTT cell viability, ELISA and RT-PCR	In normal human fibroblasts mRNA levels of MMP-1 and MMP-3were increased as early as 4 hours but after 24 hours had almost returned to basal levels. It was found that MMP-1 and MMP-3 protein and activity were increased in normal human fibroblasts over a period of 48 hours thereafter began to decrease. Collagen type I mRNA significantly decreases for up to 24 hours	N/A
(Karrer *et al.*, 2004)	Fibroblasts and Keratinocytes	100µmol/l ALA	24h	580nm-740nm	Halogen Lamp	24J/cm^2	40mW/cm^2	Dependent on assay used	6–48 h	1	0	Conditioned medium from PDR treated keratinocytes was used on the fibroblasts	XTT cell viability, ELISA and RT-PCR	Conditioned medium from keratinocytes 24h after PDR stimulated fibroblasts to increase the protein levels of MMP-1 and 3 48h later. However, after 96h the levels returned to normal. Collagen type I RNA was not altered after conditioned medium was placed on the cells. Collagen IV coated transwell were used where keratinocytes were on one side and fibroblasts on the other. Only small molecules can pass through the transwell. Induction of MMP-1 and 3 was only noted on the supernatants from the fibroblasts and not the keratinocytes. IL-1RA completely abrogated the stimulation of fibroblasts from the keratinocyte conditioned medium.	N/A

Reference	No. of Patients	PS & conc	PS incubation period	Wavelength of Light	Light Source	Energy/ Energy Density	Power/ Power Density	No. of Follow up	Follow up time	No. of treatments	Intervals between treatments	Application	Assessment method	Comment	Side Effects
(Marmur *et al.*, 2005)	7 patients; Mean age: 51 years	ALA	1h	550-1200nm with 550nm cut-off filter	IPL	24J/cm^2	N/A	1	3 month	2	1 month	Split-faced	Dependent investigators. Punch biopsies were also taken 3 months after treatment for electron microscopy.	Greater shift towards collagen type I production than collagen type III and had an increase in fibre number. Increase in collagen type I in ALA-IPL treated cells could be due to the thermal effects of IPL and the ROS-generating reaction of activated ALA. It was noted that there was a subjective improvement in the skin overall however, there was no difference between those treated with IPL or with IPL and ALA.	No mottled pigmentation, blistering, or crusting occurred. Transient, mild erythema and burning occurred on both sides on the face and was resolved within 24 hours.
(Orringer *et al.*, 2008)	24 patients; All patients over the age of 40 years. Mean age: 68 years	20% ALA	3hr	595nm	PDL	7.5J/cm^2	N/A	4-5	Up to 6 months	1	0	Forearm skin	RT-PCR, immunohistochemistry (IHC). 3mm punch biopsies taken.	MMP-1 gene expression increased 20-fold and returned to basal levels within 24 hours. Prolyl-4-hydroxylase, an enzyme involved in post-translation modification of collagen, was elevated 3-fold one month after treatment. RT-PCR results indicated that collagen type I and III mRNA levels were significantly increased after 30 days. Procollagen type I and III mRNA peaked at 30 days and decreased, but not to basal levels.	Procedure well tolerated. Erythema and focal crusting was noted after treatment.
(Almeida Issa *et al.*, 2009)	14 Patients aged 55-60 years; Mean age: 57.6 years	MAL	2h	635nm	LED	37J/cm^2	N/A	2	3 and 6 months	2	4 weeks	Full face	Biopsies were taken for histology and (IHC) results were examined by three independent observers.	At 3 months - Elastotic material becomes more diffuse and collagen appears between the elastic fibres. MMP-9 and collagen type I. IHC staining was moderately increased from before treatment. At 6 months - Collagen fibres increased further between the elastotic fibres and a band of collagen was noted in the upper papillary dermis in some patients. Fragmented elastic fibres were decreased substantially and there was a stronger staining for collagen type I compared to 3 months.	N/A

Reference	No. of Patients	PS & conc	PS incubation period	Wavelength of Light	Light Source	Energy/ Energy Density	Power/ Power Density	No. of Follow up	Follow up time	No. of treatments	Intervals between treatments	Application	Assessment method	Comment	Side Effects
(Park *et al.*, 2010)	14 Korean patients; Mean age: 62 years	20% ALA	4h	Red	Halogen	100J/cm^2	100mW/ cm^2	1	1 month	2	1 month	ALA mixed with petrolatum was applied to actinic keratotic lesions	Biopsies were taken for histological and IHC processing at the follow up times.	The histological results showed a decrease in epidermal thickness & smoothing of the skin. An increase in total collagen & decrease in elastotic material was seen. When IHC was used, TGF-β & TGF-βIIR increased mainly in the epidermis & fibrillin-1 in dermis, an increase in procollagen type I & III protein in the papillary dermis & decrease of MMP-1, 3, 12. The increase in TGF-β, its receptor & collagen type I & III mRNA support an increase in collagen synthesis. In contrast, the decrease in MMPs has not be seen in other studies but as these results are only from one time point.	Variable degrees of erythema and oedema which was resolved in a few days. Some patients reported mild to moderate pain which did not need intervention.
(Issa *et al.*, 2010)	14 Patients aged 55-60 years; Mean age: 57.6 years	MAL	2h	635nm	LED	37J/cm^2	N/A	2	3 and 6 months	2	4 weeks	Full face	Biopsies were taken for histology using h haematoxylin-eosin (HE), orcein, and picrosirius. Results were examined by 2 independent observers.	At 6 months – 10 patients had improvement in skin texture, roughness and fine lines. Some patients' elastosis was reduced significantly. There was an increase in collagen density in the papillary dermis.	

Reference	No. of Patient	PS & conc	PS incubation period	Wavelength of Light	Light Source	Energy/ Energy Density	Power/ Power Density	No. of Follow up	Follow up time	No. of treat-ments	Intervals between treatments	Application	Assessment method	Comment	Side Effects
(Choi *et al.*, 2010)	Female ICR mice	16% MAL	3hr	613–645 nm	LED	25J	35mW/ cm^2	7	day 1, 2, 4, 8, 12, 16, 21	1	0	MAL was applied to a 2cm area on the back of the mice.	Western blot, RT-PCR, histology and zymography	An increase in IL-1, TNF-α and TGF-β1 mRNA was seen at day 2 after treatment but not in the controls. The increase of IL-1 & TNF-α correspond to the changes in MMP expression. An increase in MMP-2 mRNA & enzyme activity, MMP-3 mRNA & protein, & MMP-9 enzyme activity were observed at day 1, 2 & 4. Procollagen type I mRNA & protein began to increase after PDR treatment but at time points after 16 days. Procollagen type III mRNA & protein was not strongly affected but still showed an increase at the later time points.	N/A

Table 1.5.2 Summary of molecular studies that used PDR

1.5.3. Hypericin as a novel photosensitizer

Hypericin, an extract from St Johns Wort, was discovered in animals that grazed on it and developed photodermatitis, erythema and oedema illustrating photosensitization (Kiesslich *et al.*, 2006). Hypericin is a second generation PS and has many attributes that make it a potent photosensitizing compound. Among others, it has low dark cytotoxicity, high quantum yield, no dark mutagenicity or carcinogenicity and a higher clearance rate from the body compared to other PS (Chen *et al.*, 2001; Kiesslich *et al.*, 2006; Kocanová *et al.*, 2003; Krammer & Verwanger, 2012; O'Connor *et al.*, 2009). Its mode of action is similar to that of ALA-PDR where upon light activation with specific wavelengths, according to its absorption coefficient, it generates reactive oxygen species with its interaction with oxygen (Agostinis *et al.*, 2002; Kiesslich *et al.*, 2006). Hypericin's maximum absorption peaks are 300nm-360nm (UVA) and 530-600nm (yellow light) (Figure 1.5.2). Yellow light, therefore, maximally activates hypericin but this PS has an added advantage in PDR as it could be activated by a variety of light sources. When it is irradiated, both Type I and Type II photochemical reactions takes place generating both singlet oxygen and superoxide anion amongst others (Figure 1.5.1) (Lubart *et al.*, 2007). It is generally accepted that the Type II reactions generating singlet oxygen play the main role in the biological photoactivity of hypericin (Agostinis *et al.*, 2011; Kiesslich *et al.*, 2006; Kocanova *et al.*, 2006).

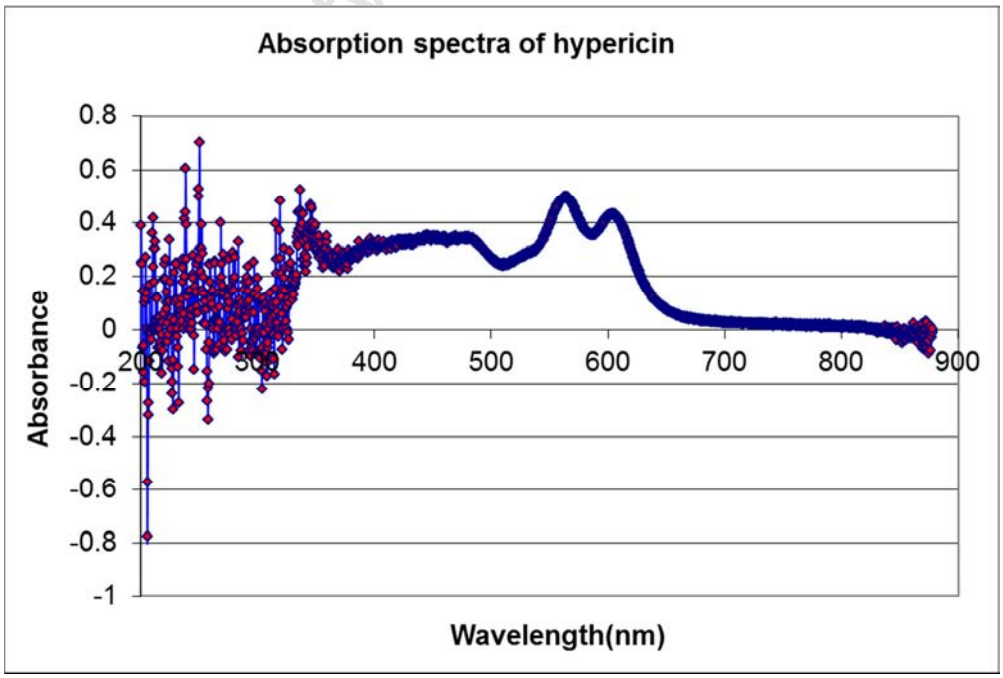

Figure 1.5.2 Absorption Spectrum of hypericin.

Hypericin is lipophilic and thus easily enters cells through the cell membrane. It has also been shown to bind to various serum proteins, such as human serum albumin (HSA) and low-density lipoprotein (LDL) in the blood. Bound to these proteins, hypericin enters the cells through different mechanisms and not solely through passive diffusion (Buriankova *et al.*, 2011; Das *et al.*, 1999; Gbur *et al.*, 2009; Huntosova *et al.*, 2010; Kascakova *et al.*, 2005; Mukherjee *et al.*, 2008; Roelants *et al.*, 2011; Siboni *et al.*, 2002; Uzdensky *et al.*, 2001). Its subcellular localization depends on how it enters the cells and this seems to determine its path and final location.

Hypericin has been shown to localise with four major cellular organelles: ER, Golgi apparatus, mitochondria and lysosomes. Each organelle provides a specific and vital function within the cell. The ER is involved in lipid and protein synthesis, protein secretion, metabolism of carbohydrates and detoxification of drugs (Campbell & Reece, 2002). The proteins are modified in the ER and leave in transport vesicles to the Golgi apparatus. The Golgi apparatus is involved in sorting, storing and moving these proteins to different locations and out of the cell (Campbell & Reece, 2002). The mitochondria are the power houses in cell, generating the energy in the form of adenosine triphosphate (ATP) (Campbell & Reece, 2002). Lysosomes are double membrane bound organelles containing lytic enzymes which breakdown waste materials and cellular debris. They are part of the endosomal pathway where an endosome will bud off from the Golgi apparatus and fuse with hydrolytic enzymes to create a lysosome (Campbell & Reece, 2002).

Table 1.5.3 indicates a great disparity in the literature regarding hypericin's end location in the cell i.e. ER, Golgi apparatus, mitochondria or lysosome. This table attempts to summarise the intracellular location of hypericin and clearly shows that hypericin appears in the perinuclear region in most cell types and that this location is independent of hypericin concentration and incubation times. However, the exact location of hypericin in specific organelles differed in most reports. From this data, it appears that hypericin has the ability to localise to all the major organelles i.e. ER, Golgi apparatus, mitochondria and lysosome. Moreover, culture characteristics affect its location, this includes: cell type, supplementation of medium, incubation time and time of visualization (Siboni *et al.*, 2002; Theodossiou *et al.*, 2009).

Hypericin has been used in the clinical treatment of a number of dermatological conditions such as acne, psoriasis and actinic keratoses (Hager *et al.*, 2009; Kascakova *et al.*, 2008; Najafizadeh *et al.*, 2012; Oztürk *et al.*, 2007). In addition, it has been used to treat basal cell and squamous cell carcinomas, and other cancers of the bladder, brain and endobronchial

tract (Bublik *et al.*, 2006; Chung *et al.*, 2000; Couldwell *et al.*, 2011; Davids *et al.*, 2009; Du *et al.*, 2007; D'Hallewin *et al.*, 2002; Thong *et al.*, 2006). While not used for melanoma treatment clinically, its efficacy *in vitro* has shown great promise (Davids *et al.*, 2008, 2009). Hypericin is a good candidate PS as it was noted that the occurrence of side effects in patients after treatment was low, and if it did occur, it was resolved within 24 hours (Kacerovská *et al.*, 2008).

Although hypericin's use in PDR has not been reported before, it shows promise due to its success in treating other dermatological conditions. The high quantum yield indicates minimal energy is needed to activate hypericin to generate ROS. This bypasses the use of high energy and power densities that cause phototoxic reactions.

Author	Cell Type	Hypericin Location	Hypericin Concentration	Hypericin incubation time	Organelle Marker	Organelle	Colocalization with Hypericin	Special circumstances
(Sattler *et al.*, 1997)	Caco 2 cells	Cellular & nuclear membranes	0.2-0.7mM	1h				
(Vandenbogaerde *et al.*, 1998)	A431 and HeLa cells	Perinuclear	71nM	24h				Suggest Golgi apparatus or ER localization
(English *et al.*, 1999)	Neurons from El 8 Sprague-Dawley rats	Membranes within the cell	10µg/ml	30min	NBD C6 ceramide	Golgi apparatus	Partial colocalization	
(Delaey *et al.*, 2001)	HeLa	Perinuclear	1µM					Suggest Golgi apparatus and ER localization
(Uzdensky *et al.*, 2001)	Adenocarcinoma WiDr, Carcinoma NHIK 3025 and Glioblastoma D54Mg cells	Perinuclear	1µM	1h	LysoTracker Blue DND-22	Lysosome	No colocalization	No hypericin in the plasma membranes
					ERTracker Blue-White DPX	ER	Partial colocalization	
					MitoTracker Green FM	Mitochondria	No colocalization	
(Agostinis *et al.*, 2002)	HeLa	Perinuclear	0.5µM	16h	MitoTracker Green FM	Mitochondria	No colocalization	
(Ali & Olivo, 2002)	CNE2 & TW0-1 nasopharyngeal carcinoma cells	Cytoplasmic staining, perinuclear	1.25µM	2h	MitoTracker Green	Mitochondria	Significant colocalization	
					LysoTracker Green DND-22	Lysosome	Significant colocalization	
(Siboni *et al.*, 2002)	murine colon carcinoma CT26 cells	Perinuclear	1µM	20h	LysoSensor	Lysosome	Significant colocalization	Serum supplemented medium
		Perinuclear	1µM	1h	$DiOC_5$	ER	Significant colocalization	Serum free medium
(Theodossiou *et al.*, 2004)	PAM 212 murine keratinocytes	Perinuclear	5µM	3h	LysoTracker Green DND-26	Lysosome	Significant colocalization	Serum supplemented medium

Author	Cell Type	Hypericin Location	Hypericin Concentration	Hypericin incubation time	Organelle Marker	Organelle	Colocalization with Hypericin	Special circumstances
					ER-Tracker Blue-White DPX	ER	Significant colocalization	
					LysoTracker Green DND-26	Lysosome	Significant colocalization	
(Buytaert *et al.*, 2006)	HeLa, T24 cells and MEFs	Perinuclear	0.5µM	16h	Rhodamine 123	Mitochondria	Little colocalization	
(Bublik *et al.*, 2006)	Squamous Cell Carcinomas	Perinuclear	N/A	1h				
(Pfaffel-Schubart *et al.*, 2006)	U373 human glioblastoma cells	Perinuclear	1µM	1h	MitoTracker Green	Mitochondria	Partial colocalization	Serum supplemented medium
(Kascakova *et al.*, 2008)	U-87 MG Cells	Perinuclear	30nM	5h	LysoTracker Green	Lysosome	Significant colocalization	Medium with/without serum or LDL supplementation
	Keratinocytes, UCT Mel-3 melanoma cells	Perinuclear	1µM	4h	MitoTracker Green	Mitochondria	Significant Colocalization	
(Davids *et al.*, 2008)	Melanocytes, UCT Mel-1 melanomas cells	Diffuse staining in the cytoplasm	1µM	4h	MitoTracker Green	Mitochondria	No Colocalization	Suggests Golgi apparatus and ER
					MitoTracker™	Mitochondria	Significant Colocalization	Colocalization diminished at 5h
					LysoTracker™	Lysosome	Partial colocalization	
					ER tracker™	ER	Significant Colocalization	Slightly decreased colocalization at 5h
(Galanou *et al.*, 2008)	DU145 cells human prostate carcinoma cells	Perinuclear	5µM	1h	Bodipy™ FL C_5-ceramide	Golgi Apparatus	Significant Colocalization	Significant at 5h
(Ritz *et al.*, 2008)	U373 MG glioblastoma	Perinuclear	1µM	2h	Lectin GS-II from	Golgi apparatus	Partial	
					ER Tracker Green	ER	Significant colocalization	
(Sanovic *et al.*, 2009)	WI38 human lung fibroblasts	Perinuclear	200ng/ml	16h				Suggest Golgi apparatus and ER
(Huntosova *et al.*, 2010)	U87 glioma cells	Perinuclear	0.4µM	1h<				Suggest Golgi apparatus and ER

Author	Cell Type	Hypericin Location	Hypericin Concentration	Hypericin incubation time	Organelle Marker	Organelle	Colocalization with Hypericin	Special circumstances
		Perinuclear and small areas in the nucleus						Fixed cells with hypericin exposure in fixative
		Cytoplasm equally stained						Fixed cells with hypericin exposure in serum supplemented medium
		Intensity decreased from the plasma membrane to nucleus						Fixed cells with hypericin exposure in medium without serum
(Vuong *et al.*, 2011)	HeLa		2μM	30min				

Table 1.5.3 A summary of subcellular localization of hypericin within different organelles. Each studies shows different hypericin concentrations, incubation times, culture conditions and cell types used. ($DiOC_5$: 3,3-dipentyloxacarbo- cyanine iodide; ER: endoplasmic reticulum)

1.6. Project Objective

The overall objective of this project was to develop and optimise an *in vitro* PDR protocol using the PS hypericin, activated by various wavelengths of light, on primary human dermal fibroblasts.

Our laboratory and others have shown that hypericin is a good potential candidate for PDR as it has shown positive results in treating non-melanoma skin cancer, actinic keratosis, acne and psoriasis (Alecu *et al.*, 1998; Chung *et al.*, 1994, 2000; Najafizadeh *et al.*, 2012). As not much is known about the cellular consequences of PDR on skin cells, we investigated its hypericin-mediated effects on primary human fibroblasts.

Aim 1

PDR protocols were established using various hypericin concentrations activated by three different wavelengths of light of varying energy and power density.

Aim 2

The effect of PDR on growth, migration and ROS production in primary human dermal fibroblasts was determined.

Aim 3

The subcellular location of hypericin within primary human dermal fibroblasts was determined, along with its association with different cellular organelles.

2. Chapter 2: Materials and Methods

2.1. Tissue Culture - General maintenance

Primary human dermal fibroblasts were donated by Dr Ingrid Baumgarten (Dept of Chemical Pathology, University of Cape Town) and cultured in our laboratory by Toni Wiggins under ethical approval REC REF: 493/2009. Cells were cultured in complete medium which comprised: Dulbecco's Modified Eagle Medium (DMEM) (Highveld Biological Pty, Ltd., Johannesburg, South Africa) and supplemented with 10%(v/v) heat inactivated fetal bovine serum (Highveld Biological Pty, Ltd., Johannesburg, South Africa), 100U/ml Penicillin (Sigma, Schelldorf, Germany) and 100µg/ml of Streptomycin (Sigma, Schelldorf, Germany) (Appendix A for individual solutions). Cells were kept in a humidified incubator (Sanyo MCO-175M, Sanyo Electric Co., Osaka, Japan) with 5% Carbon Dioxide (CO_2) atmosphere at 37°C.

Fibroblasts were passaged by washing with phosphate buffered saline (PBS) solution before being incubated with 0.05% trypsin: 0.02% ethylenediaminetetraacetic acid (EDTA) solution for 4 minutes at 37°C. Cells passaged 10 times or less were used. Cells prepared for experiments were manually counted using a haemocytometer (Neubauer improved bright-line, Marienfeld, Lauda-Konigshofen, Germany). Cells were examined regularly using a phase contrast microscope (Olympus Microscope Model CK2, Olympus Microscopes Tokyo, Japan) and photomicrographs were taken using the coupled camera system (Canon camera, Power shot S50, Canon Tokyo, Japan) before and after treatment to determine any morphological changes.

Cells were tested regularly for the presence of mycoplasma using a Hoechst dye protocol (see Appendix A.1.2). All cell culture involving hypericin, cell viability and ROS assay reagents were performed under subdued light conditions.

Hypericin powder (Sigma Aldrich, Schelldorf, Germany) was diluted in Dimethyl Sulfoxide (DMSO) to a concentration of 2mM in light subdued conditions and aliquots were stored at -80ºC. Twenty microliter aliquots in use were kept at -20ºC.

2.2. Uptake Assay

The uptake assay was used to determine the time for maximum hypericin uptake into the cells. The hypericin concentrations were chosen from the literature as they have been shown

to be non-cytotoxic in other cell types (Davids *et al.*, 2008). These concentrations were: 0.25μM, 0.5μM, 1μM hypericin (in complete medium).

Similar to previous protocols (Berlanda *et al.*, 2010), cells were seeded at a density of $3x10^4$ fibroblasts in a 35mm tissue culture dish. The following day, the medium was removed and the 3 different hypericin concentrations were added to different dishes. Hypericin was incubated for 2, 4, 6, 10, 16 and 24h. At the end of the time periods, hypericin containing medium was removed and the cells were washed with ice-cold PBS and placed on ice. Each tissue culture dish had 40μl RIPA extraction buffer (Appendix A.4) added and the lysates collected with a rubber policeman. The lysates were centrifuged at 4°C for 20min at 12000rpm. The supernatants were divided for the determination of protein content using the BCA assay (Appendix A.2) and for the quantification of hypericin on a fluorimeter. Hypericin fluoresces in the red light spectrum, therefore, its concentration is relative to the level of fluorescence detected using the fluorimeter (Cary Eclipse Fluorimeter, Varian Inc., Palo Alto, California, United States of America) with the following settings: 488nm excitation (ex) and 608nm emission (em) wavelength. Hypericin content is represented as arbitrary fluorescent units (AFU) per microgram of protein and experiments were performed at least three times for all time points (n=3).

2.3. Irradiation Protocol

Three light sources were used:

I) Eight lamps in a transilluminator emitted light in the ultraviolet range (UVA) (320nm to 400nm: Peak ~365nm).

II) A DPSS solid state laser emitted continuous wavelength of light at 635nm.

III) A DPSS solid state laser emitted continuous wavelength of light at 561nm. Figure 2.3.1 shows the experimental setup for the 561nm DPSS laser in our laboratory.

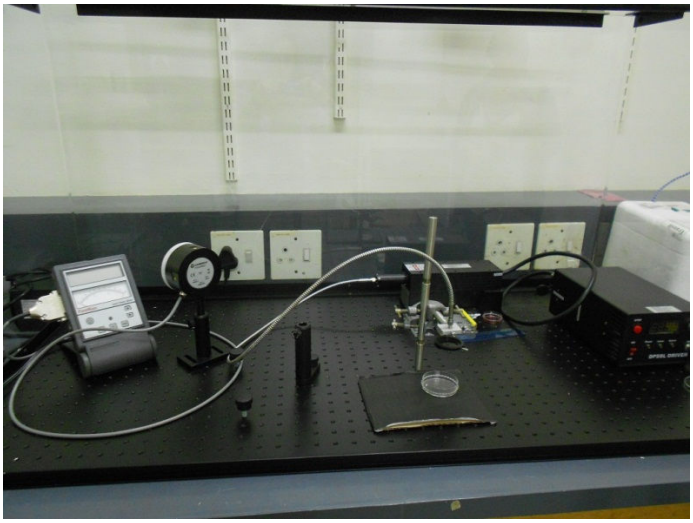

Figure 2.3.1 Setup for the DPSS 561nm laser

Before irradiation with any light source, the medium was removed from the dishes and washed with PBS. Fresh PBS was added to the cells before irradiation to prevent dehydration.

The energy density was generally determined from the literature (Table 1.5.1) with the power density limited due to practical constraints of the lasers. The following equation was used to determine the irradiation time:

$$Time = \frac{Dose\ (J/cm^2))}{Power\ Density\ (W/cm^2)}$$

Equation 1.4.1 Equation used to determine, energy and power density and exposure time.

2.4. Cell Viability Assay

Cell viability was assessed using the XTT cell proliferation kit II (Roche, Germany). This colorimetric assay is based on the conversion of yellow tetrazolium salt to orange formazan product by mitochondrial enzymes of metabolically active cells. The change in colour is determined on an ELISA plate reader (VERSAmax™ tuneable microplate reader, Molecular Devices, Sunnyvale, CA, USA; Software: Softmax Pro version 4.3.1) with an absorbance of 450nm.

Cells were seeded at a density of $3x10^4$ cells per well in 200µl of complete medium in a 96-well plate and left to adhere overnight. The following day the medium was replaced with the three hypericin concentrations (0.25µM, 0.5µM and 1µM) in complete medium, along with a vehicle (DMSO) containing complete medium or fresh medium for an untreated control, for 16h. After this time, the wells were washed with PBS then irradiated in 100µl PBS with

the various light sources using several energy and power densities to determine a non-cytotoxic irradiation protocol. Table 2.4.1 presents the various irradiation times and energy and power densities. One plate was used when irradiating with the 635nm DPSS laser and the UV transilluminator lamps. One side was irradiated and the opposite side was covered with foil and served as the sham or unirradiated control. It is important to note that when the 561nm DPSS laser was used, the unirradiated cells were seeded on a separate plate because, at high energy doses and power densities, the unirradiated control was affected by scattered light through the transparent plate. The unirradiated or sham controls would determine if hypericin on its own has any effect on primary human dermal fibroblasts.

	Diameter (cm)	Area (cm^2)	Dose (J/cm^2)	Power (mW)	Power Density (W/cm^2)	Time of Exposure (sec)	Assay
Yellow	0.5	0.20	0.1	2	0.0102	9.821	Cell Viability
Yellow	0.5	0.20	0.25	2.00	0.0102	24.554	Cell Viability
Yellow	0.5	0.20	0.50	2.00	0.0102	49.107	Cell Viability
Yellow/Red	0.5	0.20	1.00	10.00	0.0509	19.643	Cell Viability
Yellow/Red	0.5	0.20	2.50	10.00	0.0509	49.107	Cell Viability
Yellow/Red	0.5	0.20	5.00	10.00	0.0509	98.214	Cell Viability
Yellow	0.5	0.20	1.00	20.00	0.1018	9.821	Cell Viability/ROS
Yellow	0.5	0.20	2.50	20.00	0.1018	24.554	Cell Viability
Yellow	0.5	0.20	5.00	20.00	0.1018	49.107	Cell Viability
UVA	0.5	0.20	0.50				Cell Viability
UVA	0.5	0.20	1.00				Cell Viability/ROS
Yellow	1.5	1.77	1.00	179.00	0.1013	9.876	Growth Curve/ROS/Scratch
UVA	3.5	9.63	0.50				Growth Curve
Red	3.5	9.63	2.50	24.00	0.0025	1002.604	Growth Curve
Yellow	3.5	9.63	5.00	20	0.0020	240.625	Growth Curve

Table 2.4.1 Variables used in the different irradiation protocols for each wavelength of light. Yellow is light from the 561nm DPSS laser, Red is light from the 635nm laser and UVA is light from the transilluminator lamps. Diameters: 0.5cm = 96-well plate, 1.5cm = 24-well plate, 3.5cm = 6-well plates/35mm tissue culture dish.

Following irradiation, PBS was removed and 200µl of complete medium was added for a 24h recovery period. Four hours before the end of this recovery period the XTT solution (Roche, Germany) was prepared according to the manufacturer's instructions (Appendix A.6) and 50µl of the combined solution was added to all the wells in subdued light conditions. Twenty four hours after the irradiation, plates were analysed on an ELISA plate reader where the absorbance of XTT was determined at 450nm. The percentage of viable cells was established by normalization to the combined values of unirradiated, untreated and vehicle treated controls. Figure 2.4.1 is a schematic of the timeline for the cell viability assay.

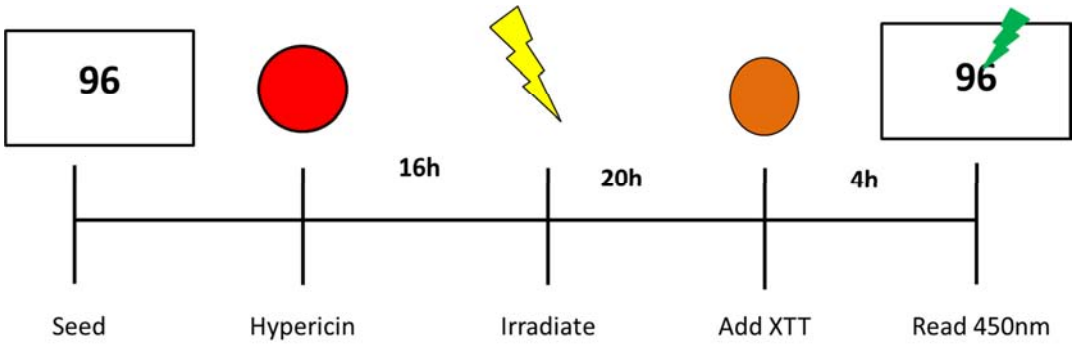

Figure 2.4.1 A timeline showing the protocol for the cell viability assay (96 = 96 well plate)

2.5. Growth Curve

Cells analysed to establish growth curves were seeded in either 35mm diameter dishes, 6-well plates or 24-well plates both at a density of $1x10^4$ cells per dish or well and allowed to adhere overnight. The following day hypericin in medium was added to those dishes to be treated with PDR. Table 2.5.1 summarises the hypericin concentrations used with each light source.

	Hypericin Concentration (μM)	Energy dose (J/cm^2)	Power Density (W/cm^2)
UVA lamps	0.25	0.5	
635nm DPSS Laser	0.5	2.5	0.0025
561nm DPSS Laser	0.25	1	0.102

Table 2.5.1 Summary of hypericin concentrations, energy doses and power densities

After 16h hypericin incubation, the cells were washed with PBS and 1ml or 0.5ml of PBS was added to the 35mm dish or 24-well plate well, respectively. The dishes were irradiated with the energy dose and power density indicated in Table 2.5.1

When the 561nm DPSS laser was used, the growth rate of cells treated with the laser beam and the vehicle (0.0125v/v% DMSO) alone was also determined. This was performed to see the effect of the laser alone on the cells.

Cells were counted using a haemocytometer (Neubauer improved bright-line, Marienfeld, Lauda-Konigshofen, Germany) 24h post-irradiation and every alternate day thereafter for 7 days. Medium was changed every 3 days in all the dishes or wells. Except with the 561nm DPSS laser where the medium was only changed once on day 3. Of note, the red and UVA light growth curves had 3 intra-experiments repeats but only one inter-experiment repeat due to limited access to these light sources.

2.6. Reactive Oxygen Species (ROS) Assay

2.6.1. FACS Method

Reactive oxygen species (ROS) were quantified using initially the non-fluorescent dye, 5(6)-Carboxy-2′,7′-dichlorofluorescein diacetate (DCF-DA) (Sigma-Aldrich, Schnelldorf, Germany), whereupon interaction with ROS, is converted to an oxidized state and fluoresces green. The fluorescence can be detected on a fluorescent activated cell sorter (FACS) using the 488nm argon laser.

One hundred thousand cells ($1x10^5$) were seeded into 35mm dishes. After 24h, the medium was replaced with the relevant hypericin concentration in complete medium for each light source. Cells to be treated with the UV transilluminator and yellow laser (561nm DPSS) were both incubated with 0.25µM hypericin for 16h. Following irradiation (Table 2.5.1), the medium was replaced with fresh medium that contained 40µM DCF-DA (Appendix A.7) for 30 minutes at 37°C in the incubator. It is important to note, for this method the power was at 20mW. This meant the power density was $0.002W/cm^2$. Following this, the cells were washed with PBS and collected by trypsinization. The cells were pelleted at 2500rpm at room temperature and rinsed in 1ml PBS and re-pelleted. Cells were re-suspended in in 500µl PBS, transferred to FACS tubes (BD Falcon tubes, BD Biosciences, Becton Dickinson International, Erembodegem, Belgium) and analysed on the FACS machine (FACS Calibur, Division of Immunology, UCT).

DCF-DA was detected in the FLH-1 channel with hypericin being detected in the FLH-3 channel and 10 000 events/cells were analysed. All data generated were analysed using CellQuestPro software (version 5.2.1, BD Biosciences, California, United States of America). Results are presented as a percentage of the control, which indicated basal levels of ROS. All samples were gated to only analyse live cell events in the population.

2.6.2. Fluorimeter Method

For a comparison between FACS analyses of ROS, a fluorimeter-based assay was developed. Ninety-six well white tissue culture plates (Greiner Bio-One, Frickenhausen, Germany) were seeded with $3x10^4$ cells per well, the same number used in the cell viability assay with the design setup in Figure 2.6.1. Cells were treated with either 0.25µM hypericin or 0.0125% DMSO for 16h and irradiated with the yellow laser ($1J/cm^2$, $100mW/cm^2$) or UVA ($1J/cm^2$). Following this, cells were incubated with 10µM DCF-DA for 30 minutes in the incubator at 37°C. After this, the cells were washed and 100µl PBS was added to each well. The plate was analysed on a fluorimeter at an excitation of 488nm and emission of 535nm. The blank for the experiment were the untreated cells, which had not been exposed

to DCF-DA. The results were normalized to the DCF-DA only treated cells. The following experimental setup was used:

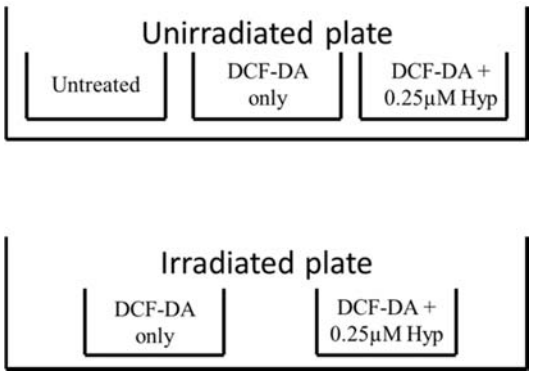

Figure 2.6.1 Experimental design for the two 96-well plates for the fluorimeter based assay where DCF-DA's fluorescence to determine ROS generated. Irradiated plate was either exposed to yellow laser light (1J/cm^2, 100mW/cm^2) or UVA (1J/cm^2) whereas the unirradiated plate was kept in the dark.

2.7. Scratch Assay

Figure 2.7.1 shows the experimental setup for the scratch assay. Two plates were used with one kept in the dark and the other irradiated with laser light. One hundred thousand cells were seeded in a 24-well tissue plate and allowed to adhere overnight. The following day the medium was replaced with 10ug/ml of mitomycin C in complete medium for 2-3h to halt proliferation of the dividing cells. The cells were thoroughly washed with PBS four times before complete medium was added. A scratch was made across the well with a pipette tip. Photographs of the scratch were taken immediately using a Zeiss Axiovert 200M fluorescent microscope (Carl Zeiss Microscopy GmbH, Germany).

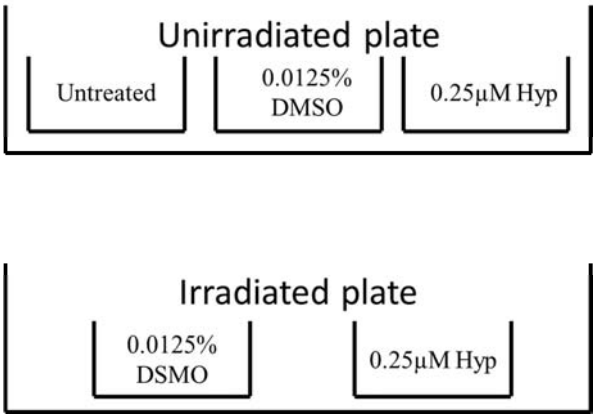

Figure 2.7.1 The experimental design for the two 24-well plates used in the scratch assay. One plate was irradiated with 1J/cm^2, 100mW/cm^2 yellow laser light and the other was kept in the dark.

Cells were exposed to either 0.25µM hypericin or 0.0125% (v/v) DMSO for 16h and thereafter irradiated with the same parameters as the yellow laser growth curve (1J/cm^2, 100mW/cm^2). Eight hours after irradiation with the laser, a total of 24h after making the scratch, photographs were taken to determine the decrease in the area of the scratch. The photographs were aligned in GIMP (GNU Image Manipulation Program, version 2.6.11) and the area was determined using the software programme Axiovision (Carl Zeiss MicroImaging GmbH, Germany, Version 4.8.2.0). The results are shown as a percentage of wound closure after 24h. Figure 2.7.2 is the timeline for this experiment.

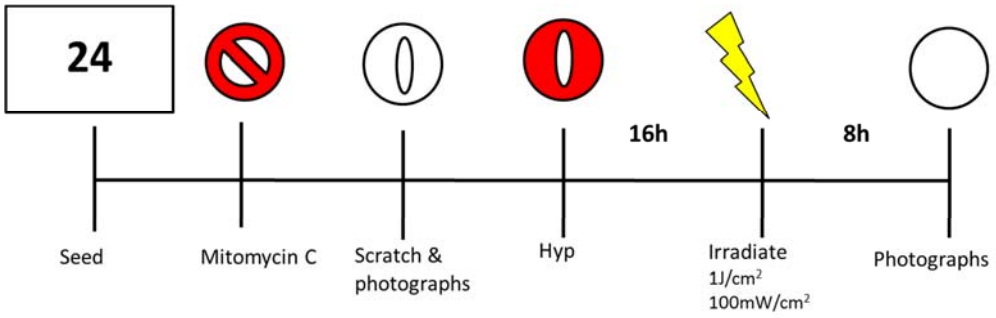

Figure 2.7.2 Timeline for the scratch assay (24 = 24 well-plate; Hyp = hypericin)

2.8. Subcellular Localization using Transfection

To determine the subcellular localization of hypericin, we used plasmids targeted to specific organelles expressing fluorescent proteins and used scanning confocal microscopy to visualize the fluorescence (Zeiss Axiovert 200M LSM 510 META Confocal microscope, Carl Zeiss Microscopy GmbH, Germany). The table below describes the targeted organelles, parent plasmid, gene used to specify each organelle and the colour of the fluorescent protein tag (Table 2.8.1). Plasmid maps and references are in the Appendix A.9.

Organelle	Plasmid	Targeting sequence/Gene	Fluorescent Protein
ER	pEYFP	Calreticulin	Yellow
Golgi apparatus	pEGFP-C1	Rab7WT	Green
Mitochondria	pEGFP-N1	OTC	Green

Table 2.8.1 Plasmids used in the subcellular localization experiments indicating: organelle targeted, parent plasmid, gene inserted in plasmid and the colour of the fluorescent protein.

Transfections were performed by seeding cells (1x10^5 cells) to obtain approximately 70% confluency on 22mm^2 glass coverslips placed inside 35mm diameter tissue culture dishes. The Jet Pei transfection reagent (PolyPlus Transfections, New York, USA) was used for the transfections and the protocol followed the manufacturer's instructions. Briefly, for each

sample, 0.5µg plasmid DNA was added to 50µl of 150mM NaCl. The mixture was vortexed and centrifuged. In a separate centrifuge tube, 2µl of Jet Pei transfection reagent was added to 50µl of 150mM NaCl, vortexed and centrifuged. The solution containing the plasmid was added to the transfection reagent solution and gently triturated. The combined solution was left at room temperature for 15-20 minutes and then added to the dishes, without changing the complete medium, in a drop-wise manner.

The dishes were left in the incubator at 37°C for 24h after which 0.25µM hypericin in complete medium was replaced in specified dishes while the control dishes were left. All the dishes were left for a further 16h. At the termination of the experiment all the dishes were stained with 5µg/ml Hoechst in medium for 30 minutes at 37°C (Appendix A1.1). The Hoechst was removed and replaced with fresh medium until viewing.

Immediately before viewing the dishes were taken out of the incubator and the coverslips were mounted onto glass slides in medium without fetal calf serum and viewed live on the confocal microscope. The blue argon 488nm laser on the confocal microscope visualized the GFP and YFP localised in the organelles. The laser used to visualise the hypericin in the cell was the same type of laser used during the other experiments (DPSS 561nm laser). We, therefore, have the ability to activate the cells in a similar way and see their reaction immediately after irradiation. However, the energy and power density will not be same as the cell viability assay as the power needed to detect hypericin's fluorescence is higher as for visualisation on the microscope. The two-photon infra-red laser was used to detect the Hoechst localized in the nucleus. The order of detecting each label using the individual lasers was kept the same so we could visualize the organelles before hypericin activation (GFP/YFP<hypericin<nucleus). To determine colocalization in the cells, profiles and scatterplots were used to interpret the images using the LSM and Zen software (2009, Carl Zeiss Microscopy GmbH, Germany)

2.9. Statistical Analyses

The statistical program Graphpad Prism (Version 5, Graphpad Software Inc., California, United States of America) was used for all analysis. Differences in values were stated as significant if the p-value was less than 0.05.

3. Chapter 3: Results

3.1. Cellular Uptake of Hypericin

To determine hypericin's maximum cellular uptake, primary human fibroblasts were incubated with three different hypericin concentrations (0.25µM, 0.5µM, 1µM) over a time course (2.5h-24h). After each time period, cell lysates were collected for analysis. The total cellular protein concentration was quantified using a BCA assay (Section A.2) and the fluorescence of hypericin was determined on a fluorimeter with the settings 488nm for excitation and 608nm for emission. Hypericin is an autofluorescent compound, thus the amount of fluorescence is related to its concentration within a cell (Kascakova *et al.*, 2008; Sattler *et al.*, 1997; Theodossiou *et al.*, 2004). The results are presented as Arbitrary Fluorescent Units per microgram of protein (AFU/µg of protein).

The three hypericin concentrations (0.25µM, 0.5µM, 1µM) were shown to be non-toxic in other cell types. Over the time course of the experiment (2.5-24h), cellular uptake displayed a time-dependent increase in fluorescence with all three concentrations peaking between 10-16h (Figure 3.1.1).

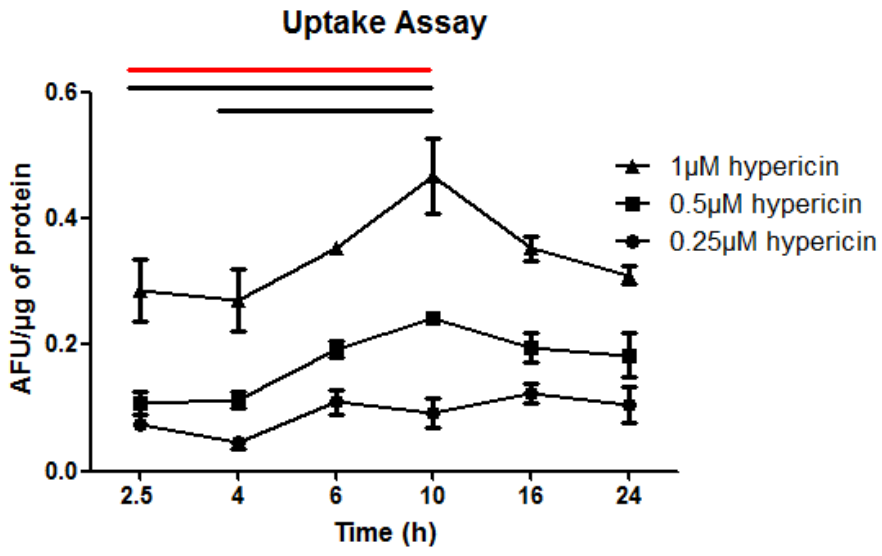

Figure 3.1.1 The cellular uptake of hypericin over 2.5-24h for three hypericin concentrations (0.25µM, 0.5µM and 1µM) in primary human dermal fibroblasts. Results measured in AFU per µg of protein and represented as mean±SEM (n=3). Solid black lines signifies p<0.05 for 0.5µM time points and the solid red line signifies p<0.05 for 1µM times points. Significance calculated using ANOVA with the Bonferroni post-test.

The lowest hypericin concentration (0.25µM) showed a gradual increasing trend with peak fluorescence at 16h (Figure 3.1.1). There was no significant difference between any of the

time points ($p>0.05$). The 0.5µM hypericin concentration peaked at 10h and showed a significant increase from the two earlier time points (2.5h and 4h) with no significant difference displayed between 10h and later time points (16h and 24h). In contrast, the highest hypericin concentration (1µM) used, showed a significant increase between 4 and 10h. Similarly to the 0.5µM hypericin concentration, the 1µM hypericin showed the greatest AFU/µg of protein at 10h with no difference between this peak and later time points. In comparing the three concentrations' value to one another, the 1µM concentration had a highest AFU/µg of protein values with 0.5µM being second and 0.25µM having the lowest values at all time points (Figure 3.1.1). These results were semi-quantitatively confirmed using fluorescent microscopy (see images Figure A.8.1)

In experiments that followed, 16h exposure was chosen as it had the highest AFU/µg of protein values for 0.25µM hypericin. In addition, there was no significant difference between 10h and 16 h for both 0.5µM and 1µM hypericin. This incubation time is in line with the literature where 16h has the greatest uptake of hypericin in other cell types such as A431 human epidermoid carcinoma, T24, HeLa cells and mouse embryonic fibroblasts (Berlanda *et al.*, 2010; Hendrickx *et al.*, 2005).

3.2. Cell Viability of Fibroblasts after PDR Treatment

PDR involves the uptake of the PS and subsequent irradiation of the cells with an activating wavelength of light. The variables in the irradiation protocol, such as energy, power density and irradiation time, are important to consider for the best possible outcome for this therapy. To test this, a cell viability assay was performed using three light sources to determine an irradiation protocol that was non-cytotoxic with 3 hypericin concentrations. The assay used tetrazolium salt which is indicative of mitochondrial metabolic function and correlates to cell viability. As this therapy will be used for clinical applications in skin rejuvenation, cytotoxic reactions are not desirable and must be avoided.

Two different types of light sources, lamps and lasers, were used to activate the three hypericin concentrations (0.25µM, 0.5µM and 1µM) used in the uptake assay. A bank of eight lamps in a transilluminator delivered light in the UVA range (320nm-400nm) with a peak output of 365nm. Two solid state DPSS lasers emitted continuous-wave, coherent light at 632nm (red) and 561nm (yellow). The 561nm laser (now referred to as the yellow laser) and UVA lamps were chosen as these wavelength were shown to be maximally absorbed by hypericin according to its absorbance spectrum (See Figure 1.5.2). Light from the 632nm laser (now referred to as the red laser) is approximately one third as effectively absorbed by hypericin but this wavelength is often used in dermatology to treat skin conditions and is

therefore readily available in dermatological clinics (Dierickx & Anderson, 2005; Peplow, Chung, & Baxter, 2012a)

Energy and power density refer to energy delivered and its rate within a certain area, respectively. The energy density is most often reported in the literature as a defining variable for the irradiation protocol in previous PDR studies (Table 1.5.1). Reports ranging from photorejuvenation, PDT and PDR trials were used to determine a range of energy densities that would not be detrimental to cell survival or demonstrate skin phototoxicity. Low level energy and power densities were chosen as they have been shown to be stimulatory to fibroblasts (Lubart *et al.*, 2005). Our overall aim was to determine a protocol where minimal energy was used to activate hypericin to prevent phototoxic reactions occurring during PDR. However, the energy must still be at a level where ROS is produced to be stimulatory.

3.2.1. Red (635nm) Laser

Red light is able to penetrate deep into the dermis due to its long wavelength (Agostinis *et al.*, 2011; Peng *et al.*, 2008). Although red light does not activate hypericin to the same extent as UVA and yellow light, it may be beneficial due to its penetration into the skin.

Cells were exposed to the three hypericin concentrations (0.25μM, 0.5μM and 1μM) for 16h and irradiated with three different energy densities at one power density. The lowest energy density, 1J/cm^2, displayed no difference in cell viability compared to the control (Figure 3.2.1). In contrast, 2.5J/cm^2 displayed a significant increase in cell viability of cells exposed to 0.25μM (111.7±9.95%) and 0.5μM (117.5±8.49%) hypericin. Interestingly, 5J/cm^2 showed no significant change at any of the hypericin concentrations (See Figure 3.2.1). Based on these results, 2.5J/cm^2 red laser light seemed to be the threshold amount for cell stimulation using the red laser while higher energy density led to no change in cell viability.

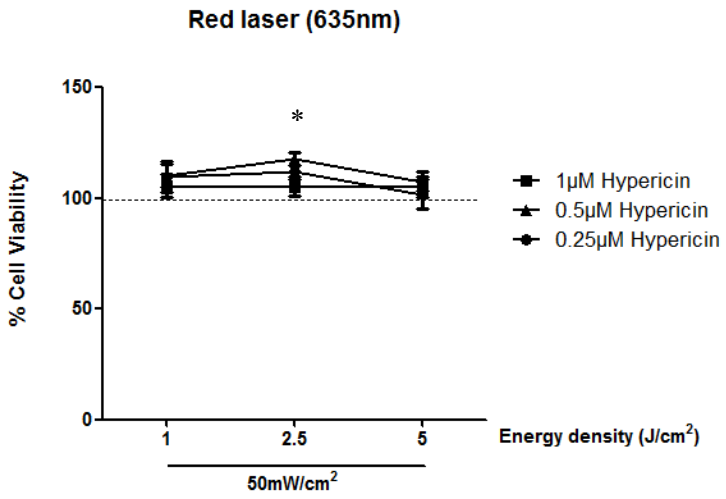

Figure 3.2.1 The percentage of viable cells 24h after PDR treatment with 3 hypericin concentrations activated by red laser light using 3 different energy densities. Results were normalised to a 100% against the dark control and represented as mean±SEM (n=3). * represent p values <0.05 for 0.5μM hypericin using the student's t-test to the unirradiated control.

3.2.2. UV transilluminator

UVA light was investigated not only because of its high absorbance coefficient with hypericin but through its ability to penetrate the dermis (Figure 1.5.2) (Peng *et al.*, 2008). A drawback of UVA is its propensity to generate high ROS levels. This led us to use a dose of 1J/cm^2 or less as higher energy densities may generate adverse side effects. Twenty four hours after hypericin activation with 0.5J/cm^2 UVA light, results showed a significant decrease in cell viability at 1μM hypericin (Figure 3.2.2). Interestingly, there was a slight increase (112.4±25.12%) in cell viability at the lower hypericin concentration (0.25μM) when irradiated with 1J/cm^2 (Figure 3.2.2). Conversely, there was a drastic decrease in cell viability when 1μM was irradiated with 1J/cm^2 (Figure 3.2.2). Interestingly, previous work done in our group showed that 1μM hypericin with 1J/cm^2 was not cytotoxic in melanoma cells. This indicates that fibroblasts are more sensitive to UVA activated hypericin compared to melanoma cells which indicate a possible cell type dependency with this therapy.

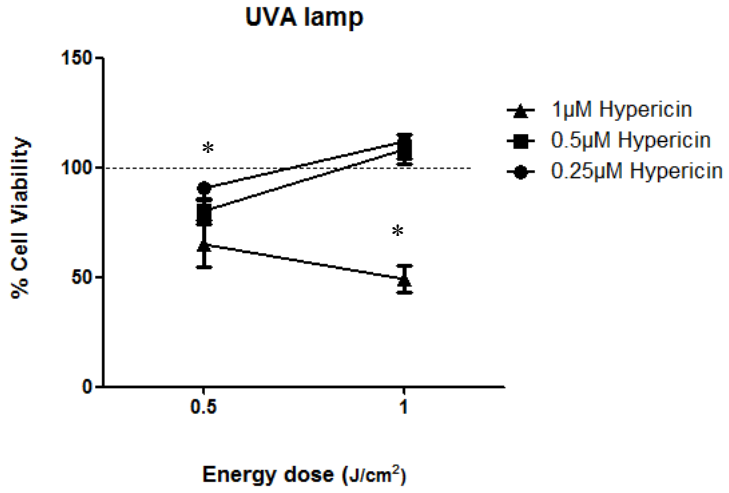

Figure 3.2.2 The percentage of viable cells 24h after PDR treatment with 3 hypericin concentrations activate by UVA light using 2 different energy densities. Results were normalised to a 100% against the control and represented as mean±SEM (n=3). * represent p-values <0.05 for 1µM hypericin using the student's t-test to the unirradiated control.

One limitation in using the UVA transilluminator was that only energy density was available. This meant the power or power density could not be fully investigate, thus, limiting the use of UVA as an activating light source in our PDR protocol. A laser can overcome this as power is used to determine the energy density through the time of exposure (Equation 1.4.1). We, thus, investigated the effect of varying, not only the energy density, but also the power density using the yellow laser.

3.2.3. Yellow (561nm) Laser

Due to the optimal spectral characteristics of hypericin where 563nm light is maximally absorbed, yellow light (561nm) was used. In contrast to UVA and red light, most of this wavelength of light is captured by hypericin. This implies that less energy could be used to result in the same downstream effects, i.e. ROS generation, compared to other wavelengths. It follows that less energy, power and exposure time would most likely negate side-effects caused by overexposure to light, such as erythema and oedema.

Following the data gathered from the red laser and UV transilluminator, a range of energy density from 0.1 J/cm^2 to 5J/cm^2, with associated power densities, were tested. The results show a clear increase in cell viability at the lower energy densities (Figure 3.2.3). As the energy and power increased, there was both a hypericin- and energy dependent decrease in cell viability (Figure 3.2.3). Similarly, to the red light, there is a threshold point where the PDR treatment changed from being beneficial and having a positive effect on the cell to one where it was cytotoxic. This tipping point occurs at the higher hypericin concentration (0.5µM and 1µM) and energy densities above 2.5J/cm^2.

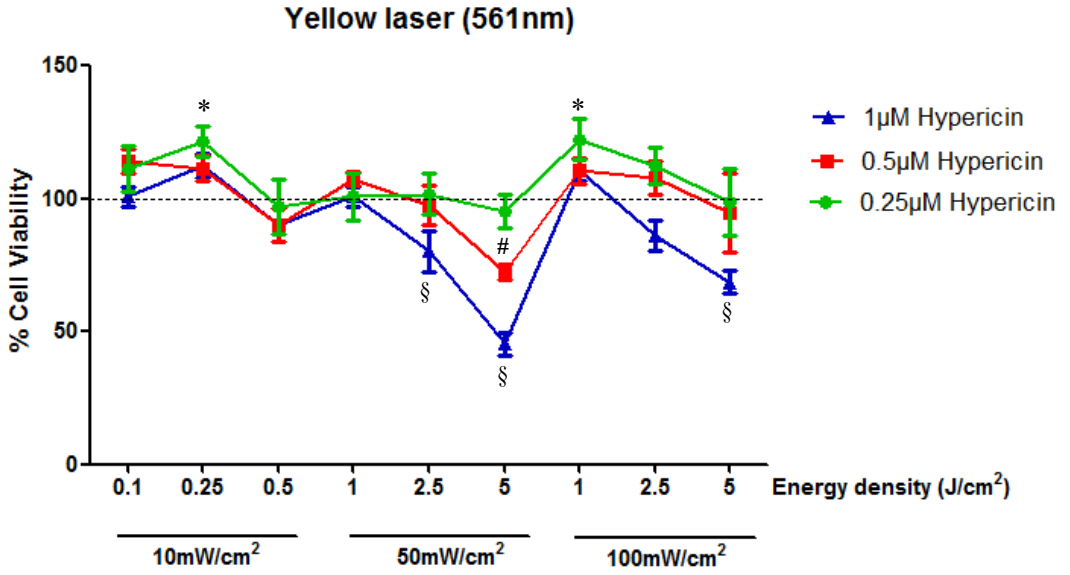

Figure 3.2.3 The percentage of viable cells 24h after PDR treatment with 3 hypericin concentrations activated by yellow laser light using several different energy and power densities. Results were normalised to a 100% against the control and represented as mean±SEM (n=3). * represents p-value<0.05 for 0.25μM hypericin, # represents p-value<0.05 for 0.5μM hypericin, § represents p-value <0.05 for 1μM hypericin using the student's t-test to the unirradiated control.

It appears the low energy density within each power density showed an increase in viability whereas the higher energy results in a decrease. The most drastic reduction was observed with 5J/cm^2 (50mW/cm^2) of light and 1μM hypericin (45.36±12.4%), resulting in a major loss of viable cells. In contrast, the 100mW/cm^2 power density, with its associated energy densities, did not result in as drastic a decrease compared to those using 50mW/cm^2. This could be explained by the length of time of irradiation being twice as long for 50mW/cm^2 compared to the 100mW/cm^2 for the same energy density. This arises from the inverse relationship between power and time (Equation 1.4.1) therefore by doubling the power from 50 to 100mW/cm^2, the time would be halved for the same energy. The extended time might have negative effects of excessive heating or prolonged activation of hypericin thereby generating overwhelming amounts of ROS.

The increase in cell viability was seen constantly with 0.25μM hypericin and low energy densities. Interestingly, both 10 and 100mW/cm^2 had an increase of 20% in cell viability (Figure 3.2.3). Noteworthy, is that an increase in this assay could indicate an increased cell number or mitochondrial function as compared to the control. The therapy could, therefore, causes an increase in proliferation or activation of cell metabolism through mitochondrial stimulation. To investigate the increase seen in cell viability and its relation to the proliferation rate, growth curves were performed for each light source.

3.3. Effect of PDR on the Growth of Fibroblasts

The growth curves were conducted over seven days to determine PDR's effect on cell proliferation. Similarly to the cell viability assay, the effect of hypericin activation with 3 different wavelengths of light on growth was assessed.

3.3.1. Red (635nm) Laser

Fibroblasts were seeded into 6-well plates and were either treated with 0.5μM hypericin for 16h or left untreated. The hypericin treated cells were washed and irradiated with 2.5J/cm^2 (2.5mW/cm^2) of red laser light. Three wells are counted on the first day after hypericin activation and every alternate day over the 7 day period. The results of each day were standardised to the average cell count 24h post-irradiation and represented as a fold increase. The proliferation rates of both untreated (no hypericin or light) and PDR treated cells showed an exponential increase 3 days after PDR treatment (Table 3.3.1 and Figure 3.3.1). Red light from any light source has been shown to stimulate fibroblasts which may explain the slight increase in proliferation of the treated cells compared to the control cells (Figure 3.3.1) (Peplow, Chung, & Baxter, 2012a).

	Control	Red laser light and hypericin
	Mean±SD	Mean±SD
1	1.0±0.3	1.0±0.2
3	1.1±0.5	1.2±0.4
5	4.7±1.8	4.5±1.3
7	10.4±3.9	13.0±3.4

Table 3.3.1 Fold increase of cell number: after PDR treatment using 2.5J/cm^2 (2.5mW/cm^2) red light to activate 0.5μM hypericin and control cells. SD – standard deviation.

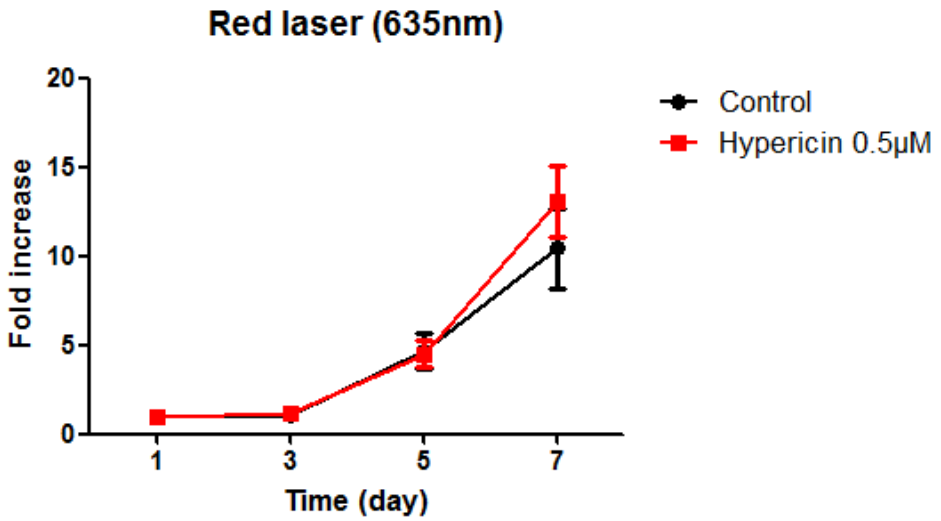

Figure 3.3.1 A growth curve of primary human fibroblasts over 7 days. Solid red line represents cell after PDR treatment using 0.5µM hypericin and 2.5J/cm^2 (2.5mW/cm^2) red laser light. The solid black line represents control cells. The results are presented as mean ±SEM (n=1)

3.3.2. UV transilluminator

The experiments using the UVA transilluminator as the activating light source followed the same rationale as the red laser (Section 2.5). All hypericin treated dishes were placed in the transilluminator and simultaneously irradiated with 0.5J/cm^2. Results showed no significant difference between the PDR treated and untreated control cells. The treated cells showed a slightly slower proliferation rate (Table 3.3.2) compared to the untreated cells over a period of 7 days (Figure 3.3.2). UVA light on its own may cause a lower proliferation rate. This is due to this wavelength's ability to generate ROS. The combined effect of UVA and PDR in generating ROS appears, therefore, may cause a transient retardation in the proliferation rate of fibroblasts.

	Control	UVA light and hypericin
	Mean±SD	Mean±SD
1	1.0±0.4	1.0±0.1
3	2.4±0.4	1.6±0.2
5	4.6±0.6	3.8±1.2
7	7.9±2.1	6.1±0.6

Table 3.3.2 Fold increase of cell number: after PDR treatment using 0.5J/cm^2 UVA light to activate 0.25µM hypericin and control cells. SD – standard deviation.

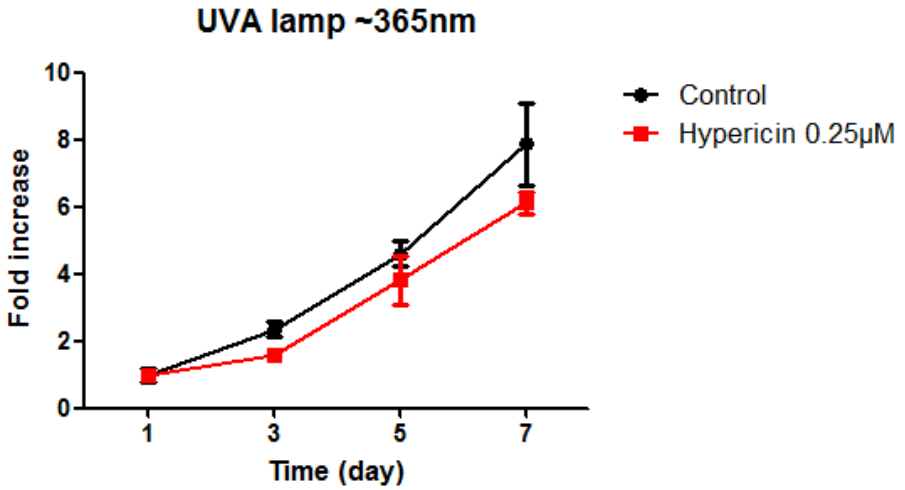

Figure 3.3.2 A growth curve of primary human fibroblasts over 7 days. Solid line represents cell after PDR treatment with 0.25µM hypericin and 0.5J/cm^2 UVA. The solid black line represents control cells. The results are presented as fold increase after day 1. Data represented as mean±SEM. (n=1)

3.3.3. Yellow (561nm) Laser

To determine the effect of yellow laser-activated hypericin on the growth rate of fibroblast, cells were firstly seeded into 24-well plates. The smaller diameter meant that the same power density as the cell viability assays was used. This required increasing the power output of the laser itself (see Table 2.4.1). Interestingly, there was no significant difference between the irradiated cells only and the PDR-treated cells (Figure 3.3.3). However, similar to the PDR treated cell using UVA, a slight decrease in the proliferation rate of the irradiated and PDR treated cells compared to the control cells (Figure 3.3.3).

	Control	Yellow laser light	Yellow laser light and hypericin
Day	Mean±SD	Mean±SD	Mean±SD
1	1.0±0.2	1.0±0.2	1.0±0.2
3	2.3±0.7	2.2±0.7	2.2±1.0
5	3.5±0.6	2.9±1.7	2.8±1.2
7	4.2±0.9	4.2±1.8	3.9±1.2

Table 3.3.3 Fold increase of cell number after: PDR treatment where yellow laser light (1J/cm², 100mW/cm²) activated 0.25µM hypericin, yellow laser light irradiated cells only and the control cells. SD – standard deviation.

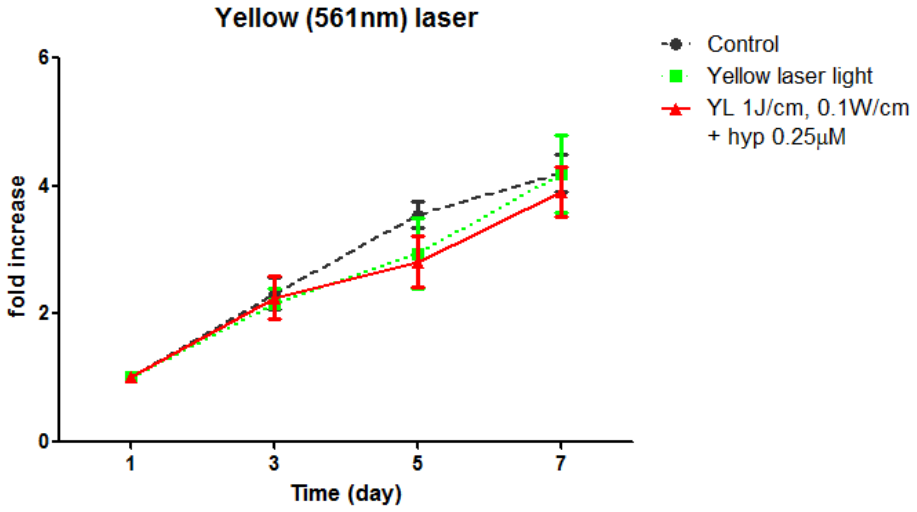

Figure 3.3.3 A growth curve of primary human fibroblasts over 7 days. Solid red line represents cell after PDR treatment with 0.25µM hypericin and 1J/cm^2 (100mW/cm^2) yellow laser light. Fine green dashed line represent cells irradiated with 1J/cm^2 (100mW/cm^2) yellow light only. The coarse black dashed line represents control cells. The results are presented as fold increase after day 1. Data represented as mean±SEM (n=3).

In summary, these data show irradiating hypericin-treated fibroblasts with different wavelengths of light have different effects on growth. The red laser activation of hypericin was tending toward an increase in proliferation rate and UVA and yellow wavelengths showed a slight decrease in growth. All three wavelengths had no significant effect on proliferation on hypericin-treated fibroblasts as growth returned to normal after several days i.e. the cells did not become cytostatic. As previously mentioned, the increase in the cell viability assay seen with each wavelength (Section 3.2) either reflects increased growth or activity in the cell. We can conclude from these growth curves, that the increase in cell viability was not related to the proliferation rate.

3.4. Effect of PDR on Migration of Fibroblasts

The response in fibroblast activity is similar in wound healing and rejuvenation regarding cytokine and growth factor alterations (Fisher *et al.*, 2008; Grotendorst *et al.*, 2004; Varga *et al.*, 1987). The scratch assay was performed as it simulates a wound situation. This allows for a 2 dimensional analysis of the impact of various treatments on the cell. The fibroblasts were treated with 10µg/µl mitomycin C which stops proliferation by inhibiting DNA synthesis and allows for the assessment of migration alone. In the experiments cells were grown to a confluent monolayer in a well. A "wound"/scratch was then made in the tissue culture plate well. Photographs of the entire wound were taken at this and one other time point (before and 8h after irradiation) to monitor the rate of fibroblast migration and results were presented as a percentage of wound closure over 24h.

After 16h incubation with hypericin, the irradiation plate was exposed to 1J/cm^2 (100mW/cm^2) of yellow laser light. Eight hours post-irradiation, and 24h after the initial scratch was made, the wells were photographed. The photographs were processed and the area of the entire wound was determined before and after the PDR treatment.

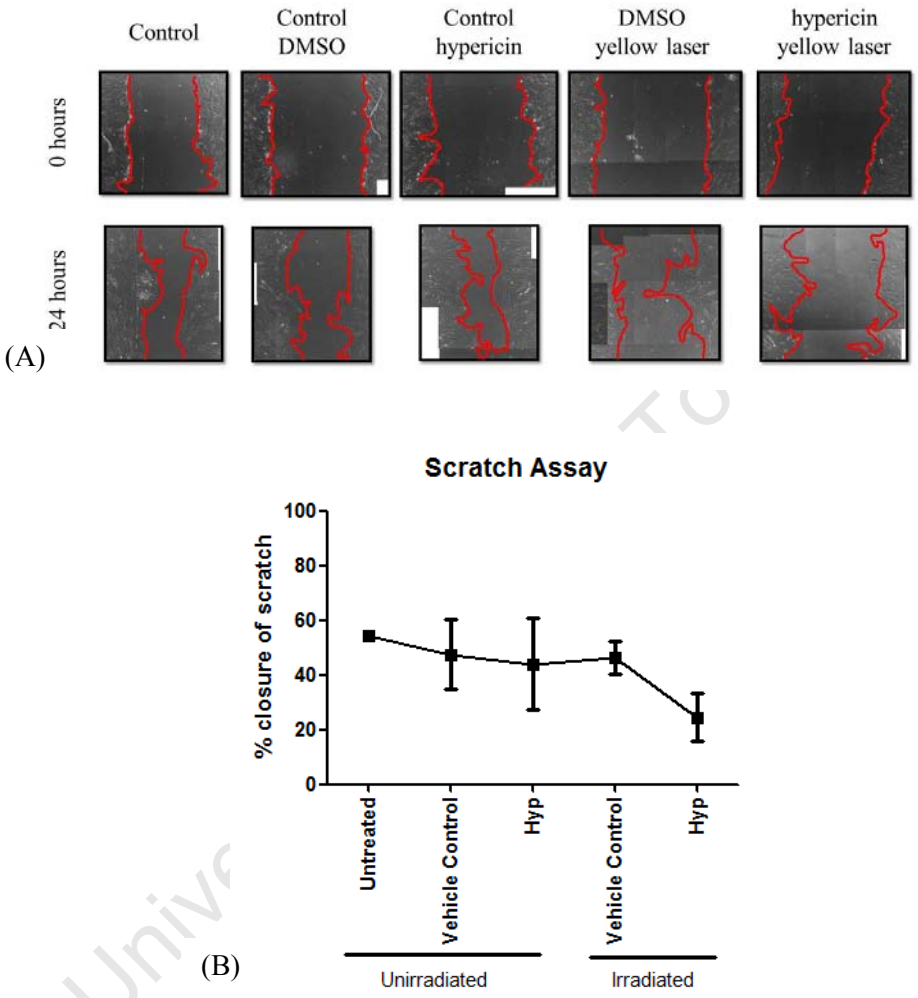

Figure 3.4.1 Cell were treated with 0.25µM hypericin for 16h and irradiated with 1J/cm^2 (100mW/cm^2) yellow laser light. The wound closure was determined 24h after the scratch was made and 8h after yellow laser irradiated. (A) Representative images of a cross sectional of a "wound"/scratch made in a confluent fibroblast monolayer with the red lines marking the borders of the wound. These borders were used to calculate the area using AxioVision software. (B) The results are represented as the percentage of wound closure between 0-24h and shown as mean±SEM (n=3).

Twenty four hours after making the scratch, the untreated and unirradiated cells had 54±2.427% wound closure. The unirradiated (47.47±22.06%) and irradiated vehicle (46.37±10.14%) controls and unirradiated hypericin (44.07±29.01%) controls had a similar amount of closure as the untreated, unirradiated cells (Figure 3.4.1 (B)). Surprisingly, the irradiated cells exposed to hypericin displayed a significantly slower closure rate (24.42±15.06%), compared to the controls (Figure 3.4.1 (B)). This raises the possibility that

yellow laser-activated hypericin seems to significantly affect wound closure through the decreased rate of fibroblast migration. This lack of movement by the cell indicates that alternative cellular energy processes may be activated through PDR (See Section 4).

3.5. Determination of Reactive Oxygen Species (ROS) after PDR treatment

ROS is the product of PDR and a potential mediator of this therapy. The effectiveness of PDR can, therefore, be monitored by quantifying the amount of ROS generated. A ROS assay was performed to confirm the hypericin concentration and irradiation protocols were indeed generating ROS. We performed a ROS assay using the dye DCF-DA. When this compound is oxidised by ROS it fluoresces green. It can detect various ROS and reactive nitrogen species (RNS) (Halliwell & Gutteridge, 2007b). The fluorescence can be visualised through various methods. This study used two methods to determine fluorescence - flow cytometry, where cell were passed through a fluorescent activated cell sorting (FACS) machine, and a fluorimeter, to determine fluorescence levels in a white tissue culture plate.

3.5.1. ROS assay: FACS method

Cells were seeded into 35mm tissue culture dishes and underwent PDR therapy. Following irradiation, cells were incubated with 40µM DCF-DA in complete medium for 30min at 37°C. Cells were collected, washed and resuspended in FACS tubes.

Both yellow laser and UVA light were used to measure their activation of 0.25µM hypericin. UVA (1J/cm^2) treated cells served as the upper limit of ROS generation. Yellow laser light treated cells were irradiated with 1J/cm^2 and 20mW. The power was not adjusted for the change in area from a 96-well plate (cell viability assay) to a 35mm tissue culture dish as this would require an extraordinary higher power output beyond that of the laser used. Instead the power density was calculated to be 0.002W/cm^2, which translated to the cells receiving 8min of irradiation (Table 2.4.1).

The results were normalized to 100% of the untreated, unirradiated control which represented basal levels as seen in Figure 3.5.1. Cells irradiated with the yellow laser light alone showed an increase of 72±83.52% in ROS generation. Whereas yellow laser irradiated-hypericin treated fibroblasts showed a 96±23.55% increase in ROS levels higher than the control (Figure 3.5.1). Incubation with hypericin and yellow laser light irradiation showed ROS generation was 24% higher than light alone. UVA irradiated cells exposed to hypericin had the highest ROS generated with 186±22.66% compared to the control.

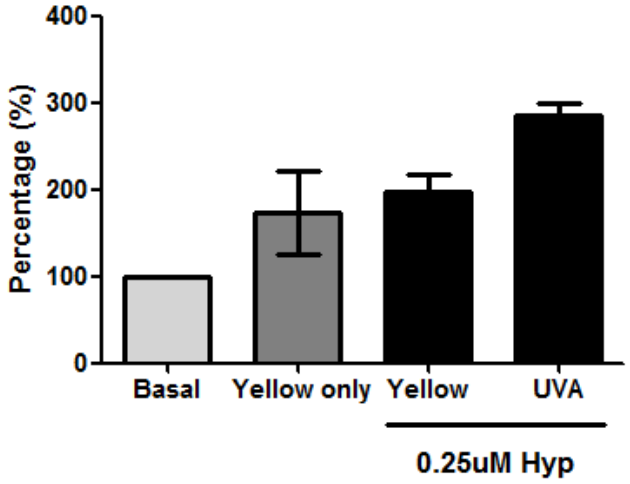

Figure 3.5.1 Results of ROS assay using flow cytometry based method. Basal represents basal ROS levels where only DCF-DA was added to the cells. Yellow only are cells irradiated with 1J/cm^2 (100mW/cm^2) yellow laser light only, 0.25µM was added to two samples where one was irradiated with 1J/cm^2 (100mW/cm^2) yellow laser light and the other 1J/cm^2 UVA. Data represented as mean±SEM (n=3).

3.5.2. ROS assay: Fluorimeter method

An additional method of ROS detection was employed to clarify results presented in Section 3.5.1. A 96-well based assay was developed which used a fluorimeter to detect the green fluorescence of oxidised DCF-DA. Cells were seeded onto white tissue culture grade 96-well plates at a density of $3x10^4$ cells per well. White plates, as opposed to clear tissue culture plates, were used as they allow for sensitive fluorescence readings using a fluorimeter, as well as stopping light from scattering during irradiation.

The hypericin concentration was 0.25µM and the irradiation protocol used was yellow laser light delivered at 1J/cm^2 (100mW/cm^2) and for the UVA treated plate it was 1J/cm^2 (the same irradiation used during the cell viability assay). After irradiation, 10µM DCF-DA in complete medium was added to each well and incubated for 30min at 37°C. Each well had 100µl PBS added to it before the fluorimetric reading. The cells were not removed from the wells and the fluorimeter was set at 488nm for excitation and 535nm for emission to analyse the total fluorescence present in each well.

The cells treated with yellow laser light alone showed no difference to the control (5±75.65% increase) (Figure 3.5.2). In contrast, cells incubated with hypericin and irradiated with yellow laser light showed a 42±75.54% increase in ROS levels (Figure 3.5.2). However, the variance in the sample was large which made standard statistical test inappropriate thus the Welch's test was used to account for this. It was found that yellow laser-activated hypericin was not significantly different to the control (p-value = 0.057).

Interestingly, hypericin and UVA light resulted in a significant increase (56±53.82%) in ROS levels in the fibroblasts (Figure 3.5.2) (p-value 0.0116).

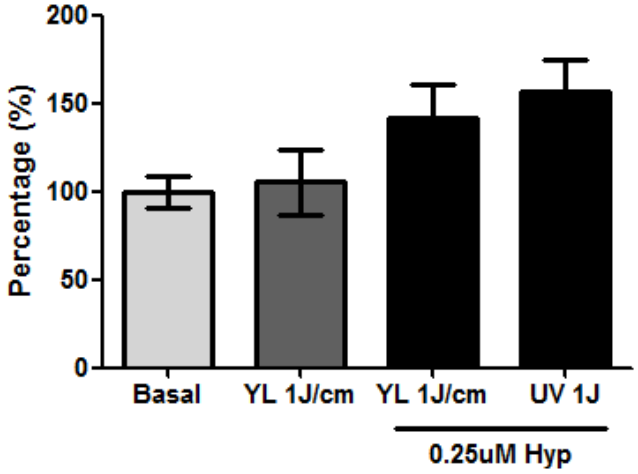

Figure 3.5.2 ROS levels using fluorimeter based method. Basal represents basal ROS levels where only DCF-DA was added to the cells. Yellow only are cells irradiated with 1J/cm^2 (100mW/cm^2) only, 0.25µM was added to two samples where one was irradiated with 1J/cm^2 (100mW/cm^2) yellow laser light and the other 1J/cm^2 UVA. Data represented as mean±SEM (n=3).

Overall, both methods showed that activating hypericin with either yellow laser or UVA light, led to an increase in ROS. Moreover, UVA light consistently generated more ROS than yellow laser light in activating hypericin. This indicates that ROS generated through hypericin activated by yellow laser light will, most likely, not have negative effects on human dermal cells and may in fact have downstream effects on cellular metabolism regarding the dermal matrix.

3.6. Hypericin colocalization with organelle specific labels

Colocalization of hypericin has been shown to influence the cellular response (Buytaert *et al.*, 2006; Theodossiou *et al.*, 2004). Hypericin is reported to localise in different organelles depending on the cell type (Table 1.5.3). Moreover, its cellular effect has been associated with its localization in mitochondria, Golgi apparatus, endoplasmic reticulum (ER) and lysosome. It has been reported the hypericin concentration and incubation time also play a role in its position in a cell (Crnolatac *et al.*, 2007; Siboni *et al.*, 2002). We, therefore, investigated hypericin's location within fibroblasts and its association with 3 major organelles: ER, Golgi apparatus, and mitochondria.

The initial experiments determined hypericin location in the cell over a time course as a visual confirmation of the uptake assay. All three hypericin concentrations and time points

showed hypericin to be localised in the cytoplasm surrounding the nucleus (Figure A.8.1). Figure 3.6.1 is a representation image of hypericin in a fibroblast using confocal microscopy. At no time or concentration did hypericin enter the nucleus (Figure 3.6.1).

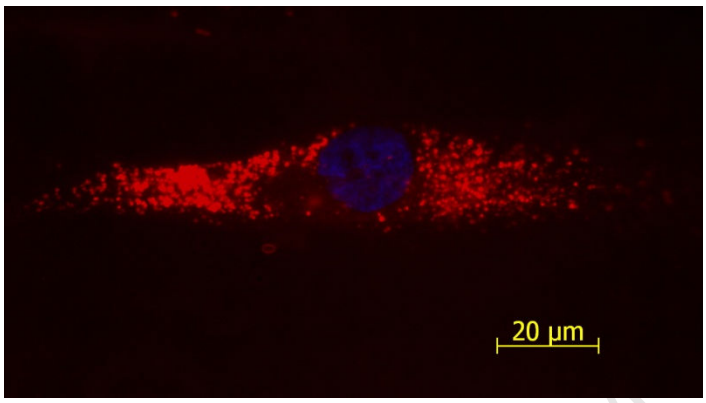

Figure 3.6.1 Representative image demonstrating hypericin's (Red) general localization was around the nucleus (Blue) in the cytoplasm.

3.6.1. Organelle-specific fluorescent proteins

3.6.1.1. Endoplasmic reticulum

The ER serves as centre of protein and lipid synthesis in the cell. In this study, fibroblasts were transfected with an ER specific plasmid expressing yellow fluorescent protein. Figure 3.6.2 displays the ER located perinuclearly and extending throughout the cytoplasm. Hypericin-treated cells transfected with this plasmid did not show conclusive colocalization between hypericin and the ER (Figure 3.6.2 (C), (D)). However, as colocalization may have been obscured by the extensive nature of ER in the cell, a 2 dimensional profile histogram for each colour was done to determine any overlap between the ER and hypericin (Figure 3.6.2). The profile histogram indicated that hypericin staining (red peaks Figure 3.6.2 (E), (F)) did not correlate with ER (yellow intensity peaks Figure 3.6.2 (E), (F)) indicating, semi-quantitatively, no exclusive colocalization between hypericin and the ER.

3.6.1.2. Golgi apparatus

The Golgi apparatus, also located in the perinuclear region, is responsible for the processing, post-translation modification and transportation of proteins (Campbell & Reece, 2002). Plasmid transfection with a Golgi apparatus-specific protein, Rab7WT, was performed. This proteins forms part of the protein regulators for vesicle transport and is located in specific intracellular compartments such as the Golgi apparatus (Choudhury *et al.*, 2002). Similarly to the ER, the Golgi apparatus showed as a diffuse aggregation around the nucleus with stronger punctate staining (Figure 3.6.3 (A), (B)). In contrast to the ER location, when hypericin was incubated, the punctate staining correlated with the labelled organelle (Figure

3.6.3. (C), (D)). Further analysis of this colocalization profiling displayed 16h hypericin treatment accumulates in the Golgi apparatus in primary human fibroblasts (Figure 3.6.3 (E), (F)). The scatterplots quantitatively investigated the colocalization by plotting the fluorescent intensities of red hypericin (y-axis) and the green fluorescent protein of the Golgi apparatus (x-axis) (Figure 3.6.4). This confirmed the results seen in Figure 3.6.3 (E), (F).

3.6.1.3. Mitochondria

The mitochondria are the power house of the cell in generating energy rich compounds such as adenosine triphosphate (ATP). Mitochondria oscillate between states of fusion and fission in the cell. They can appear as tubules in their state of fusion and during fission they are independent bean-shaped organelles (Westermann, 2010).

Mitochondria are known to generate ROS through cellular respiration (Campbell & Reece, 2002) It has been shown, in other cell types, that hypericin does localise in this organelle and is possibly linked to its mechanism of action due to its proximity with oxygen used during cellular respiration (Theodossiou *et al.*, 2006).

Ornithine transcarbamylase is a mitochondrial-specific protein present in the matrix of the mitochondria (Davids, 2003). In our system, the cells without hypericin displayed mitochondria were in a state of fusion shown by the appearance of tubular-like structures. When the cells were treated with 0.25μM hypericin however, there was mild colocalization with mitochondria, but not to the same degree as was evident with the Golgi apparatus (Figure 3.6.5 (E), (F)). The laser needed to visualise hypericin on the confocal microscope was the same yellow laser used in previous experiments in this project (Section 3.2-3.5). Unexpectedly, this caused a change in mitochondrial morphology. The mitochondria went immediately from the tubular shape to a beaded appearance (Figure 3.6.6 (C-F)). This transition was seen only in hypericin treated cells and not in control cells displaying the plasmid. This instant change was mostly likely due to the activation of hypericin. It should be noted that this state was probably induced by the massive increase in ROS generated by activated hypericin. The power of the confocal laser was 250 times more than that used in the cell viability, growth curve, scratch and ROS assays. It is important to note that this state may not occur in fibroblasts treated with $1J/cm^2$ and $100mW/cm^2$.

In conclusion, these subcellular experiments show clearly that hypericin localizes to the perinulcear region of the cell. It strongly colocalizes with the Golgi apparatus, to a lesser extent the mitochondria and has no apparent colocalization with the ER. The high power, and therefore high energy density, delivered by the confocal microscope laser caused the mitochondria to become segmented, indicating a stress response, in hypericin treated cells.

This reaction may be an artefact of the experiment and one must exercise caution to extrapolate it as a reaction of the fibroblast to hypericin mediated PDR.

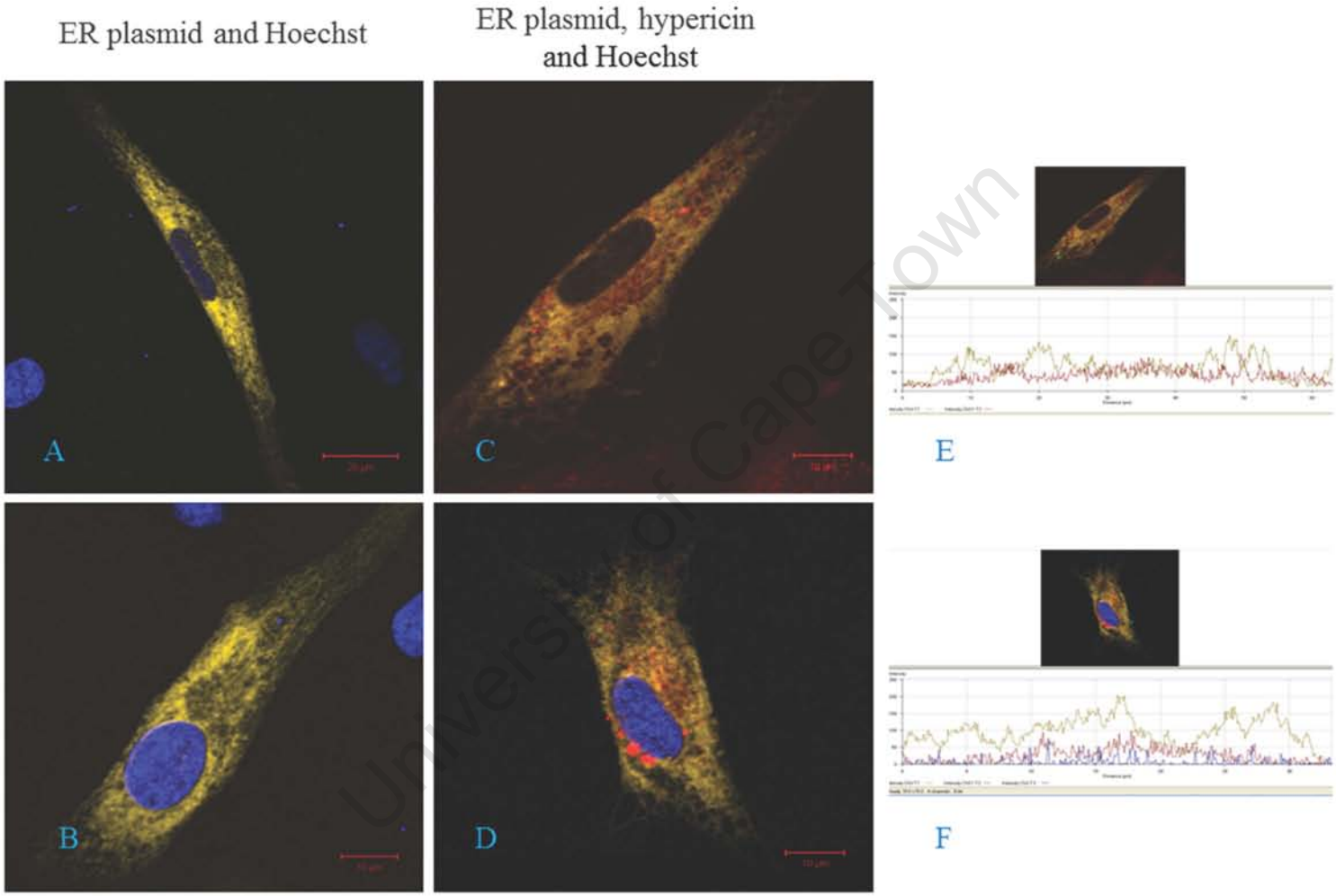

Figure 3.6.2 Representative images of fibroblasts transfected with ER-specific YFP plasmid to determine hypericin's colocalization with this organelle. (A), (B) are fibroblasts with ER plasmid (yellow) and the nuclear stain Hoechst (Blue). (C), (D) are fibroblasts treated with 0.25μM hypericin (Red), ER plasmid and Hoechst. (E) is the histogram profile of (C) and (F) is the histogram plot of (D). Both (E) and (F) indicate there is no specific colocalization between the peaks of the yellow ER and red hypericin peaks. (n=2)

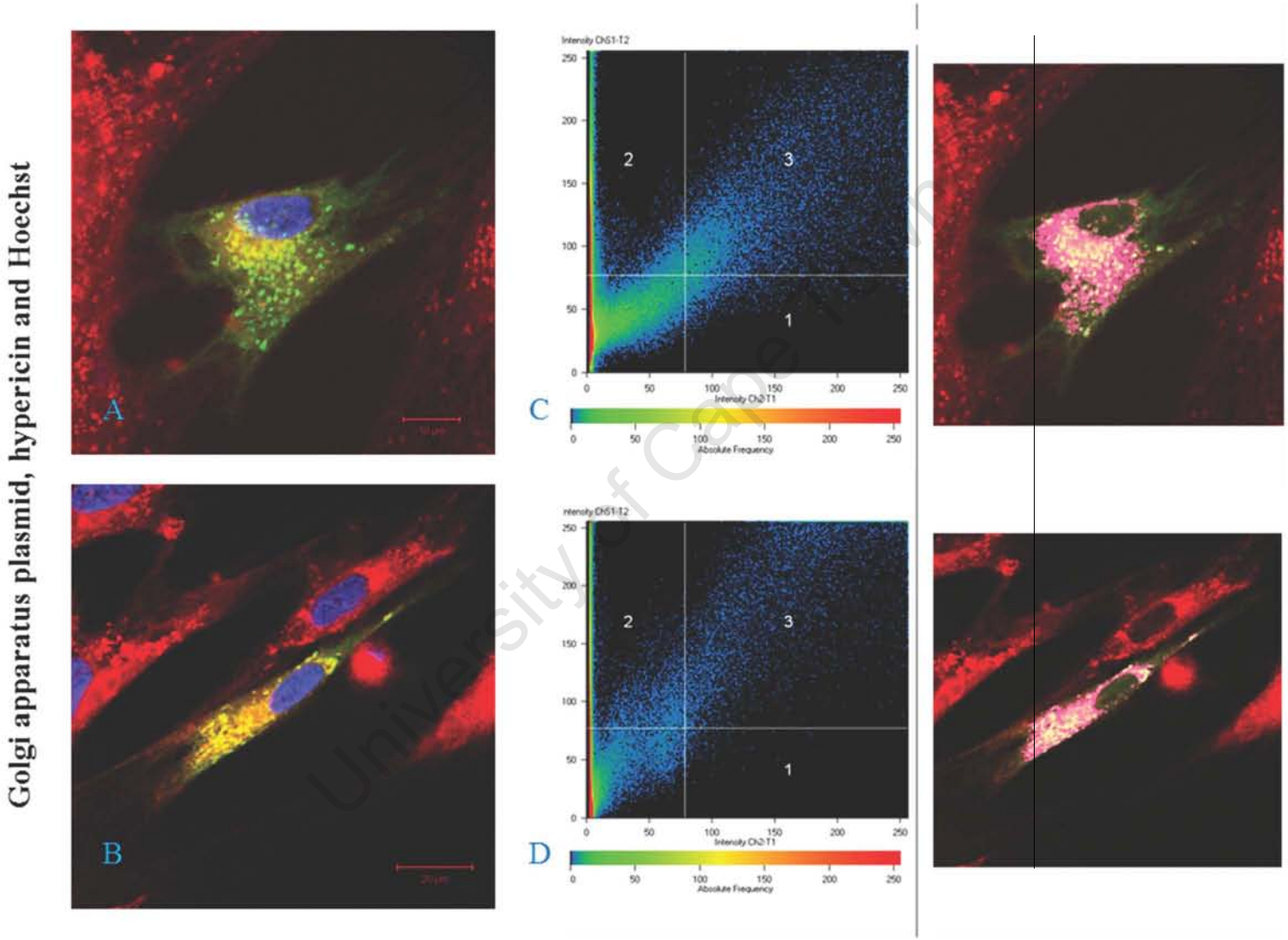

Figure 3.6.4 (A), (B) indicated hypericin located in the Golgi apparatus of the fibroblasts. (C), (D) Scatterplots indicating the colocalization of red fluorescent intensities (0.25µM hypericin) on the y-axis and green fluorescent intensities (Golgi labelled with GFP) on the x-axis in fibroblasts.

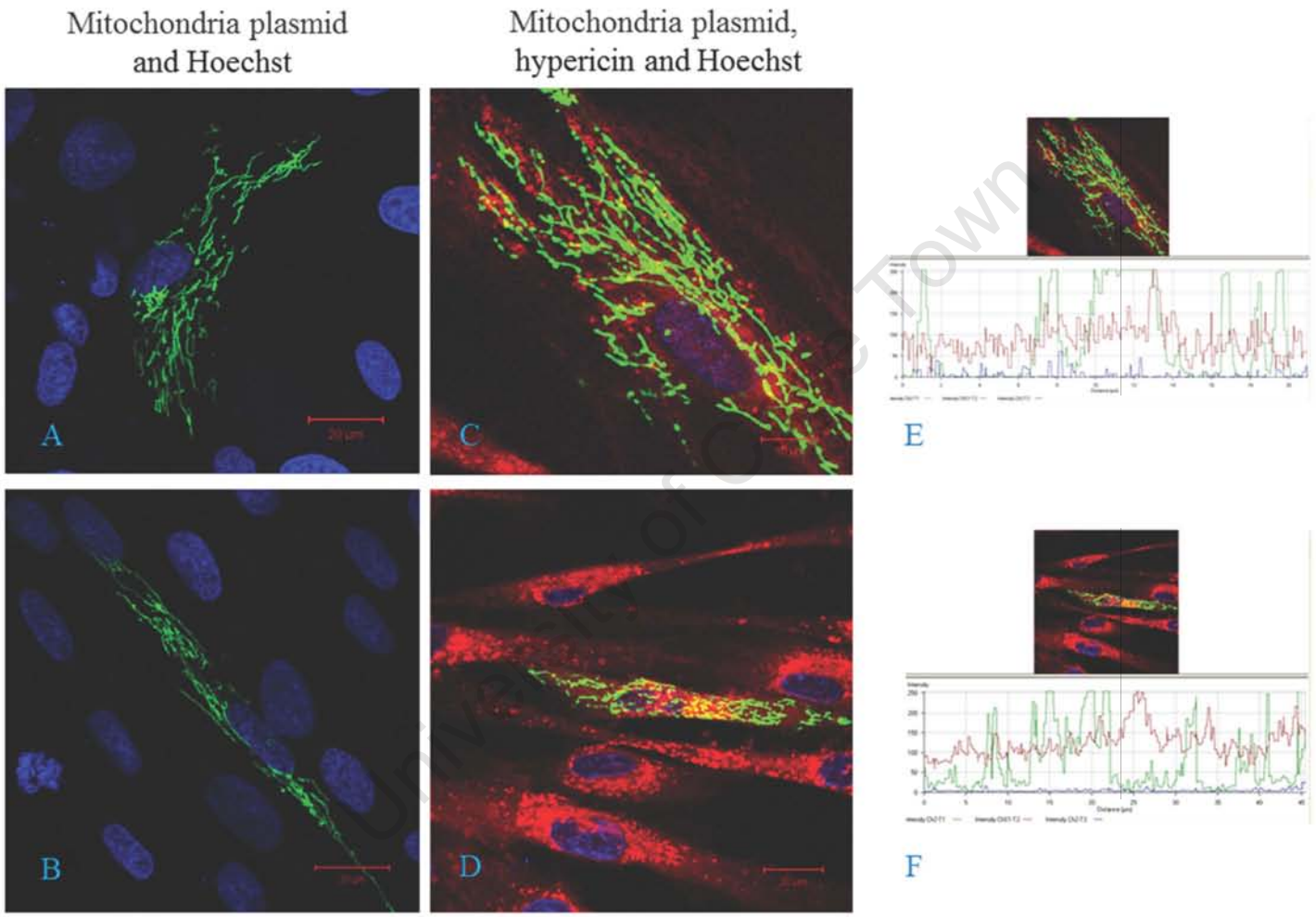

Figure 3.6.5 Representative images of fibroblasts transfected with mitochondria-specific GFP plasmid to determine hypericin's colocalization with this organelle. (A), (B) are fibroblasts with mitochondria plasmid (Green) and the nuclear stain Hoechst (Blue). (C), (D) are fibroblasts treated with 0.25µM hypericin (Red), mitochondrial plasmid and Hoechst. (E) is the histogram profile of (C) and (F) is the histogram plot of (D). Both (E) and (F) indicate no exclusive colocalization between the peaks of the green peaks of the mitochondria and red hypericin peaks. (n=3)

4. Chapter 4: Discussion

Photodynamic therapy (PDR) is a relatively new dermatological treatment used to reverse the signs of photoageing. It has been successfully used since 2002 (Ruiz-Rodriguez *et al.*, 2002). There have been several developments and improvements to this therapy over recent years. This has resulted in excellent outcomes for many patients. Although a substantial body of work has been reported on the clinical outcomes of PDR, there remains a shortfall in knowledge about the actual mechanism of PDR, including its *in vitro* effect on human skin cells. Moreover, there is still a need for an ideal protocol where minimal photosensitizer (PS) is used and optimised irradiation parameters are defined (Agostinis *et al.*, 2002; Kiesslich *et al.*, 2006; MacGregor & Dover, 2010)

The concept of PDR involves a topically applied PS activated by a specific wavelength of light to generate reactive oxygen species (ROS) in the presence of oxygen. Both the PS and activating wavelength are integral to the success of the treatment. The PS used in this project is hypericin, a photosensitizing pigment compound from the plant *Hypericum perforatum* (St John's Wort) (Agostinis *et al.*, 2002; Kiesslich *et al.*, 2006). Hypericin is a second generation PS offering a high quantum yield for triplet state generation and is, thus, able to generate ROS (Agostinis *et al.*, 2002; Berlanda *et al.*, 2010; Kiesslich *et al.*, 2006). It has shown promise as a PS in treating various skin conditions such as acne, psoriasis and in wound healing (Hager *et al.*, 2009; Kiesslich *et al.*, 2006; Najafizadeh *et al.*, 2012; Oztürk *et al.*, 2007). Due to this clinical success, this project investigated its *in vitro* efficacy in PDR on human dermal fibroblasts.

The purpose of this study was three-fold: firstly, to develop an optimised PDR protocol on primary human dermal fibroblasts using three different wavelengths of light to activate hypericin. Secondly, hypericin-mediated PDR treatment on fibroblast growth, migration and ROS production was determined. Thirdly, hypericin's subcellular location within fibroblasts was shown as this relates to its mechanism of action.

In line with the first aim of this study, the uptake assay was designed to determine the time at which the maximum amount of hypericin was present in fibroblasts. This information was important as too low hypericin concentrations would need higher energy and power densities to generate enough ROS to cause the PDR reactions and overcompensating with light energy and power may result in phototoxic reactions. Moreover, high PS concentrations will lead to post-treatment photosensitivity (Avram *et al.*, 2006; Chen *et al.*, 2001).

Three hypericin concentrations (0.25μM, 0.5μM and 1μM) were diluted in serum-supplemented medium and the amount of fluorescence within fibroblasts was quantified. These concentrations have been demonstrated to be non-cytotoxic in other cell types (Davids *et al.*, 2008). The results showed that using the low concentration of hypericin (0.25μM), maximum uptake occurred at 16h. The two higher concentrations (0.5μM and 1μM hypericin) peaked at 10h and showed only a slight, non-significant decrease at 16-24h. Our results showed a consistent concentration dependence on hypericin uptake. At no time point were the three concentrations similar with regards to their fluorescence values (Figure 3.1.1). These results were corroborated by microscopy analyses. In addition, micrographs of the fibroblasts consistently showed an accumulation in the perinuclear area with fluorescent intensity increasing with time (Figure A.8.1).

Hypericin can enter a cell through various mechanisms. These mechanisms depend on the medium in which hypericin is diluted and presented to the cell. In medium without any supplement (e.g. fetal bovine serum) this lipophilic compound can diffuse across the cell membrane freely (Castano *et al.*, 2004). This method has been documented to be the fastest way for hypericin to enter a cell (Crnolatac *et al.*, 2007; Siboni *et al.*, 2002). The higher the extracellular hypericin concentration, the faster the rate of diffusion (Buriankova *et al.*, 2011). Another mechanism of entry is hypericin bound to serum proteins such as low-density lipoprotein (LDL) and Human Serum Albumin (HSA) (Buriankova *et al.*, 2011; Das *et al.*, 1999; Gbur *et al.*, 2009; Huntosova *et al.*, 2010; Kascakova *et al.*, 2005; Mukherjee *et al.*, 2008; Roelants *et al.*, 2011; Siboni *et al.*, 2002; Uzdensky *et al.*, 2001). The serum protein that hypericin is bound to will ultimately determine its mechanism of entry into a cell and its final location. When it is attached to the serum protein it can enter a cell via endocytosis (hypericin associated with LDL) or pinocytosis (hypericin associated with HSA) (Siboni *et al.*, 2002). The different mechanisms affect the time taken for hypericin to enter the cell. Some authors have suggested that incubation of hypericin with serum supplemented medium causes competition between LDL-mediated hypericin uptake and passive diffusion (Crnolatac *et al.*, 2007).

Our results correlate with the serum-protein mediated uptake of hypericin into the cell. Hypericin's uptake peaked at 10-16h which is far longer than faster diffusion rates reported in the literature (2-3h) (Crnolatac *et al.*, 2007; Siboni *et al.*, 2002). In this study, hypericin was shown to be located in the Golgi apparatus of fibroblasts and correlates with the LDL mechanism of entry into the cell following endocytosis of the LDL receptor.

An important consideration in hypericin's uptake is its potential to form aggregates. Hypericin aggregates are non-fluorescent and occur when hypericin is in an aqueous

solution or at high concentrations (10μM<) (Kascakova *et al.*, 2005). Once inside the cell, the aggregates are believed to separate into single compounds (Buriankova *et al.*, 2011). This is a point of concern in that aggregates result in self-quenching where not only the quantum yield is lower, thus affecting ROS generation, but the fluorescent signal decreases as well (Buriankova *et al.*, 2011; Gbur *et al.*, 2009; Theodossiou *et al.*, 2004). These aggregates make it difficult to use hypericin's autofluorescence and relate it to its concentration. When aggregates are present the concentration, interpreted through its fluorescent intensity, will appear lower than its real value (Buriankova *et al.*, 2011; Huntosova *et al.*, 2010; Kascakova *et al.*, 2005; Theodossiou *et al.*, 2004). However, as we were not looking for an exact quantification but rather determined at what time maximum hypericin uptake occurred relative to other incubation times, this method served our purpose. In addition, over long periods of time a decrease in hypericin's fluorescence has been documented in other cell types which was attributed to aggregate formation (Buriankova *et al.*, 2011; Huntosova *et al.*, 2010; Theodossiou *et al.*, 2004). At no time in this experiment did the fluorescence of hypericin decrease, indicating a distinct lack of aggregation formation.

Hypericin incubation time of 16h was used for all further experiments. This time was the most practical in PDR for all three hypericin concentrations and correlated with literature (Berlanda *et al.*, 2010; Hendrickx *et al.*, 2005). Once the time for maximum uptake was defined, a non-cytotoxic, irradiation protocol was determined for three different activating wavelengths of light.

PDR has the potential to generate high levels of ROS which can overwhelm the cell, leading to its death. It is, therefore, important that the protocol established in this project had no negative effects on cell survival. To this end we used the XTT cell viability assay (Section 2.2) to find a PDR protocol that was non-cytotoxic to fibroblasts. This assay is based on viable cellular metabolism resulting in the colorimetric conversion of tetrazolium salt from yellow to orange via mitochondrial enzymes. In establishing our PDR protocol, two variables were analysed - hypericin concentration and the irradiation protocol.

As hypericin stock solutions are dissolved in DMSO, we noted the effect of this diluent on the cells. It was found to have no effect on cell viability which is in line with the literature where >1.25% is considered cytotoxic (Berlanda *et al.*, 2010). Dark cytotoxicity of hypericin in the literature ranges from 3.13μM, 31.5μM and 250μM in human epidermoid carcinoma cell line A431, colon adenocarcinoma and murine keratinocytes, respectively (Berlanda *et al.*, 2010; Theodossiou *et al.*, 2004; Uzdensky *et al.*, 2001). This indicates a cell type

dependence on hypericin tolerance without light activation. In this project the highest hypericin concentration (1μM) showed no dark cytotoxic effects on fibroblasts.

Next we investigated the three hypericin concentrations (0.25μM, 0.5μM and 1μM) activated by three different wavelengths of light. The specific wavelengths of light were delivered by two types of light sources: lasers and lamps. Two solid state lasers were used, one emitted a continuous wave light at 561nm (yellow colour) and the other at 635nm (red colour). In using a laser, all three variables from Equation 1.4.1 (Section 1.3.1.1) can be controlled or altered. A laser allows for an exact irradiation protocol, regarding all three variables, to be optimised whereas when using a lamp only energy density and time can be changed (Pryor *et al.*, 2011).

It is common to test the efficacy of different PS with several wavelengths of light (Bjerring *et al.*, 2009; Blank *et al.*, 2002; Clementoni *et al.*, 2010; Kubin *et al.*, 1996). It has been reported that different wavelengths used in PDR can treat different aspects of photoageing (Bjerring *et al.*, 2009; Ruiz-Rodriguez & López-Rodriguez, 2006). Three wavelengths (635nm- red, ~365nm - UVA, 561nm - yellow) were chosen as each provides a benefit in treating skin conditions and/or activating hypericin.

Besides photorejuvenation, red light has been used in dermatology to treat other skin conditions including diabetic and chronic wounds (Abrahamse & D, 2009; Houreld & Abrahamse, 2007; Peplow, Chung, & Baxter, 2012a, 2012b). Its advantage of deep penetration into the skin (Agostinis *et al.*, 2011; MacGregor & Dover, 2010; Peng *et al.*, 2008) allows for the light to not only affect the epidermal cells but also the fibroblasts situated deeper in the dermis.

Three energy densities delivered by the red laser light were used to activate the three hypericin concentrations. A significant increase in cell viability was seen 24h after treatment when fibroblasts were pretreated with 0.25μM and 0.5μM hypericin and irradiated with 2.5J/cm^{2}red light (Figure 3.2.1). Overall, it appears that hypericin activated by red light had minimal effect in fibroblasts. In addition, there was a threshold affect where the therapy changed from being ineffective at low energy densities to increasing cell viability at higher energy densities. However, at the highest energy density (5J/cm^2) the therapy showed no change in cell viability. This indicates that ROS levels could have changed from being beneficial to causing an upregulation of the antioxidant system where ROS are scavenged. These results point to a potential threshold level of activation where a range of red light energy is effective.

Red wavelengths of light have been shown to increase fibroblast proliferation and their activity in the wound bed (De Sousa *et al.*, 2010; Houreld & Abrahamse, 2007; Peplow *et al.*, 2010; Peplow, Chung, & Baxter, 2012a). PDR therapy that used IPL (550nm-1200nm) had great success in treating the global appearance of photoageing and fine lines, and to lesser extent mottled pigmentation and roughness (Table 1.5.1). It is interesting to note that the two most commonly used PS, ALA and MAL, only absorb approximately 10% of red light yet still result in satisfactory outcomes according to most patients and clinicians (Gold & Goldman, 2004; Haddad *et al.*, 2011; MacCormack, 2008; Peng *et al.*, 1997) (Table 1.5.1). Interestingly, hypericin absorbs only up to 33% red light (Figure 1.5.2), yet we do not see the positive effects as demonstrated with ALA and MAL in other PDR protocols. Despite this, the potential of using red light in PDR is enticing due to its penetrating depth and relative availability in dermatological clinics (Agostinis *et al.*, 2011; Peng *et al.*, 2008). It would appear that red light activation of hypericin, under these conditions, had a small effect on cellular activity of the fibroblasts. Potentially increasing the power density, thereby increasing the energy density, may result in a different outcome and should be considered in the future.

UVA light (~365nm) was the next wavelength investigated. UVA wavelengths can penetrate into the skin to the upper dermal layer (Pillai *et al.*, 2005). Moreover, hypericin has two major peaks in its absorption spectra with one being in the UVA range (Figure 1.5.2). A fine line exists between UVA being beneficial in generating low levels of ROS in PDR on the one hand and being cytotoxic on the other. UV radiation from sunlight, which is composed of UVA and UVB wavelengths of light, is the main effector in photoageing and has been linked to carcinogenesis (Fisher *et al.*, 2008; Halliwell & Gutteridge, 2007c; Macfarlane, 1992; Pillai *et al.*, 2005). This, thus, highlights the need to fully optimise the irradiation protocol so a minimum amount of energy is used to maximally activate the PS to generate low ROS levels.

The three hypericin concentrations (0.25μM, 0.5μM and 1μM) were activated with 0.5J/cm^2 and 1J/cm^2 of UVA. The lower concentrations of hypericin had no effect or a slight increase in cell viability, whereas 1J/cm^2 hypericin had a significant decrease in cell viability at the high hypericin concentration (1μM) (Figure 3.2.2). Similar to red laser light, where an increase in cell viability occurred at 2.5J/cm^2 with 0.5μM hypericin, UVA light showed an increase with a low energy density of 1J/cm^2 and low 0.25μM hypericin concentration. This is due to hypericin's ability to absorb more of UVA's light energy compared to red light. By effectively absorbing energy, a similar level of ROS was generated with less energy and lower PS concentrations but resulted in the same positive cellular effect. A threshold for cell viability was seen again, as noted with the red laser, where high hypericin concentrations

and high energy resulted in a decrease in cell viability but low energy and low hypericin concentrations resulted in an increase.

It would seem counterintuitive to use UVA in PDR seeing that UV radiation is the main agent in the development of the signs of skin ageing (Fisher *et al.*, 1997, 2002; Pillai *et al.*, 2005; Rittié & Fisher, 2002). However, there are many therapies to date that use UVA to treat skin conditions. Examples include, psolarens and UVA (PUVA) therapy to treat vitiligo, psoriasis, T-cell lymphoma and acne vulgaris (McEvoy & Muller, 1992; Mosher *et al.*, 1992; Satra & DeLeo, 1992). However, these therapies are used within established dermatological institutions where the patients are constantly monitored.

The third wavelength investigated was yellow light, specifically 561nm. Hypericin maximally absorbs light with a wavelength of 563nm and we were able to use a laser which emits light at 561nm. We, therefore, could activate hypericin to its full potential. Kubin *et al* reported activating hypericin with different wavelengths and found 532nm light was more efficient at photosensitization of hypericin treated human skin than 630nm (Kubin *et al.*, 1996). This indicates hypericin's high energy absorption of this range of wavelengths and subsequent high level ROS generation under a specific irradiation protocol. This is in agreement with results reported in this project.

We investigated the effect of yellow laser light activation of hypericin on fibroblasts using 3 different power densities in a similar manner to Head *et al* (Head *et al.*, 2006). Three energy densities were used with each power density as seen in Figure 3.2.3. Very low energy densities (0.1J/cm^2, 0.25J/cm^2, 0.5J/ cm^2) were used with the lowest power density (10mW/cm^2). However, these low energy densities had the same irradiation time as those energy densities used with higher power densities. This allowed us to investigate if exposure time had any effect on cell viability (Table 2.4.1). There was little change among the three hypericin concentrations irradiated with 10mW/cm^2 light at any of the energy densities. However, 0.25μM hypericin showed an increase in viability when irradiated with 0.25J/cm^2. At higher energy densities with a power density of 50mW/cm^2, there was a hypericin concentration and energy density-dependent decrease in cell viability. This decrease was somewhat mirrored at the higher power density of 100mW/cm^2. At the highest power density (100mW/cm^2), however, there was an increase in cell viability with the lowest energy density (1J/cm^2) and 0.25μM hypericin.

It, therefore, appears juxtaposed that both the low and high energy and power densities would result in an increase in viability. Regarding the low energy and power density (0.25J/cm^2, 10mW/cm^2), this may be due to the longer irradiation time resulting in more hypericin being activated and reacting within the cell. In contrast, the short burst of high

power delivering a small amount of energy in a short time could result in a similar ROS generation but may elicit a different signalling pathway. Both protocols appear to result in a positive outcome.

Consistently, when cells were irradiated with yellow laser light, the 0.25μM hypericin concentration caused an increase in cell viability. This activated hypericin concentration most likely generates low levels of ROS which have a positive impact on the cell.

Green/Yellow light alone has been shown to have an advantageous effect on fibroblast proliferation at 24h (Vinck *et al.*, 2003). This wavelength, therefore, has benefits similar to red and UVA light where it has shown positive outcomes with regard to increased cell proliferation. Yellow light is able to penetrate between 1 - 1.6mm into tissue (Nootheti & Goldman, 2006; Peng *et al.*, 2008). It is, therefore, possible that yellow light can activate hypericin in the papillary dermis as the epidermis has a thickness of about 0.1mm depending on the location in the body (Blank *et al.*, 2002; Gambichler *et al.*, 2006). Blank *et al* reported the potent *in vivo* effect of hypericin activated with 550nm and 590nm light in mouse skin. Although this treatment was PDT-mediated tumour destruction, it highlighted that the depth of tissue response to activated hypericin was about 10mm, far beyond the predicted depth of 1mm reported for 550-590nm light (Blank *et al.*, 2002). This further emphasises how successful yellow light is in activating hypericin to the level of the dermis. Yellow light activation has indirectly been reported with other PS with PDR therapies using IPL systems, which include the yellow range of wavelengths (550nm-1200nm), and have been successful in resolving the signs of photoageing (Table 1.5.1).

It is important to note that many PDR therapies have not been optimised with regards to the specific wavelength activation of the PS or energy and power densities as demonstrated in the variety of protocols represented in Table 1.5.1. In this work we demonstrate a threshold where activated hypericin changes from being beneficial to cytotoxic. This is an important contribution to future hypericin mediated PDR and is often not demonstrated in other PDR studies.

As the cell viability assay indicates mitochondrial function, an increase could mean two things: an increase in proliferation or mitochondrial activity. An increase due to proliferation would indicate the therapy has had an effect on the growth rate of the cells. Alternatively mitochondrial activity could signify that the cells may not have increased in number, and may in fact have decreased, but their collective activity or cellular metabolism is higher than the control cells. To investigate whether this increase was due to an increase in proliferation rate, growth curves for each wavelength of light were performed over a period of 7 days.

In investigating PDR's effect on growth, the protocol which gave the greatest increase in the cell viability for each wavelength was used for a growth curve. In the case of red light, 0.5μM hypericin was irradiated with 2.5J/cm^2 (Figure 3.3.1). The growth rate of the red laser light-PDR treated cells was not significantly different to control cells. An issue for this growth curve was that the power density was not the same as the cell viability assay. Due to the practical limitations of laser, the highest power output was used for the growth curve and the power density was calculated retrospectively. Interestingly, there was a lag in growth between day 1 and 3. This could be due to the long irradiation times (16min for each well) for this specific wavelength that might have stressed the cell causing a slowing in proliferation. When the growth curve with 0.5J/cm^2 UVA and 0.25μM hypericin was performed, there was a lag between the normal control and the PDR treated cells (Figure 3.3.2). A similar outcome was noted when 0.25μM hypericin was activated by 1J/cm^2 (100mW/cm^2) yellow laser light (Figure 3.3.3). In both cases the slowing in growth was not permanent and the cells regained a rate of proliferation similar to the control cells after a few days. In addition, the yellow laser growth curve included cells that irradiated with the vehicle (0.0125% DMSO) only. The irradiated cells had a similar growth pattern to the PDR treated cells where there was a slight reduction in the growth rate of the fibroblasts. This indicates the light itself could have an effect which is resolved and the normal growth rate returns (as compared to the control). Interestingly, some reports have shown that hypericin on its own, without light activation, can slow down the proliferation of fibroblasts (Oztürk *et al.*, 2007). Noteworthy, is that the red laser and UVA light activation growth curves were repeated once with an intra-triplicate repeat. In contrast, the growth curve with hypericin activated by yellow laser light was repeated in three individual experiments. For these data to be confirmed, more replicates would need to be done for the other wavelengths. Unfortunately, we only had limited access to these light sources (UVA transilluminator and red laser), therefore, could not repeat these experiments within the time frame of this project. We would, therefore, need further testing to verify these results.

Here, it seems that the ROS generated by PDR may cause a slight slowing in cell growth which disappears after a few days. Interestingly, the opposite response is generally reported where ROS is associated with proliferation (Halliwell & Gutteridge, 2007a). In our case, however, this contradiction is likely due to the PDR protocol used. Our main aim was to generate a non-cytotoxic PDR protocol on primary human fibroblasts and not necessarily affect the proliferation rate of fibroblasts. Furthermore, this also indicates these protocols will most likely not cause a hyperproliferative state in fibroblasts. Hyperproliferation is linked with fibrosis where an unregulated, overproduction of collagen occurs as in the case of keloid scarring (Halliwell & Gutteridge, 2007a; Lim *et al.*, 2001; Murrell *et al.*, 1990). In

addition, results from our scratch assay show a change in cell morphology after PDR treatment. The change in shape from long and spindle to a shorter, rounded shape indicate the cells are not in a proliferative state (Murrell *et al.*, 1990; Oztürk *et al.*, 2007). This non-significant growth inhibition could be linked with the fibroblast's antioxidants systems scavenging the ROS and causing an overall slowing of proliferation as was highlighted in the study by Murrell *et al* (Murrell *et al.*, 1990). Moreover, experiments using "low dose PDT" with hypericin indicate cellular growth arrest and suggest it is caused by alterations to signalling molecules such as the anti-apoptotic protein Bcl-2 and cycle regulator protein cyclin-dependent protein kinase 1 (CDK-1) (Piette *et al.*, 2003; Vandenbogaerde *et al.*, 1998). An alternative interpretation could be that the cell is funnelling energy towards other metabolic processes. Two studies have shown that fibroblast proliferation and collagen synthesis are mutually exclusive when regulated under combinations of various cytokines such as TGF-β, connective tissue growth factor (CTGF) and epidermal growth factor (EGF) (Grotendorst *et al.*, 2004; Varga *et al.*, 1987). We propose that the metabolic process upregulated may be collagen synthesis. This correlates with the results seen in the scratch assay.

As the growth rate did not change after treatment, the increase in cell viability indicates a possible increase in other cellular activities. Cellular reactions of fibroblasts in late wound healing regarding collagen synthesis and remodelling are similar to those in skin rejuvenation regarding collagen neogenesis and the breakdown of the fragmented ECM through MMP (Fisher *et al.*, 2008; Grotendorst *et al.*, 2004; Varga *et al.*, 1987; Welch *et al.*, 1990). Furthermore, it has been shown that fibroblast migration occurs mutually exclusively from collagen synthesis in the wound healing sequence (Singer & Clark, 1999; Welch *et al.*, 1990).

The scratch assay was used to determine the rate of wound closure and, therefore, the speed of cell migration after PDR treatment. The cells are blocked from entering mitosis with a 3h incubation with mitomycin C which stops DNA synthesis. This allows migration to be analysed without the effect of proliferation. Only one time point (24h from initial scratch) was assessed as multiple photographs exposed the cells to bouts of light that could potentially reactivated hypericin.

Interestingly, the yellow laser-irradiated hypericin-treated fibroblasts only migrated 22% compared to 54% wound closure of the control cells. The other controls in the experiment, hypericin or irradiated only, fibroblasts migrated at the same rate as the control cells. This indicates that neither hypericin nor light irradiation on its own had an effect on migration. The difference in wound size between the control and the PDR treated cells was obvious in

the photographs (Figure 3.4.1). This correlates with other studies investigating activated hypericin's inhibitory effect on migration (Buytaert *et al.*, 2008; Hendrickx *et al.*, 2005; Martínez-Poveda *et al.*, 2005; Zhang *et al.*, 1997). However, it should be noted that this results stem from a 2 dimensional interpretation of fibroblast function. As fibroblasts function is dependent on its attachment to the matrix, these results may differ when cells are treated within a 3D matrix (Varani *et al.*, 2004; Welch *et al.*, 1990). The other wavelengths were not analysed as we did not have access to them at the time these experiments were being performed.

These results, along with the growth curve data and wound healing literature, could suggest that when cells are not growing or migrating they are actively producing matrix proteins due to an increase in activity (Grotendorst *et al.*, 2004; Oztürk *et al.*, 2007; Singer & Clark, 1999; Varga *et al.*, 1987; Welch *et al.*, 1990). On the basis of our data, we propose that due to the slowing of proliferation and inhibition of migration, fibroblasts after PDR treatment are funnelling metabolic energy to other processes, such as collagen synthesis. This theory was supported by Oztürk *et al* where hypericin treated cells resulted in a slowing of proliferation and the formation of collagen granules in fibroblasts (Oztürk *et al.*, 2007).

Reactive oxygen species (ROS) are thought to be the main effector in PDR. As in skin ageing, ROS stimulates pathways and cytokines to be released to effect changes in cellular metabolism. A ROS assay was performed to confirm that ROS generation had, indeed, occurred after PDR treatment. This would support the fact that all changes demonstrated in the previous experiments were related to ROS produced by PDR and not solely by the light. In this assay a dye (DCF-DA) was used that once oxidised, fluoresces green, and detects various ROS (Halliwell & Gutteridge, 2007b). Two methods were used to analyse ROS production in the cells. The first method used flow cytometry to analyse the fluorescence within each individual cell and the second employed a 96-well based assay where the cell's fluorescence was determined using a fluorimeter. Both methods proved successful.

In using the two methodologies, it was shown that irradiated hypericin caused an increase in ROS in human dermal fibroblasts. Yellow and UVA light alone showed low ROS levels in comparison to the activated hypericin-treated cells. The ROS levels generated were not at overwhelming or cytotoxic levels as the PDR protocol was exactly the same as the cell viability assay where no cell death occurred. In addition, we showed that the protocol is indeed generating ROS and that the results are most likely not from the light irradiation alone. Low level ROS has been shown to be beneficial and affect signalling pathways in the cell to elicit positive reaction such as an increase in cellular activity (Halliwell & Gutteridge, 2007a; Lubart *et al.*, 2005, 2007).

Although the results gave the same conclusion, there were differences between the two methods' values. The flow cytometry method showed yellow laser light activated hypericin generates ROS 96±23.55% higher than basal where in the fluorimeter based assay the increase was only 42%±75.54. When UVA-irradiated hypericin was tested, the increase in ROS using flow cytometry was 186%±22.66 compared to 56%±53.82 using the fluorimeter. These differences between the two methods may be due to several reasons. Firstly, due to the nature of primary fibroblasts cultured from different patients used in each method, an inherent genotypic variation may account for the cell's response to activated hypericin. Secondly, the power density differences between 2 methods (irradiating 35mm dish and well in a 96-well plate), and the time of exposure differences, would have had an impact on the result. Finally, during the flow cytometric method it is most likely that the collection of cells through trypsinization, subsequent washes and resuspension in PBS could stress the cells, raising the levels artificially (Halliwell & Gutteridge, 2007d). However, the individual cell's fluorescence determined via flow cytometry is, perhaps, more accurate as it is a mean fluorescent signal from each individual cell compared to an overall fluorescence reading from a well of a plate.

When hypericin is irradiated it mainly generates singlet oxygen in an oxygen-dependent photochemical type II reaction (Agostinis *et al.*, 2002; Kiesslich *et al.*, 2006). Other ROS, such as superoxide anion, and hypericin radicals are also generated in similar photochemical reactions but to a lesser extent (English *et al.*, 1999; Gbur *et al.*, 2009). The intrinsic lifetime of singlet oxygen in a lipid environment is 13– 35μs and about 4μs in pure water (Buytaert *et al.*, 2007; Gbur *et al.*, 2009). This extremely short time makes detection of this ROS very difficult and needs specialised instruments such as spin trapping coupled with electron paramagnetic resonance spectroscopy (Lubart *et al.*, 2007). When ROS, such as singlet oxygen, are metabolised in the cell, hydrogen peroxide is generated. For this reason, DCF-DA was used and its green fluorescent emission made it an excellent choice as there was no overlap in spectral readings between it and hypericin.

As important as confirming ROS production, the location of the PS within the cell is intimately linked with PDR's mechanism of action. The subcellular location of hypericin closely relates to the area in which ROS can react (Huntosova *et al.*, 2010; Siboni *et al.*, 2002; Uzdensky *et al.*, 2001). It has been suggested that the biological photosensitization and cellular uptake of a PS and its final location can be more relevant to its efficacy than its basic photophysical properties (Siboni *et al.*, 2002).

We investigated hypericin's location in primary human dermal fibroblast after 16h incubation of hypericin in complete (serum supplemented) medium and its colocalization within three major organelles.

The three organelles investigated were: ER, Golgi apparatus and the mitochondria. Each organelle provides a specific and vital function within the cell. The ER is involved in protein and lipid synthesis in the cell (Campbell & Reece, 2002; Sherwood, 2010). The ER has a lower antioxidant concentration than other organelles in the cell. This provides an optimum redox state for ER-specific enzymes to catalyse the disulphide bridges needed for protein folding (Halliwell & Gutteridge, 2007e). The proteins are modified in the ER and leave in transport vesicles to the Golgi apparatus. The Golgi apparatus is involved in sorting, storing and moving these proteins to different locations in and out of the cell (Campbell & Reece, 2002). The mitochondria are the power houses of cell, generating the energy in the form of adenosine triphosphate (ATP) (Campbell & Reece, 2002). Mitochondria have been associated with the ageing process since 1956 (Halliwell & Gutteridge, 2007c). ROS produced for secondary signalling by the mitochondria or by errors in oxidation phosphorylation lead to oxidative damage and, eventually, the signs of ageing (Halliwell & Gutteridge, 2007c; Ma *et al.*, 2001).

In this study it was found that hypericin colocalized with the Golgi apparatus and to a lesser degree within the mitochondria. Interestingly, hypericin was not found to colocalize within the ER. It has been suggested that the membranes of intracellular organelles, such as the Golgi apparatus and mitochondria, can serve as a pump extracting hydrophobic molecules like hypericin from a weak solution and keeping them at a low cytosolic concentration (Uzdensky *et al.*, 2001). The uptake of hypericin was a slow process, therefore, the long time needed for hypericin's uptake emphasises that hypericin's entry into the cell may be due to its association with HSA or LDL (Uzdensky *et al.*, 2001). Interestingly, other authors have shown different hypericin incubation times result in different subcellular locations (Siboni *et al.*, 2002; Vuong *et al.*, 2011). In addition, in all experiments hypericin was not found in the nucleus. As ROS only acts within a small area, any ROS generated during PDR will most likely not affect the DNA. This is beneficial as the therapy has a small chance of becoming genotoxic. This re-iterates that the use of hypericin has to be complemented with an optimised PDR protocol.

Mitochondria in fibroblasts used in this project appeared as long fibrils in the primary human fibroblasts. Mitochondria appear differently in different cell types but most commonly in organised fibrils (Westermann, 2010). For example, the mitochondria appear as granules in WiDr cells, as granules and fibrils in NHIK cells, and mostly as fibrils in

glioblastoma cells D54Mg (Uzdensky *et al.*, 2001). Although their function is mainly to produce ATP for cellular metabolism, mitochondria are indispensable for the citric acid cycle, β-oxidation of fatty acids, haem synthesis and an initiator of apoptosis (Westermann, 2010)

Visualization of hypericin on the confocal microscope led to the power being approximately 250 times higher than in previous experiments (Section 3.2-3.5). The irradiation led to an instant change in the mitochondrial morphology from fibrils to a more beaded shape (Figure 3.6.6). This drastic change in shape was unexpected and novel. A reasonable explanation for it though, is that it is related to the state of fusion and fission (Westermann, 2010).

Mitochondria exist in a state of fusion in the cell and this is often seen microscopically as fibrils. This allows the mitochondrion's outer membranes to fuse with one another allowing for quick communication and dissipation of metabolic energy (Westermann, 2010). Fission is evident during cell division and apoptotic events. As the activation of hypericin resulted in high levels of ROS, it is likely that the fission seen in our samples is related to apoptosis as there are links with dissociating mitochondria and this form of cell death (Westermann, 2010).

It must be said that the changes seen in the mitochondria of the fibroblasts are probably not seen during the PDR treatment under the protocol established in this project. The changes were due to the high power and are not representative of mitochondrial morphology during PDR.

Studies have shown that activated PS located within the ER generate a high level of free calcium which in turns causes a release of cytochrome c from the mitochondria and initiates programmed cell death – apoptosis (Buytaert *et al.*, 2007; Castano *et al.*, 2005). Hypericin at a low dose has been shown to modulate calcium but is not related to cell death (Pfaffel-Schubart *et al.*, 2006; Piette *et al.*, 2003). It is, therefore, advantageous that hypericin is not located in the ER with our protocol as it is not likely to trigger apoptosis through this mechanism. A PS located within the mitochondria cause an uncoupling of the oxidative phosphorylation chain leading to necrosis. In addition, damage to the mitochondria can trigger apoptosis via various signalling molecules and pathways as reviewed in several papers (Almeida *et al.*, 2004; Buytaert *et al.*, 2007; Castano *et al.*, 2005). In this regard, it should be treated with caution that hypericin mediated PDR may affect the mitochondria. However, due to that fact that cell viability was not decreased in earlier experiments, this most likely does not occur in our protocol. There is scant information regarding the Golgi apparatus' involvement in PDR treatment. MAP kinases are also targeted by activated hypericin however, the specific proteins upregulated and phosphorylated appears to be cell

type and protocol dependent (Assefa *et al.*, 1999; Buytaert *et al.*, 2006; Hendrickx *et al.*, 2005; Pfaffel-Schubart *et al.*, 2006; Piette *et al.*, 2003). It appears that the PS concentration and irradiation protocol are extremely important and the incorrect PDR treatment will tip the cells towards a catastrophe rather than having a beneficial effect through altering intracellular signalling cascades (Assefa *et al.*, 1999; Buytaert *et al.*, 2006; Kiesslich *et al.*, 2006; Piette *et al.*, 2003).

To this end, the *in vitro* experiments in this project lay the foundation for future hypericin-mediated PDR. This project shows the location of hypericin within the cell, and an increase in cell viability, which indicates the protocol used here most likely will not have negative or cytotoxic events and may push the cell towards collagen production.

5. Chapter 5: Conclusion and Future Directions

5.1. Conclusion

Photodynamic therapy (PDR) is a relatively new therapy used to treat the signs of ageing. However, an established protocol which gives consistent results does not exist (Table 1.5.1). In addition, little is known about the molecular mechanism of this treatment regime (Table 1.5.2). The main objective of this project, therefore, was to optimise a protocol based on PDR using the photosensitizer (PS) hypericin and characterise its effects on primary human dermal fibroblasts. These cells were chosen as they are the chief cell type in the dermis where some of the most prominent signs of ageing occur.

In determining the time for maximum cellular uptake of the PS, three hypericin concentrations were tested. Hypericin's uptake will ultimately decide its final location in the fibroblasts and its mechanism of action during PDR treatment. It was found that hypericin reached a maximum concentration after 16h for the lowest concentration (0.25µM) and 10h for both 0.5µM and 1µM hypericin. Ultimately, 16h incubation time was decided upon as there was not a significant difference between 10 and 16h with the higher concentrations (0.5µM and 1µM) and this time was in agreement with the literature (Berlanda *et al.*, 2010; Hendrickx *et al.*, 2005).

Three different wavelengths of light were utilized to activate hypericin in this project. Moreover, different energy and power densities were used for each wavelength. These wavelengths are linked to the absorbance spectrum of hypericin and are related to the manner in which this compound captures different wavelengths of light (Figure 1.5.2). All the wavelengths displayed an increase in cell viability with low hypericin concentrations (0.25-0.5µM). Once a hypericin concentration and irradiation protocol was decided upon for each wavelength, we sought to characterise its effect on the fibroblasts.

The increase in cell viability could relate to an affect on the proliferation rate or cellular activity. We investigated its effect on growth and showed PDR treatment did not affect the proliferation of fibroblast with any of the wavelengths and their associated hypericin concentration. We investigated cellular activity through a scratch assay to determine if the migration rate of the fibroblasts was affected. We found that yellow laser light activation of hypericin significantly decreased the rate of wound closure compared to the control fibroblasts. As reactive oxygen species (ROS) is believed to be the main mediator in altering signalling toward rejuvenation in PDR, we confirmed that ROS was being generated through

this therapy using the oxidation-sensitive dye, DCF-DA. Both yellow laser and UVA light activation of 0.25μM hypericin caused an increase in ROS.

Taken together these results show hypericin used in PDR did not affect the growth rate of cells, instead inhibited the migration of the cells and resulted in an immediate, non-toxic increase in ROS production.

Finally, we sought to uncover hypericin's location within the fibroblast and its colocalization with major cellular organelles. Hypericin colocalized to the Golgi apparatus and to a lesser degree to the mitochondria. Interestingly, hypericin was not found in the ER or the nucleus. This was considered advantageous as ROS generated in the ER could cause free calcium to leak from the organelle initiating apoptosis. In addition, its absence in the nucleus would not result in genotoxic mutations of DNA in the nucleus. Partial colocalization with the mitochondria should be raised as a point of concern as this organelle is linked with inducing apoptosis and necrosis if the ROS levels are too high.

This work underlines the importance of *in vitro* characterization of PDR therapy as inappropriate hypericin concentrations and irradiation protocol result in a decrease in viable cells (Section 3.2) and further detrimental effects.

Overall this optimised protocol shows PDR using hypericin has the potential to cause an increase in cellular activity. This increase in activity could be an upregulation of cellular metabolism resulting in regulation of the ECM as demonstrated in other studies (Najafizadeh *et al.*, 2012; Oztürk *et al.*, 2007). This would require further investigation into the gene and protein expression levels of dermal matrix proteins and characterization in other skin cell types.

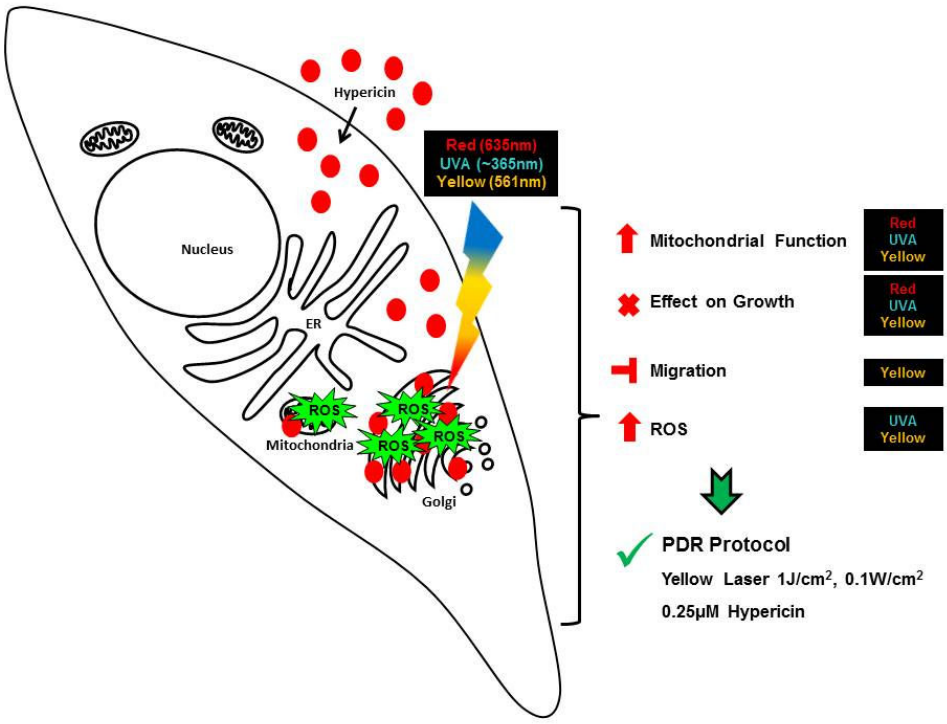

Figure 5.1.1 The diagram represents a summary of the work reported in this dissertation. Hypericin (seen here as red dots) moved into the cell and was mainly located in the Golgi apparatus and to a lesser degree in the mitochondria. Hypericin was not seen exclusively in the endoplasmic reticulum (ER). When hypericin was irradiated with the three different wavelengths of light reactive oxygen species (ROS) were generated. The effects of this PDR therapy are reported on the right-hand side of this diagram where an increase of mitochondrial function was noted with all three wavelengths. There was no effect on growth when PDR was performed. Yellow laser light activated hypericin resulted in an inhibition of fibroblast migration and hypericin irradiated with yellow laser and UVA light resulted in non-cytotoxic levels of ROS being formed. Overall, the hypericin activated with yellow laser shows promise as a PDR treatment.

5.2. Future Directions and Considerations

The work from this project forms a strong base in establishing a PDR protocol using hypericin. While there is still much work to be done before hypericin mediated PDR could be considered viable for clinical applications, the data presented here makes a compelling case for hypericin-mediated PDR to be considered as a strong candidate in cosmetic biology.

Human skin fibroblasts were the only cell type used in this research. However, investigations following the same rationale could be employed on the other two major skin cell types i.e. keratinocytes and melanocytes. Furthermore, a three-dimensional model representing all three cell types would be ideal as this would simulate an *in vivo* situation. In this scenario, fibroblasts are seeded into collagen matrices simulating the dermis and keratinocytes and melanocytes seeded together to form a stratified layer on top of the matrix in a similar manner to the epidermis. In this way paracrine signalling between the cells could occur during and after PDR treatment. In addition, an environment where fibroblasts can attach to the ECM may give a more realistic view of what may occur in the skin. This is due to the fibroblasts, not only being stimulated through signalling cascades, but through their mechanosensing attachment to the matrix affecting their metabolism.

To fully elucidate the molecular mechanism behind PDR treatment using hypericin analysis, ECM genes and proteins would need to be determined at several time points in three skin cell types, individually or combined in a 3 dimensional model. Initial candidates for analyses include: collagen type I and MMP-1. Transient alterations in collagen synthesis and active MMP secretions would contribute to the elucidation of PDR treatment and, thus, illuminate novel rejuvenation processes. Both collagen type I and MMP-1 are secreted proteins and, thus, cell lysates cannot be used for their analysis via western blots. However, procollagen could be detected from cell lysates and this would relate to overall collagen synthesis. Serum-free conditioned medium would be used for MMP-1 detection. Furthermore, zymography could be used to confirm the activity of this enzyme to assure that it is not kept in its inactive zymogen/inhibited form.

Following the interesting results seen in the subcellular colocalization experiments, another organelle that would be fascinating to follow up on would be intracellular lysosomes. Lysosomes are important for removing cellular debris and are formed from endosomes generated by the Golgi apparatus. There is, thus, an integral link between the two organelles. Hypericin has been shown to colocalize with lysosomes in other cell types (Ali & Olivo, 2002; Buytaert *et al.*, 2006; Galanou *et al.*, 2008; Kascakova *et al.*, 2008; Siboni *et al.*, 2002; Theodossiou *et al.*, 2004) and the information gleaned from these further experiments would

provide a more complete picture of hypericin's location is relation to all the major cellular organelles.

This research will not only provide a solid foundation in hypericin's use for PDR but may also uncover the molecular mechanism common to this therapy regardless of PS or light source used. However, caution should always be employed when extrapolating *in vitro* result to an *in vivo* application.

6. Chapter 6: References

Abrahamse, H. & D, P. 2009. Molecular perspectives of wound healing--cellular models. *Photomedicine And Laser Surgery*. 27(5):693-4.

Agostinis, P., Berg, K., Cengel, K.A., Foster, T.H., Girotti, A.W., Gollnick, S.O., Hahn, S.M., Hamblin, M.R., Juzeniene, A., Kessel, D., Korbelik, M., Moan, J., Mroz, P., Nowis, D., Piette, J., Wilson, B.C., & Golab, J. 2011. Photodynamic therapy of cancer: an update. *CA: A Cancer Journal for Clinicians*. 61(4):250-81.

Agostinis, P., Vantieghem, A., Merlevede, W., & de Witte, P.A.M. 2002. Hypericin in cancer treatment: more light on the way. *The International Journal of Biochemistry & Cell Biology*. 34(3):221-41.

Alberts, B., Johnson, A., Lewis, J., Raff, M., Roberts, K., & Walter, P. 2002. Molecular Biology of the Cell. Garland Science: New York, pp. 118-127.

Alecu, M., Ursaciuc, C., Hãlãlãu, F., Coman, G., Merlevede, W., Waelkens, E., & de Witte, P. 1998. Photodynamic treatment of basal cell carcinoma and squamous cell carcinoma with hypericin. *Anticancer Research*. 18(6B):4651-4.

Alexiades-Armenakas, M.R. & Geronemus, R.G. 2003. Laser-mediated photodynamic therapy of actinic keratoses. *Archives of Dermatology*. 139(10):1313-20.

Ali, S.M. & Olivo, M. 2002. Bio-distribution and subcellular localization of Hypericin and its role in PDT induced apoptosis in cancer cells. *International Journal of Oncology*. 21(3):531-40.

Allison, R.R. & Sibata, C.H. 2010. Oncologic photodynamic therapy photosensitizers: a clinical review. *Photodiagnosis and Photodynamic Therapy*. *Elsevier B.V.* 7(2):61-75.

Almeida Issa, M.C., Piñeiro-Maceira, J., Farias, R.E., Pureza, M., Raggio Luiz, R., & Manela-Azulay, M. 2009. Immunohistochemical expression of matrix metalloproteinases in photodamaged skin by photodynamic therapy. *The British Journal of Dermatology*. 161(3):647-53.

Almeida, R.D., Manadas, B.J., Carvalho, A.P., & Duarte, C.B. 2004. Intracellular signaling mechanisms in photodynamic therapy. *Biochimica et Biophysica acta*. 1704(2):59-86.

Armstrong, R. 1992. Photobiology of Ultraviolet radiation. Abel, E. (Ed.), Photochemotherapy in Dermatology. Igaku-Shoin Medical Publishers: New York, Tokyo, p. 28.

Assefa, Z., Vantieghem, A., Declercq, W., Vandenabeele, P., Vandenheede, J.R., Merlevede, W., de Witte, P., & Agostinis, P. 1999. The activation of the c-Jun N-terminal kinase and p38 mitogen-activated protein kinase signaling pathways protects HeLa cells from apoptosis following photodynamic therapy with hypericin. *The Journal of Biological Chemistry*. 274(13):8788-96.

Avram, M.R., Tsao, S., Tannous, Z., & Avram, M. 2006. Color Atlas of Cosmetic Dermatology. McGraw-Hill Professional.

Berlanda, J., Kiesslich, T., Engelhardt, V., Krammer, B., & Plaetzer, K. 2010. Comparative in vitro study on the characteristics of different photosensitizers employed in PDT. *Journal of Photochemistry and Photobiology. B, Biology*. *Elsevier B.V.* 100(3):173-80.

Bickers, D.R. & Athar, M. 2006. Oxidative stress in the pathogenesis of skin disease. *The Journal of Investigative Dermatology*. 126(12):2565-75.

Bjerring, P., Christiansen, K., Troilius, A., Bekhor, P., & de Leeuw, J. 2009. Skin fluorescence controlled photodynamic photorejuvenation (wrinkle reduction). *Lasers in Surgery and Medicine*. 41(5):327-36.

Blank, M., Kostenich, G., Lavie, G., Kimel, S., Keisari, Y., & Orenstein, A. 2002. Wavelength-dependent properties of photodynamic therapy using hypericin in vitro and in an animal model. *Photochemistry and Photobiology*. 76(3):335-40.

Brennan, M., Bhatti, H., Nerusu, K.C., Bhagavathula, N., Kang, S., Fisher, G.J., Varani, J., & Voorhees, J.J. 2003. Matrix metalloproteinase-1 is the major collagenolytic enzyme responsible for collagen damage in UV-irradiated human skin. *Photochemistry and Photobiology*. 78(1):43-8.

Brenneisen, P., Sies, H., & Scharffetter-Kochanek, K. 2002. Ultraviolet-B irradiation and matrix metalloproteinases: from induction via signaling to initial events. *Annals of the New York Academy of Sciences*. 973:31-43.

Brenneisen, P., Wenk, J., Klotz, L.O., Wlaschek, M., Briviba, K., Krieg, T., Sies, H., & Scharffetter-Kochanek, K. 1998. Central role of Ferrous/Ferric iron in the ultraviolet B irradiation-mediated signaling pathway leading to increased interstitial collagenase (matrix-degrading metalloprotease (MMP)-1) and stromelysin-1 (MMP-3) mRNA levels in cultured human dermal fibrobl. *The Journal of Biological Chemistry*. 273(9):5279-87.

Bruscino, N., Rossi, R., Dindelli, M., Ghersetich, I., & Lotti, T. 2010. Therapeutic Hotline: Facial skin rejuvenation in a patient treated with photodynamic therapy for actinic keratosis. *Dermatologic Therapy*. 23(1):86-9.

Bublik, M., Head, C., Benharash, P., Paiva, M., Eshraghi, A., Kim, T., & Saxton, R. 2006. Hypericin and pulsed laser therapy of squamous cell cancer in vitro. *Photomedicine and Laser Surgery*. 24(3):341-7.

Buggiani, G., Troiano, M., Rossi, R., & Lotti, T. 2008. Photodynamic therapy: off-label and alternative use in dermatological practice. *Photodiagnosis and Photodynamic Therapy*. 5(2):134-8.

Buriankova, L., Buzova, D., Chorvat, D., Sureau, F., Brault, D., Miskovský, P., & Jancura, D. 2011. Kinetics of hypericin association with low-density lipoproteins. *Photochemistry and Photobiology*. 87(1):56-63.

Buytaert, E., Callewaert, G., Hendrickx, N., Scorrano, L., Hartmann, D., Missiaen, L., Vandenheede, J.R., Heirman, I., Grooten, J., & Agostinis, P. 2006. Role of endoplasmic

reticulum depletion and multidomain proapoptotic BAX and BAK proteins in shaping cell death after hypericin-mediated photodynamic therapy. *FASEB journal : official publication of the Federation of American Societies for Experimental Biology*. 20(6):756-8.

Buytaert, E., Dewaele, M., & Agostinis, P. 2007. Molecular effectors of multiple cell death pathways initiated by photodynamic therapy. *Biochimica et Biophysica acta*. 1776(1):86-107.

Buytaert, E., Matroule, J.Y., Durinck, S., Close, P., Kocanova, S., Vandenheede, J.R., de Witte, P. a, Piette, J., & Agostinis, P. 2008. Molecular effectors and modulators of hypericin-mediated cell death in bladder cancer cells. *Oncogene*. 27(13):1916-29.

Callaghan, T.M. & Wilhelm, K.-P. 2008. A review of ageing and an examination of clinical methods in the assessment of ageing skin. Part I: Cellular and molecular perspectives of skin ageing. *International Journal of Cosmetic Science*. 30(5):313-22.

Campbell, N.A. & Reece, J.B. 2002. A tour of the cell. Biology. Pearson Education: San Fransico, pp. 108-126.

Castano, A.P., Demidova, T.N., & Hamblin, M.R. 2004. Mechanisms in photodynamic therapy: part one—photosensitizers, photochemistry and cellular localization. *Photodiagnosis and Photodynamic Therapy*. 1(4):279-293.

Castano, A.P., Demidova, T.N., & Hamblin, M.R. 2005. Mechanisms in photodynamic therapy: part two—cellular signaling, cell metabolism and modes of cell death. *Photodiagnosis and Photodynamic Therapy*. 2(1):1-23.

Chen, B., Xu, Y., Roskams, T., Delaey, E., Agostinis, P., Vandenheede, J.R., & de Witte, P. 2001. Efficacy of antitumoral photodynamic therapy with hypericin: relationship between biodistribution and photodynamic effects in the RIF-1 mouse tumor model. *International Journal of Cancer. Journal International du Cancer*. 93(2):275-82.

Choi, J.Y., Park, G.T., Na, E.Y., Wi, H.S., Lee, S.-C., & Lee, J.-B. 2010. Molecular changes following topical photodynamic therapy using methyl aminolaevulinate in mouse skin. *Journal of dermatological science*. *Japanese Society for Investigative Dermatology*. 58(3):198-203.

Choudhury, A., Dominguez, M., Puri, V., Sharma, D.K., Narita, K., Wheatley, C.L., Marks, D.L., & Pagano, R.E. 2002. Rab proteins mediate Golgi transport of caveola-internalized glycosphingolipids and correct lipid trafficking in Niemann-Pick C cells. *The Journal of Cinical Investigation*. 109(12):1541-50.

Christiansen, K., Bjerring, P., & Troilius, A. 2007. 5-ALA for photodynamic photorejuvenation--optimization of treatment regime based on normal-skin fluorescence measurements. *Lasers in Surgery and Medicine*. 39(4):302-10.

Chung, K.Y., Agarwal, A., Uitto, J., & Mauviel, A. 1996. An AP-1 binding sequence is essential for regulation of the human alpha2(I) collagen (COL1A2) promoter activity by transforming growth factor-beta. *The Journal of Biological Chemistry*. 271(6):3272-8.

Chung, P.S., Rhee, C.K., Kim, K.H., Paek, W., Chung, J., Paiva, M.B., Eshraghi, A.A., Castro, D.J., & Saxton, R.E. 2000. Intratumoral hypericin and KTP laser therapy for transplanted squamous cell carcinoma. *The Laryngoscope*. 110(8):1312-6.

Chung, P.S., Saxton, R.E., Paiva, M.B., Rhee, C.K., Soudant, J., Mathey, A., Foote, C., & Castro, D.J. 1994. Hypericin uptake in rabbits and nude mice transplanted with human squamous cell carcinomas: study of a new sensitizer for laser phototherapy. *The Laryngoscope*. 104(12):1471-6.

Clementoni, M.T., B-Roscher, M., & Munavalli, G.S. 2010. Photodynamic photorejuvenation of the face with a combination of microneedling, red light, and broadband pulsed light. *Lasers in Surgery and Medicine*. 42(2):150-9.

Couldwell, W.T., Surnock, A. a, Tobia, A.J., Cabana, B.E., Stillerman, C.B., Forsyth, P. a, Appley, A.J., Spence, A.M., Hinton, D.R., & Chen, T.C. 2011. A phase 1/2 study of orally administered synthetic hypericin for treatment of recurrent malignant gliomas. *Cancer*. 117(21):4905-15.

Crnolatac, I., Huygens, A., Agostinis, P., Kamuhabwa, A.R., Maes, J., van Aerschot, A., & De Witte, P. a M. 2007. In vitro accumulation and permeation of hypericin and lipophilic analogues in 2-D and 3-D cellular systems. *International Journal of Oncology*. 30(2):319-24.

Da Silva, J.P., Da Silva, M.A., Almeida, A.P.F., Lombardi Junior, I., & Matos, A.P. 2010. Laser therapy in the tissue repair process: a literature review. *Photomedicine and Laser Surgery*. 28(1):17-21.

Das, K., Smirnov, a V., Wen, J., Miskovsky, P., & Petrich, J.W. 1999. Photophysics of hypericin and hypocrellin A in complex with subcellular components: interactions with human serum albumin. *Photochemistry and Photobiology*. 69(6):633-45.

Davids, L.M. 2003. Mitochondrial targeting of wild-type and mutant human protoporphyrinogen oxidase (PPOX). University of Cape Town.

Davids, L.M., Kleemann, B., Cooper, S., & Kidson, S.H. 2009. Melanomas display increased cytoprotection to hypericin-mediated cytotoxicity through the induction of autophagy. *Cell Biology International*. 33(10):1065-72.

Davids, L.M., Kleemann, B., Kacerovská, D., Pizinger, K., & Kidson, S.H. 2008. Hypericin phototoxicity induces different modes of cell death in melanoma and human skin cells. *Journal of Photochemistry and Photobiology. B, Biology*. 91(2–3):67-76.

De Sousa, A.P.C., Santos, J.N., Dos Reis, J. a, Ramos, T. a, de Souza, J., Cangussú, M.C.T., & Pinheiro, A.L.B. 2010. Effect of LED phototherapy of three distinct wavelengths on fibroblasts on wound healing: a histological study in a rodent model. *Photomedicine and Laser Surgery*. 28(4):547-52.

Delaey, E.M., Obermuëller, R., Zupkó, I., De Vos, D., Falk, H., & de Witte, P. a. 2001. In vitro study of the photocytotoxicity of some hypericin analogs on different cell lines. *Photochemistry and Photobiology*. 74(2):164-71.

Dierickx, C.C. & Anderson, R.R. 2005. Visible light treatment of photoaging. *Dermatologic Therapy*. 18(3):191-208.

Dong, K.K., Damaghi, N., Picart, S.D., Markova, N.G., Obayashi, K., Okano, Y., Masaki, H., Grether-Beck, S., Krutmann, J., Smiles, K.A., & Yarosh, D.B. 2008. UV-induced DNA damage initiates release of MMP-1 in human skin. *Experimental Dermatology*. 17(12):1037-44.

Dover, J.S., Bhatia, A.C., Stewart, B., & Arndt, K.A. 2005. Topical 5-aminolevulinic acid combined with intense pulsed light in the treatment of photoaging. *Archives of Dermatology*. 141(10):1247-52.

Du, H.-Y., Olivo, M., Mahendran, R., Huang, Q., Shen, H.-M., Ong, C.-N., & Bay, B.-H. 2007. Hypericin photoactivation triggers down-regulation of matrix metalloproteinase-9 expression in well-differentiated human nasopharyngeal cancer cells. *Cellular and Molecular Life Sciences : CMLS*. 64(7–8):979-88.

D'Hallewin, M.-A., Kamuhabwa, a R., Roskams, T., De Witte, P. a M., & Baert, L. 2002. Hypericin-based fluorescence diagnosis of bladder carcinoma. *BJU international*. 89(7):760-3.

English, D.S., Doyle, R.T., Petrich, J.W., & Haydon, P.G. 1999. Subcellular distributions and excited-state processes of hypericin in neurons. *Photochemistry and Photobiology*. 69(3):301-5.

Fagot, D., Asselineau, D., & Bernerd, F. 2002. Direct role of human dermal fibroblasts and indirect participation of epidermal keratinocytes in MMP-1 production after UV-B irradiation. *Archives of Dermatological Research*. 293(11):576-83.

Farage, M. a, Miller, K.W., Elsner, P., & Maibach, H.I. 2008. Intrinsic and extrinsic factors in skin ageing: a review. *International Journal of Cosmetic Science*. 30(2):87-95.

Fisher, G.J., Datta, S., Wang, Z., Li, X.Y., Quan, T., Chung, J.H., Kang, S., & Voorhees, J.J. 2000. c-Jun-dependent inhibition of cutaneous procollagen transcription following ultraviolet irradiation is reversed by all-trans retinoic acid. *The Journal of Clinical Investigation*. 106(5):663-70.

Fisher, G.J., Datta, S.C., Talwar, H.S., Wang, Z.Q., Varani, J., Kang, S., & Voorhees, J.J. 1996. Molecular basis of sun-induced premature skin ageing and retinoid antagonism. *Nature*. 379(6563):335-9.

Fisher, G.J., Kang, S., Varani, J., Bata-Csorgo, Z., Wan, Y., Datta, S., & Voorhees, J.J. 2002. Mechanisms of photoaging and chronological skin aging. *Archives of Dermatology*. 138(11):1462-70.

Fisher, G.J., Quan, T., Purohit, T., Shao, Y., Cho, M.K., He, T., Varani, J., Kang, S., & Voorhees, J.J. 2009. Collagen fragmentation promotes oxidative stress and elevates matrix metalloproteinase-1 in fibroblasts in aged human skin. *The American Journal of Pathology*. 174(1):101-14.

Fisher, G.J., Talwar, H.S., Lin, J., Lin, P., Mcphillips, F., Wang, Z., Li, X., Wan, Y., Kang, S., & Voorhees, J.J. 1998. Retinoic acid inhibits induction of c-Jun protein by ultraviolet radiation

that occurs subsequent to activation of Mitogen-activated Protein Kinase pathways in human skin in vivo. *The Journal of Clinical Investigation*. 101(6).

Fisher, G.J., Varani, J., & Voorhees, J.J. 2008. Looking older: fibroblast collapse and therapeutic implications. *Archives of Dermatology*. 144(5):666-72.

Fisher, G.J. & Voorhees, J.J. 1998. Molecular mechanisms of photoaging and its prevention by retinoic acid: ultraviolet irradiation induces MAP kinase signal transduction cascades that induce Ap-1-regulated matrix metalloproteinases that degrade human skin in vivo. *The Journal of Investigative Dermatology. Symposium proceedings / the Society for Investigative Dermatology, Inc. [and] European Society for Dermatological Research*. 3(1):61-8.

Fisher, G.J., Wang, Z.Q., Datta, S.C., Varani, J., Kang, S., & Voorhees, J.J. 1997. Pathophysiology of premature skin aging induced by ultraviolet light. *The New England Journal of Medicine*. 337(20):1419-28.

Frigo, L., Fávero, G.M., Lima, H.J.C., Maria, D.A., Bjordal, J.M., Joensen, J., Iversen, V.V., Marcos, R.L., Parizzoto, N.A., & Lopes-Martins, R.A.B. 2010. Low-level laser irradiation (InGaAlP-660 nm) increases fibroblast cell proliferation and reduces cell death in a dose-dependent manner. *Photomedicine and Laser Surgery*. 28 Suppl 1(0):S151-6.

Galanou, M.C., Theodossiou, T. a, Tsiourvas, D., Sideratou, Z., & Paleos, C.M. 2008. Interactive transport, subcellular relocation and enhanced phototoxicity of hypericin encapsulated in guanidinylated liposomes via molecular recognition. *Photochemistry and Photobiology*. 84(5):1073-83.

Gambichler, T., Matip, R., Moussa, G., Altmeyer, P., & Hoffmann, K. 2006. In vivo data of epidermal thickness evaluated by optical coherence tomography: effects of age, gender, skin type, and anatomic site. *Journal of Dermatological Science*. 44(3):145-52.

Gbur, P., Dedic, R., Chorvat, D., Miskovsky, P., Hala, J., & Jancura, D. 2009. Time-resolved luminescence and singlet oxygen formation after illumination of the hypericin-low-density lipoprotein complex. *Photochemistry and Photobiology*. 85(3):816-23.

Gene Entrez. 2011. http://www.ncbi.nlm.nih.gov/gene [WWW Document].

Ghaffari, A., Kilani, R.T., & Ghahary, A. 2009. Keratinocyte-conditioned media regulate collagen expression in dermal fibroblasts. *The Journal of Investigative Dermatology*. 129(2):340-7.

Gilchrest, B.A. 1996. A review of skin ageing and its medical therapy. *The British Journal of Dermatology*. 135(6):867-75.

Gilchrest, B.A. 2006. Skin aging with 24 tables. Springer: Berlin.

Glogau, R.G. 1996. Aesthetic and anatomic analysis of the aging skin. *Seminars in Cutaneous Medicine and Surgery*. 15(3):134-8.

Gold, M.H., Bradshaw, V.L., Boring, M.M., Bridges, T.M., & Biron, J. a. 2006. Split-face comparison of photodynamic therapy with 5-aminolevulinic acid and intense pulsed light versus intense pulsed light alone for photodamage. *Dermatologic Surgery : official*

publication for American Society for Dermatologic Surgery [et al.]. 32(6):795-801; discussion 801-3.

Gold, M.H. & Goldman, M.P. 2004. 5-aminolevulinic acid photodynamic therapy: where we have been and where we are going. *Dermatologic Surgery : official publication for American Society for Dermatologic Surgery [et al.]*. 30(8):1077-83; discussion 1083-4.

Goldman, M.P., Weiss, R.A., & Weiss, M.A. 2005. Intense pulsed light as a nonablative approach to photoaging. *Dermatologic Surgery : official publication for American Society for Dermatologic Surgery [et al.]*. 31(9 Pt 2):1179-87; discussion 1187.

Grotendorst, G.R., Rahmanie, H., & Duncan, M.R. 2004. Combinatorial signaling pathways determine fibroblast proliferation and myofibroblast differentiation. *FASEB journal : official publication of the Federation of American Societies for Experimental Biology*. 18(3):469-79.

Gu, W., Liu, W., Yang, X., Zhao, X., Yuan, X., Ma, H., Tian, Y., & Meng, R. 2011. Effects of intense pulsed light and ultraviolet A on metalloproteinases and extracellular matrix expression in human skin. *Photomedicine and Laser Surgery*. 29(2):97-103.

Haddad, A., Santos, I.D.D.A.O., Gragnani, A., & Ferreira, L.M. 2011. The effect of increasing fluence on the treatment of actinic keratosis and photodamage by photodynamic therapy with 5-aminolevulinic acid and intense pulsed light. *Photomedicine and Laser Surgery*. 29(6):427-32.

Hager, B., Strauss, W.S.L., & Falk, H. 2009. Cationic hypericin derivatives as novel agents with photobactericidal activity: synthesis and photodynamic inactivation of Propionibacterium acnes. *Photochemistry and Photobiology*. 85(5):1201-6.

Halliwell, B. & Gutteridge, J.M.C. 2007a. Consequence of oxidative stress: proliferation, adaptation, senescence, damage or death? Halliwell, B., Gutteridge, J.M.C. (Eds.), Free Radicals in Biology and Medicine. Oxford University Press: Oxford, pp. 188-191.

Halliwell, B. & Gutteridge, J.M.C. 2007b. Studies of “generalized” light emission (luminescence/fluorescence). ,Halliwell, B., Gutteridge, J.M.C. (Eds.), Free Radicals Biology and Medicine. Oxford University Press: Oxford, pp. 304-305.

Halliwell, B. & Gutteridge, J.M.C. 2007c. Oxidative damage: a common link between all the theories of ageing? Halliwell, B., Gutteridge, J.M.C. (Eds.), Free Radicals in Biology and Medicine. Oxford University Press: Oxford, pp. 624-626.

Halliwell, B. & Gutteridge, J.M.C. 2007d. Artefacts in cell culture. Halliwell, B., Gutteridge, J.M.C. (Eds.), Free Radicals in Biology and Medicine. Oxford University Press: Oxford, p. 28.

Halliwell, B. & Gutteridge, J.M.C. 2007e. Protein-disulphide isomerase. Halliwell, B., Gutteridge, J.M.C. (Eds.), Free Radicals in Biology and Medicine. Oxford University Press: Oxford, p. 121.

Hawkins, D.H. & Abrahamse, H. 2006. The role of laser fluence in cell viability, proliferation, and membrane integrity of wounded human skin fibroblasts following Helium-Neon laser irradiation. *Cell*. 38:74-83.

Head, C.S., Luu, Q., Sercarz, J., & Saxton, R. 2006. Photodynamic therapy and tumor imaging of hypericin-treated squamous cell carcinoma. *World Journal of Surgical Oncology*. 4:87.

Hendrickx, N., Dewaele, M., Buytaert, E., Marsboom, G., Janssens, S., Van Boven, M., Vandenheede, J.R., de Witte, P., & Agostinis, P. 2005. Targeted inhibition of p38alpha MAPK suppresses tumor-associated endothelial cell migration in response to hypericin-based photodynamic therapy. *Biochemical and Biophysical Research Communications*. 337(3):928-35.

Houreld, N.N. & Abrahamse, H. 2007. Effectiveness of Helium-Neon laser irradiation on viability and cytotoxicity of diabetic-wounded fibroblast cells. *Photomedicine And Laser Surgery*. 25(6):474-481.

Huang, J., Luo, X., Lu, J., Chen, J., Zuo, C., Xiang, Y., Yang, S., Tan, L., Kang, J., & Bi, Z. 2011. IPL irradiation rejuvenates skin collagen via the bidirectional regulation of MMP-1 and TGF-β1 mediated by MAPKs in fibroblasts. *Lasers in Medical Science*. 26(3):381-7.

Huntosova, V., Alvarez, L., Bryndzova, L., Nadova, Z., Jancura, D., Buriankova, L., Bonneau, S., Brault, D., Miskovsky, P., & Sureau, F. 2010. Interaction dynamics of hypericin with low-density lipoproteins and U87-MG cells. *International Journal of Pharmaceutics*. 389(1–2):32-40.

Ignotz, R. a & Massagué, J. 1986. Transforming growth factor-beta stimulates the expression of fibronectin and collagen and their incorporation into the extracellular matrix. *The Journal of Biological Chemistry*. 261(9):4337-45.

Imokawa, G. 2009. Mechanism of UVB-induced wrinkling of the skin: paracrine cytokine linkage between keratinocytes and fibroblasts leading to the stimulation of elastase. *The Journal of Investigative Dermatology. Symposium proceedings / the Society for Investigative Dermatology, Inc. [and] European Society for Dermatological Research*. 14(1):36-43.

Issa, M.C.A., Piñeiro-Maceira, J., Vieira, M.T.C., Olej, B., Mandarim-de-Lacerda, C.A., Luiz, R.R., & Manela-Azulay, M. 2010. Photorejuvenation with topical methyl aminolevulinate and red light: a randomized, prospective, clinical, histopathologic, and morphometric study. *Dermatologic Surgery : official publication for American Society for Dermatologic Surgery [et al.]*. 36(1):39-48.

Jenkins, G. 2002. Molecular mechanisms of skin ageing. *Mechanisms of Ageing and Development*. 123(7):801-10.

Kacerovská, D., Pizinger, K., Majer, F., & Smíd, F. 2008. Photodynamic therapy of nonmelanoma skin cancer with topical hypericum perforatum extract--a pilot study. *Photochemistry and Photobiology*. 84(3):779-85.

Karrer, S., Bosserhoff, A.K., Weiderer, P., Landthaler, M., & Szeimies, R.-M. 2004. Keratinocyte-derived cytokines after photodynamic therapy and their paracrine induction of matrix metalloproteinases in fibroblasts. *The British Journal of Dermatology*. 151(4):776-83.

Karrer, S., Bosserhoff, A.K., Weiderer, P., Landthaler, M., & Szeimies, R.-markus. 2003. Influence of 5-aminolevulinic acid and red light on collagen metabolism of human dermal fibroblasts. *The Journal of Investigative Dermatology*. 120(2):325-31.

Kascakova, S., Nadova, Z., Mateasik, A., Mikes, J., Huntosova, V., Refregiers, M., Sureau, F., Maurizot, J.-C., Miskovsky, P., & Jancura, D. 2008. High level of low-density lipoprotein receptors enhance hypericin uptake by U-87 MG cells in the presence of LDL. *Photochemistry and Photobiology*. 84(1):120-7.

Kascakova, S., Refregiers, M., Jancura, D., Sureau, F., Maurizot, J.-C., & Miskovsky, P. 2005. Fluorescence spectroscopic study of hypericin-photosensitized oxidation of low-density lipoproteins. *Photochemistry and Photobiology*. 81(6):1395-403.

Kierszenbaum, A.L. 2002a. Integumentary System. Histology and Cell Biology. Mosby: United States of America, pp. 299-318.

Kierszenbaum, A.L. 2002b. Connective Tissue. Histology and Cell Biology. Mosby: United States of America, pp. 95-129.

Kiesslich, T., Krammer, B., & Plaetzer, K. 2006. Cellular mechanisms and prospective applications of hypericin in photodynamic therapy. *Current Medicinal Chemistry*. 13(18):2189-204.

Kocanova, S., Hornakova, T., Hritz, J., Jancura, D., Chorvat, D., Mateasik, A., Ulicny, J., Refregiers, M., Maurizot, J.-C., & Miskovsky, P. 2006. Characterization of the interaction of hypericin with protein kinase C in U-87 MG human glioma cells. *Photochemistry and Photobiology*. 82(3):720-8.

Kocanová, S., Laigle, A., & Miskovsky, P. 2003. Inhibition of Protein Kinase C Activity in 3T3 Mouse Fibroblasts by Photoactive Drug Hypericin. *Laser Physics*. 13(1):30-34.

Kohl, E., Torezan, L.A.R., Landthaler, M., & Szeimies, R.-m. 2010. Aesthetic effects of topical photodynamic therapy. *Journal of the European Academy of Dermatology and Venereology : JEADV*. 24(11):1261-9.

Kosaka, S., Yasumoto, M., Akilov, O.E., Hasan, T., & Kawana, S. 2010. Comparative split-face study of 5-aminolevulinic acid photodynamic therapy with intense pulsed light for photorejuvenation of Asian skin. *The Journal of Dermatology*. 37(12):1005-10.

Krammer, B. & Verwanger, T. 2012. Molecular response to hypericin-induced photodamage. *Current Medicinal Chemistry*. 19(6):793-8.

Kubin, A., Alth, G., Jindra, R., Jessner, G., & Ebermann, R. 1996. Wavelength-dependent photoresponse of biological and aqueous model systems using the photodynamic plant pigment hypericin. *Journal of Photochemistry and Photobiology. B, Biology*. 36(2):103-8.

Leask, A. & Abraham, D.J. 2004. TGF-beta signaling and the fibrotic response. *FASEB journal : official publication of the Federation of American Societies for Experimental Biology*. 18(7):816-27.

Lim, I.J., Phan, T.T., Song, C., Tan, W.T., & Longaker, M.T. 2001. Investigation of the influence of keloid-derived keratinocytes on fibroblast growth and proliferation in vitro. *Plastic and Reconstructive Surgery*. 107(3):797-808.

Lodish, H., Berk, A., Matsudaira, P., Kaiser, C.A., Krieger, M., Scott, M.P., Zipursky, S.L., & Darnell, J. 2003. Molecular Cell Biology.

Lowe, N.J. & Lowe, P. 2005. Pilot study to determine the efficacy of ALA-PDT photo-rejuvenation for the treatment of facial ageing. *Journal of Cosmetic and Laser Therapy : official publication of the European Society for Laser Dermatology*. 7(3–4):159-62.

Lubart, R., Eichler, M., Lavi, R., Friedman, H., & Shainberg, A. 2005. Low-energy laser irradiation promotes cellular redox activity. *Photomedicine and Laser Surgery*. 23(1):3-9.

Lubart, R., Friedmann, H., Lavie, R., Longo, L., Jacobi, J., Baruchin, O., & Baruchin, A.M. 2007. A reasonable mechanism for visible light-induced skin rejuvenation. *Lasers in Medical Science*. 22(1):1-3.

Ma, W., Wlaschek, M., Tantcheva-Poór, I., Schneider, L. a, Naderi, L., Razi-Wolf, Z., Schüller, J., & Scharffetter-Kochanek, K. 2001. Chronological ageing and photoageing of the fibroblasts and the dermal connective tissue. *Clinical and Experimental Dermatology*. 26(7):592-9.

Maas-Szabowski, N., Shimotoyodome, A., & Fusenig, N.E. 1999. Keratinocyte growth regulation in fibroblast cocultures via a double paracrine mechanism. *Journal of Cell Science*. 112 (Pt 1:1843-53.

MacCormack, M. a. 2008. Photodynamic therapy in dermatology: an update on applications and outcomes. *Seminars in Cutaneous Medicine and Surgery*. 27(1):52-62.

MacGregor, J.L. & Dover, J.S. 2010. Commentary: the evolving role of photodynamic therapy for the treatment of photoaged skin. *Dermatologic Surgery : official publication for American Society for Dermatologic Surgery [et al.]*. 36(1):49-51.

Macfarlane, D. 1992. Signs of Photoaging and skin cancer. DeLeo, V. (Ed.), Topics in Clinical Dermatology: Photosensitivity. Igaku-Shoin Medical Publishers: New York, Tokyo, pp. 36-40.

Marmur, E.S., Phelps, R., & Goldberg, D.J. 2005. Ultrastructural changes seen after ALA-IPL photorejuvenation: a pilot study. *Journal of Cosmetic and Laser Therapy : official publication of the European Society for Laser Dermatology*. 7(1):21-4.

Martínez-Poveda, B., Quesada, A.R., & Medina, M.A. 2005. Hypericin in the dark inhibits key steps of angiogenesis in vitro. *European Journal of Pharmacology*. 516(2):97-103.

Mauviel, A., Chung, K.Y., Agarwal, A., Tamai, K., & Uitto, J. 1996. Cell-specific induction of distinct oncogenes of the Jun family is responsible for differential regulation of collagenase gene expression by transforming growth factor-beta in fibroblasts and keratinocytes. *The Journal of Biological Chemistry*. 271(18):10917-23.

Mbene, A.B., Houreld, N.N., & Abrahamse, H. 2009. DNA damage after phototherapy in wounded fibroblast cells irradiated with 16 J/cm(2). *Journal of Photochemistry and Photobiology. B, Biology*. *Elsevier B.V.* 94(2):131-7.

McEvoy, M.T. & Muller, S.A. 1992. PUVA treatment of Mycosis Fungiodes. , in: Abel, E. (Ed.), Photochemotherapy in Dermatology. Igaku-Shoin Medical Publishers: New York, Tokyo. Igaku-Shoin Medical Publishers: New York, Tokyo, pp. 131-150.

Meier, B., Radeke, H.H., Selle, S., Younes, M., Sies, H., Resch, K., & Habermehl, G.G. 1989. Human fibroblasts release reactive oxygen species in response to interleukin-1 or tumour necrosis factor-alpha. *The Biochemical Journal*. 263(2):539-45.

Mine, S., Fortunel, N.O., Pageon, H., Asselineau, D. 2008. Aging Alters Functionally Human Dermal Papillary Fibroblasts but Not Reticular Fibroblasts: A New View of Skin Morphogenesis and Aging. *PLoS ONE.* 3(12): e4066.

Mosher, D.B., Pathak, M., & Fitzpatrick, T.B. 1992. Photochemotherapy for Vitiligo: an approach to diagnosis and management. Abel, E. (Ed.), Photochemotherapy in Dermatology. Igaku-Shoin Medical Publishers: New York, Tokyo, pp. 109-130.

Mukherjee, P., Adhikary, R., Halder, M., Petrich, J.W., & Miskovsky, P. 2008. Accumulation and interaction of hypericin in low-density lipoprotein--a photophysical study. *Photochemistry and Photobiology*. 84(3):706-12.

Murrell, G. a, Francis, M.J., & Bromley, L. 1990. Modulation of fibroblast proliferation by oxygen free radicals. *The Biochemical Journal*. 265(3):659-65.

Najafizadeh, P., Hashemian, F., Mansouri, P., Farshi, S., Surmaghi, M.S., & Chalangari, R. 2012. The evaluation of the clinical effect of topical St Johns wort (Hypericum perforatum L.) in plaque type psoriasis vulgaris: a pilot study. *The Australasian Journal of Dermatology*. 53(2):131-5.

Nestor, M.S., Goldberg, D.J., Goldman, M.P., Weiss, R.A., & Rigel, D.S. 2000. Photorejuvenation: Non-Ablative Skin Rejuvenation Using Intense Pulsed LIght. *Skin and Aging Supplement*. :5-8.

Nishimori, Y., Pearse, a. D., Edwards, C., & Marks, R. 1998. Elastotic degenerative change and yellowish discolouration in photoaged skin. *Skin Research and Technology*. 4(2):79-82.

Nootheti, P.K. & Goldman, M.P. 2006. Advances in photorejuvenation and the current status of photodynamic therapy. *Expert Review of Dermatology*. 1(1):51-61.

Orringer, J.S., Hammerberg, C., Hamilton, T., Johnson, T.M., Kang, S., Sachs, D.L., Fisher, G., & Voorhees, J.J. 2008. Molecular effects of photodynamic therapy for photoaging. *Archives of Dermatology*. 144(10):1296-302.

Orringer, J.S., Voorhees, J.J., Hamilton, T., Hammerberg, C., Kang, S., Johnson, T.M., Karimipour, D.J., & Fisher, G. 2005. Dermal matrix remodeling after nonablative laser therapy. *Journal of the American Academy of Dermatology*. 53(5):775-82.

Oztürk, N., Korkmaz, S., & Oztürk, Y. 2007. Wound-healing activity of St. John's Wort (Hypericum perforatum L.) on chicken embryonic fibroblasts. *Journal of Ethnopharmacology*. 111(1):33-9.

O'Connor, A.E., Gallagher, W.M., & Byrne, A.T. 2009. Porphyrin and nonporphyrin photosensitizers in oncology: preclinical and clinical advances in photodynamic therapy. *Photochemistry and Photobiology*. 85(5):1053-74.

Page-McCaw, A., Ewald, A.J., & Werb, Z. 2007. Matrix metalloproteinases and the regulation of tissue remodelling. *Nature Reviews. Molecular cell Biology*. 8(3):221-33.

Park, M.Y., Sohn, S., Lee, E.-so, & Kim, Y.C. 2010. Photorejuvenation induced by 5-aminolevulinic acid photodynamic therapy in patients with actinic keratosis: a histologic analysis. *Journal of the American Academy of Dermatology*. *Elsevier Inc*. 62(1):85-95.

Peng, Q., Juzeniene, A., Chen, J., Svaasand, L.O., Warloe, T., Giercksky, K.-E., & Moan, J. 2008. Lasers in medicine. *Reports on Progress in Physics*. 71(5):056701.

Peng, Q., Warloe, T., Berg, K., Moan, J., Kongshaug, M., Giercksky, K.E., & Nesland, J.M. 1997. 5-Aminolevulinic acid-based photodynamic therapy. Clinical research and future challenges. *Cancer*. 79(12):2282-308.

Peplow, P.V., Chung, T.-Y., & Baxter, G.D. 2010. Laser photobiomodulation of proliferation of cells in culture: a review of human and animal studies. *Photomedicine and Laser Surgery*. 28 Suppl 1:S3-40.

Peplow, P.V., Chung, T.-Y., & Baxter, G.D. 2012a. Photodynamic modulation of wound healing: a review of human and animal studies. *Photomedicine and Laser Surgery*. 30(3):118-48.

Peplow, P.V., Chung, T.-Y., & Baxter, G.D. 2012b. Laser photostimulation (660 nm) of wound healing in diabetic mice is not brought about by ameliorating diabetes. *Lasers in Surgery and Medicine*. 44(1):26-9.

Petersen, M.J., Hansen, C., & Craig, S. 1992. Ultraviolet A irradiation stimulates collagenase production in cultured human fibroblasts. *The Journal of Investigative Dermatology*. 99(4):440-4.

Pfaffel-Schubart, G., Rück, A., & Scalfi-Happ, C. 2006. Modulation of cellular Ca2+-signaling during hypericin-induced photodynamic therapy (PDT). *Medical Laser Application*. 21(1):61-66.

Piette, J., Volanti, C., Vantieghem, A., Matroule, J.-Y., Habraken, Y., & Agostinis, P. 2003. Cell death and growth arrest in response to photodynamic therapy with membrane-bound photosensitizers. *Biochemical Pharmacology*. 66(8):1651-1659.

Pillai, S., Oresajo, C., & Hayward, J. 2005. Ultraviolet radiation and skin aging: roles of reactive oxygen species, inflammation and protease activation, and strategies for prevention of inflammation-induced matrix degradation - a review. *International Journal of Cosmetic Science*. 27(1):17-34.

Pryor, L., Gordon, C.R., Swanson, E.W., Reish, R.G., Horton-Beeman, K., & Cohen, S.R. 2011. Dermaplaning, topical oxygen, and photodynamic therapy: a systematic review of the literature. *Aesthetic Plastic Surgery*. 35(6):1151-9.

Quan, T., He, T., Kang, S., Voorhees, J.J., & Fisher, G.J. 2002. Ultraviolet irradiation alters transforming growth factor beta/smad pathway in human skin in vivo. *The Journal of Investigative Dermatology*. 119(2):499-506.

Quan, T., Qin, Z., Xia, W., Shao, Y., Voorhees, J.J., & Fisher, G.J. 2009. Matrix-degrading metalloproteinases in photoaging. *The journal of investigative dermatology. Symposium proceedings / the Society for Investigative Dermatology, Inc. [and] European Society for Dermatological Research*. 14(1):20-4.

Quan, T., Qin, Z., Xu, Y., He, T., Kang, S., Voorhees, J.J., & Fisher, G.J. 2010. Ultraviolet irradiation induces CYR61/CCN1, a mediator of collagen homeostasis, through activation of transcription factor AP-1 in human skin fibroblasts. *The Journal of Investigative Dermatology*. *Nature Publishing Group*. 130(6):1697-706.

Rawlings, A.V. 2006. Ethnic skin types: are there differences in skin structure and function? *International Journal of Cosmetic Science*. 28(2):79-93.

Rhie, G., Shin, M.H., Seo, J.Y., Choi, W.W., Cho, K.H., Kim, K.H., Park, K.C., Eun, H.C., & Chung, J.H. 2001. Aging- and photoaging-dependent changes of enzymic and nonenzymic antioxidants in the epidermis and dermis of human skin in vivo. *The Journal of Investigative Dermatology*. 117(5):1212-7.

Rinaldi, F. 2008. Laser: a review. *Clinics in Dermatology*. 26(6):590-601.

Rittié, L. & Fisher, G.J. 2002. UV-light-induced signal cascades and skin aging. *Ageing Research Reviews*. 1(4):705-20.

Ritz, R., Roser, F., Radomski, N., Strauss, W.S.L., Tatagiba, M., & Gharabaghi, A. 2008. Subcellular colocalization of hypericin with respect to endoplasmic reticulum and Golgi apparatus in glioblastoma cells. *Anticancer Research*. 28(4B):2033-8.

Rodrigo, S.M., Cunha, A., Pozza, D.H., Blaya, D.S., Moraes, J.F.J.F., Webber, B.J.B., de Oliveira, M.G.M.G., Weber, J.B.B., & de Oliveira, M.G.M.G. 2009. Analysis of the systemic effect of red and infrared laser therapy on wound repair. *Photomedicine And Laser Surgery*. 27(6):929-(6):929-935.

Roelants, M., Van Cleynenbreugel, B., Lerut, E., Van Poppel, H., & de Witte, P. a M. 2011. Human serum albumin as key mediator of the differential accumulation of hypericin in normal urothelial cell spheroids versus urothelial cell carcinoma spheroids. *Photochemical & Photobiological sciences : Official journal of the European Photochemistry Association and the European Society for Photobiology*. 10(1):151-9.

Rossi, R. 2011. Photodynamic Therapy/Assisted Photorejuvenation. *Journal of Cosmetics, Dermatological Sciences and Applications*. 01(02):30-35.

Ruiz-Rodriguez, R. & López-Rodriguez, L. 2006. Nonablative skin resurfacing: the role of PDT. *Journal of Drugs in Dermatology : JDD*. *Journal of Drugs in Dermatology*. 5(8):756-62.

Ruiz-Rodriguez, R., Sanz-Sánchez, T., & Córdoba, S. 2002. Photodynamic photorejuvenation. *Dermatologic Surgery : official publication for American Society for Dermatologic Surgery [et al.]*. 28(8):742-4; discussion 744.

Ruiz-Rodríguez, R., López, L., Candelas, D., & Pedraz, J. 2008. Photorejuvenation using topical 5-methyl aminolevulinate and red light. *Journal of Drugs in Dermatology : JDD*. 7(7):633-7.

Sanclemente, G., Medina, L., Villa, J.-F., Barrera, L.-M., & Garcia, H.-I. 2011. A prospective split-face double-blind randomized placebo-controlled trial to assess the efficacy of methyl aminolevulinate + red-light in patients with facial photodamage. *Journal of the European Academy of Dermatology and Venereology : JEADV*. 25(1):49-58.

Sanovic, R., Krammer, B., Grumboeck, S., & Verwanger, T. 2009. Time-resolved gene expression profiling of human squamous cell carcinoma cells during the apoptosis process induced by photodynamic treatment with hypericin. *International Journal of Oncology*. 35(4):921-939.

Satra, K.H. & DeLeo, V. 1992. PUVA for Photosensitivity and Other Skin Diseases. , in: Abel, E. (Ed.), Photochemotherapy in Dermatology. Igaku-Shoin Medical Publishers: New York, Tokyo. Igaku-Shoin Medical Publishers: New York, Tokyo, pp. 180-200.

Sattler, S., Schaefer, U., Schneider, W., Hoelzl, J., & Lehr, C.M. 1997. Binding, uptake, and transport of hypericin by Caco-2 cell monolayers. *Journal of Pharmaceutical Sciences*. 86(10):1120-6.

Schultz, G., Ladwig, G., & Wysocki, A. 2005. World Wide Wounds - Extracellular matrix: review of its role in acute and chronic wounds [WWW Document]. URL http://www.worldwidewounds.com/2005/august/Schultz/Extrace-Matric-Acute-Chronic-Wounds.html.

Sherwood, L. 2010. Human Physiology: From cells to systems. Brooks/Cole, Cengage Learning: Belmont, USA. . Brooks/Cole, Cengage Learning: Belmont, USA, pp. 25-27.

Siboni, G., Weitman, H., Freeman, D., Mazur, Y., Malik, Z., & Ehrenberg, B. 2002. The correlation between hydrophilicity of hypericins and helianthrone: internalization mechanisms, subcellular distribution and photodynamic action in colon carcinoma cells. *Photochemical & photobiological sciences : Official journal of the European Photochemistry Association and the European Society for Photobiologyhotobiological Sciences*. 1(7):483-491.

Singer, A.J. & Clark, R.A. 1999. Cutaneous wound healing. *The New England Journal of Medicine*. 341(10):738-46.

Steinbauer, J.M., Schreml, S., Kohl, E.A., Karrer, S., Landthaler, M., & Szeimies, R.-markus. 2010. Photodynamic therapy in dermatology. *Journal of the German Society of Dermatology : JDDG*. 8(6):454-64.

Szeimies, R.-M., Matheson, R.T., Davis, S. a, Bhatia, A.C., Frambach, Y., Klövekorn, W., Fesq, H., Berking, C., Reifenberger, J., & Thaçi, D. 2009. Topical methyl aminolevulinate photodynamic therapy using red light-emitting diode light for multiple actinic keratoses: a

randomized study. *Dermatologic Surgery : official publication for American Society for Dermatologic Surgery [et al.]*. 35(4):586-92.

Talwar, H.S., Griffiths, C.E.M., Fisher, G.J., Hamilton, T. a., & Voorhees, J.J. 1995. Reduced Type I and Type III Procollagens in Photodamaged Adult Human Skin. *Journal of investigative dermatology*. 105(2):285-290.

Thannickal, V.J. & Fanburg, B.L. 2000. Reactive oxygen species in cell signaling. *American Journal of Physiology. Lung cellular and Molecular Physiology*. 279(6):L1005-28.

Theodossiou, T.A., Hothersall, J.S., De Witte, P.A., Pantos, A., & Agostinis, P. 2009. The multifaceted photocytotoxic profile of hypericin. *Molecular Pharmaceutics*. 6(6):1775-89.

Theodossiou, T.A., Noronha-Dutra, A., & Hothersall, J.S. 2006. Mitochondria are a primary target of hypericin phototoxicity: synergy of intracellular calcium mobilisation in cell killing. *The International Journal of Biochemistry & Cell Biology*. 38(11):1946-56.

Theodossiou, T.A., Spiro, M.D., Jacobson, J., Hothersall, J.S., & Macrobert, A.J. 2004. Evidence for intracellular aggregation of hypericin and the impact on its photocytotoxicity in PAM 212 murine keratinocytes. *Photochemistry and Photobiology*. 80(3):438-43.

Thong, P.S.-P., Watt, F., Ren, M.Q., Tan, P.H., Soo, K.C., & Olivo, M. 2006. Hypericin-photodynamic therapy (PDT) using an alternative treatment regime suitable for multi-fraction PDT. *Journal of Photochemistry and Photobiology. B, Biology*. 82(1):1-8.

Touma, D., Yaar, M., Whitehead, S., Konnikov, N., & Gilchrest, B.A. 2004. A trial of short incubation, broad-area photodynamic therapy for facial actinic keratoses and diffuse photodamage. *Archives of Dermatology*. 140(1):33-40.

Uzdensky, A.B., Ma, L.W., Iani, V., Hjortland, G.O., Steen, H.B., & Moan, J. 2001. Intracellular localisation of hypericin in human glioblastoma and carcinoma cell lines. *Lasers in Medical Science*. 16(4):276-83.

Vandenbogaerde, a L., Delaey, E.M., Vantieghem, a M., Himpens, B.E., Merlevede, W.J., & de Witte, P. a. 1998. Cytotoxicity and antiproliferative effect of hypericin and derivatives after photosensitization. *Photochemistry and Photobiology*. 67(1):119-25.

Varani, J., Dame, M.K., Rittie, L., Fligiel, S.E.G., Kang, S., Fisher, G.J., & Voorhees, J.J. 2006. Decreased collagen production in chronologically aged skin: roles of age-dependent alteration in fibroblast function and defective mechanical stimulation. *The American Journal of Pathology*. 168(6):1861-8.

Varani, J., Schuger, L., Dame, M.K., Leonard, C., Fligiel, S.E.G., Kang, S., Fisher, G.J., & Voorhees, J.J. 2004. Reduced fibroblast interaction with intact collagen as a mechanism for depressed collagen synthesis in photodamaged skin. *The Journal of Investigative Dermatology*. 122(6):1471-9.

Varani, J., Spearman, D., Perone, P., Fligiel, S.E., Datta, S.C., Wang, Z.Q., Shao, Y., Kang, S., Fisher, G.J., & Voorhees, J.J. 2001. Inhibition of type I procollagen synthesis by damaged collagen in photoaged skin and by collagenase-degraded collagen in vitro. *The American Journal of Pathology*. 158(3):931-42.

Varga, J., Rosenbloom, J., & Jimenez, S. a. 1987. Transforming growth factor beta (TGF beta) causes a persistent increase in steady-state amounts of type I and type III collagen and fibronectin mRNAs in normal human dermal fibroblasts. *The Biochemical Journal*. 247(3):597-604.

Verrecchia, F., Tacheau, C., Schorpp-kistner, M., Angel, P., & Mauviel, A. 2001. Induction of the AP-1 members c-Jun and JunB by TGF-b / Smad suppresses early Smad-driven gene activation. *Oncogene*. :2205-2211.

Vinck, E.M., Cagnie, B.J., Cornelissen, M.J., Declercq, H. a, & Cambier, D.C. 2003. Increased fibroblast proliferation induced by light emitting diode and low power laser irradiation. *Lasers in Medical Science*. 18(2):95-9.

Vuong, T.T.K., Vever-Bizet, C., Bonneau, S., & Bourg-Heckly, G. 2011. Hypericin incorporation and localization in fixed HeLa cells for various conditions of fixation and incubation. *Photochemical & Photobiological Sciences : Official journal of the European Photochemistry Association and the European Society for Photobiology*. 10(4):561-8.

Waibel, J.S. 2009. Photorejuvenation. *Dermatologic Clinics*. 27(4):445-57, vi.

Welch, M.P., Odland, G.F., & Clark, R. a. 1990. Temporal relationships of F-actin bundle formation, collagen and fibronectin matrix assembly, and fibronectin receptor expression to wound contraction. *The Journal of Cell Biology*. 110(1):133-45.

Westermann, B. 2010. Mitochondrial fusion and fission in cell life and death. *Nature reviews. Molecular Cell Biology*. 11(12):872-84.

Whelan, H.T., Smits, R.L., Buchman, E.V., Whelan, N.T., Turner, S.G., Margolis, D. a, Cevenini, V., Stinson, H., Ignatius, R., Martin, T., Cwiklinski, J., Philippi, a F., Graf, W.R., Hodgson, B., Gould, L., Kane, M., Chen, G., & Caviness, J. 2001. Effect of NASA light-emitting diode irradiation on wound healing. *Journal of Clinical Laser Medicine & Surgery*. 19(6):305-14.

Wlaschek, M., Wenk, J., Brenneisen, P., Briviba, K., Schwarz, A., Sies, H., & Scharffetter-Kochanek, K. 1997. Singlet oxygen is an early intermediate in cytokine-dependent ultraviolet-A induction of interstitial collagenase in human dermal fibroblasts in vitro. *FEBS Letters*. *Federation of European Biochemical Societies*. 413(2):239-242.

Wong, W.-R., Shyu, W.-L., Tsai, J.-W., Hsu, K.-H., & Pang, J.-H.S. 2009. Intense pulsed light effects on the expression of extracellular matrix proteins and transforming growth factor beta-1 in skin dermal fibroblasts cultured within contracted collagen lattices. *Dermatologic Surgery : official publication for American Society for Dermatologic Surgery [et al.]*. 35(5):816-25.

Xi, Z., Shuxian, Y., Zhong, L., Hui, Q., Yan, W., Huilin, D., Leihong, X., & Gold, M.H. 2011. Topical 5-aminolevulinic acid with intense pulsed light versus intense pulsed light for photodamage in Chinese patients. *Dermatologic Surgery : official publication for American Society for Dermatologic Surgery [et al.]*. 37(1):31-40.

Young, B. & Heath, J.W. 2000. Skin. Young, B., Heath, J.W. (Eds.), Wheater's Functional Histology. Harcourt Publishers Limited: Garfos, Spain, pp. 157-171.

Zane, C., Capezzera, R., Sala, R., Venturini, M., & Calzavara-Pinton, P. 2007. Clinical and echographic analysis of photodynamic therapy using methylaminolevulinate as sensitizer in the treatment of photodamaged facial skin. *Lasers in Surgery and Medicine*. 39(3):203-9.

Zhang, W., Law, R.E., Hinton, D.R., & Couldwell, W.T. 1997. Inhibition of human malignant glioma cell motility and invasion in vitro by hypericin, a potent protein kinase C inhibitor. *Cancer Letters*. 120(1):31-8.

A. Appendix A

A.1. Hoechst Staining Protocol

Hoechst (Hoechst No. 33258 trihydrochloride ((2'-[4-hydroxyphenyl]-5-[4-methyl-1-piperazinyl]-2,5'-bi-1H-benzimidazole) (Sigma-Aldrich, Schnelldorf, Germany) was used to stain the nucleus of cells and mycobacteria potentially present in the cells. Hoechst staining was done live or on fixed cells depending on the experiment. Hoechst powder was dissolved in distilled water for a stock solution with a concentration of 5mg/ml and stored at -20°C. The slides were viewed in the DAPI channel on a fluorescent microscope (Zeiss Axiovert 200M fluorescent microscope, Carl Zeiss Microscopy GmbH, Germany) and in the infra-red range when the confocal microscope (Zeiss Axiovert 200M LSM 510 META Confocal microscope, Carl Zeiss Microscopy GmbH, Germany) was used.

A.1.1. Live Cell staining

A working stock of 0.5mg/ml Hoechst in water was used in all live cell experiments. At the end of each experiment the medium was replaced with complete medium with Hoechst diluted to 5µg/ml. The cells were exposed to Hoechst for 30 minutes at 37°C in the incubator. The Hoechst was discarded before the cells were washed thoroughly and incubated in fresh medium until viewing.

A.1.2. Fixed Cell staining

Cells were grown on coverslips for three days prior to staining. The dishes were washed with PBS and fixed with 1ml glacial acetic acid and methanol in a ratio of 1:3 for 6 minutes. The fixative was removed and the dishes were allowed to air dry. The cells were exposed to 5ug/ml Hoechst solution for 6 minutes. The Hoechst was discarded and the multiple washes with PBS were done. The coverslips were lifted and mounted onto glass slides and left at room temperature until viewing.

A.2. BCA protein quantification

The BCA protein Assay kit (Thermo Scientific, Pierce, Rockford, IL, USA) is colorimetric assay where the peptide bond is reduced by copper ions present in the green working reagent provided in the kit. These ions are chelated by bicinchoninic acid (BCA) to create a purple solution. The samples were analysed on an ELISA plate reader at 562nm with a standard curve of known protein concentrations. To generate a standard curve, bovine serum albumin (BSA) was diluted with 0.9% saline to have a concentration of 2000µg/ml. This stock

solution was further diluted using incomplete RIPA buffer to known protein concentrations ranging from 0-2000µg/ml and 25µl to each well, of a 96-well plate, in duplicate.

The protein lysates following protein extraction were diluted 5–fold using incomplete RIPA buffer and 25µl added per well in triplicate into the 96-well plate. The working reagent was prepared and 200µl added to each well. The solution was incubated at 37°C for 30 minutes in the dark as the working reagent is light sensitive. After 30 minutes the plate was cooled to room temperature and read at 562nm on a spectrophotometer plate reader. The standard curve used the absorbance values of the known protein concentrations and the two variables were plotted against one another. Following this, the unknown samples' absorbance values were used with the standard curve to generate accurate protein concentrations and the average of the triplicates was reported and represented protein concentration as µg/µl.

A.2.1. BCA Working Solution

The number of wells was multiplied by 200µl and 50 parts of Reagent A to 1 part Reagent B was calculated for each experiment. An extra well was normally added to the calculation to account for pipetting error.

A.2.2. Standard Protein Concentrations

A stock solution of 2mg/ml BSA in saline was either supplied with the kit or made in the laboratory. For the standard curve of protein concentration, serial dilutions were performed from the stock solutions using the incomplete RIPA (Appendix A.4.1) as a diluent. The concentrations were: 2mg/ml, 1mg/ml, 500µg/ml, 250µg/ml, 125µg/ml and a blank with only incomplete RIPA buffer.

A.3. Cell Culture Reagents

Dulbecco's Modified Eagle's Medium (DMEM)

27.06g DMEM powder (Highveld Biological pty. Ltd. Johannesburg, South Africa)
7.4g $NaHCO_3$
Make up to 1 litre with autoclaved double distilled water and adjust to pH 7.4
Filter sterilize medium using 0.2µm filter into autoclaved bottles
Store at 4°C

A.3.1. Fetal Bovine Serum (FBS)

Each 500ml of FBS (Highveld Biological pty. Ltd. Johannesburg, South Africa) was heat inactivated by 20 minute incubation in a 56°C water bath. It was allowed to cool and was aliquots were stored at -20°C until use.

A.3.2. Penicillin/Streptomycin

Both antibiotics were combined to have a final concentration of 100U/ml of penicillin and 100µg/ml of streptomycin sulphate salt in autoclaved distilled water. Stocks of penicillin and streptomycin were stored at -20°C.

A.3.3. Trypsin/ethylenediaminetetraacetic acid (EDTA)

0.05% trypsin and 0.02% EDTA are dissolved together in autoclaved PBS. The solution is sterilised through a 0.2µm filter and was stored at -20°C until use.

A.4. RIPA Extraction Buffer

A.4.1. Incomplete RIPA Buffer

1.5ml of 50mM NaCl

0.5ml Triton-X 100

0.5ml 10% Sodium-Dodecyl Sulphate

0.5 Tris-HCl pH 7.5

0.5g Deoxycholate

Make up to 50ml distilled water and adjust to pH 7.4

Filter sterilize

Store at 4°C

A.4.2. Complete RIPA buffer

40µl Roche Complete Protease Inhibitor Cocktail (X25)

1µl 1mg/ml Aprotinin

5µl 100mM PMSF

1µl Pepstatin

954µl incomplete RIPA buffer

Add 50µl to a 35mm tissue plate

A.5. Buffers

A.5.1. Phosphate Buffered Saline X1

8g NaCl

0.2g KCl

1.26g Na_2HPO_4

0.2g KH_2PO_4

Make up to 1 litre with autoclaved double distilled water and adjust to pH 7.4

A.6. XTT solution Reagents

XTT solution was combined according to the manufacturers (Roche, Germany) instructions in subdued conditions.

A.6.1. XTT Working Solution

50µl Solution I

1µl Solution II

Solution I and II were combined in subdued light conditions.

50µl was added to each well which contained 200µl medium.

The solution I and II volumes were multiplied by the numbers of wells being treated and included another 0.5 well to account for pipetting error.

A.7. DCF-DA solution

The DCF-DA powder was dissolved in DMSO according to manufacturer' (Sigma-Aldrich, Schnelldorf, Germany) instructions to a concentration of 100mM.

A.7.1. DCF-DA working solution

10µl 100mM DCF-DA solution

990µl PBS

Final concentration of DCF-DA in complete medium varied between 40µM and 10µM.

A.8. Hypericin Uptake Assay photographs

To confirm the fluorescent values from the uptake analysis (Section 3.1) microscopy was used to visualize hypericin within the fibroblast. Cells were seeded onto glass slides in 35mm tissue culture dishes and each was incubated with the three hypericin concentration (0.25µM, 0.5µM and 1µM) for the same time course as uptake assay (2.5-24h) (Section 2.2). At the end of the time period images were taken of the tissue culture dish using the X10 lens on the Zeiss Axiovert 200M fluorescent microscope. The exposure time for hypericin detection set on the lowest hypericin concentration (0.25µM) and the shortest time (2.5h) for all the images. In this way, we could visually determine the amount of hypericin through its fluorescent intensity (Figure A.8.1).

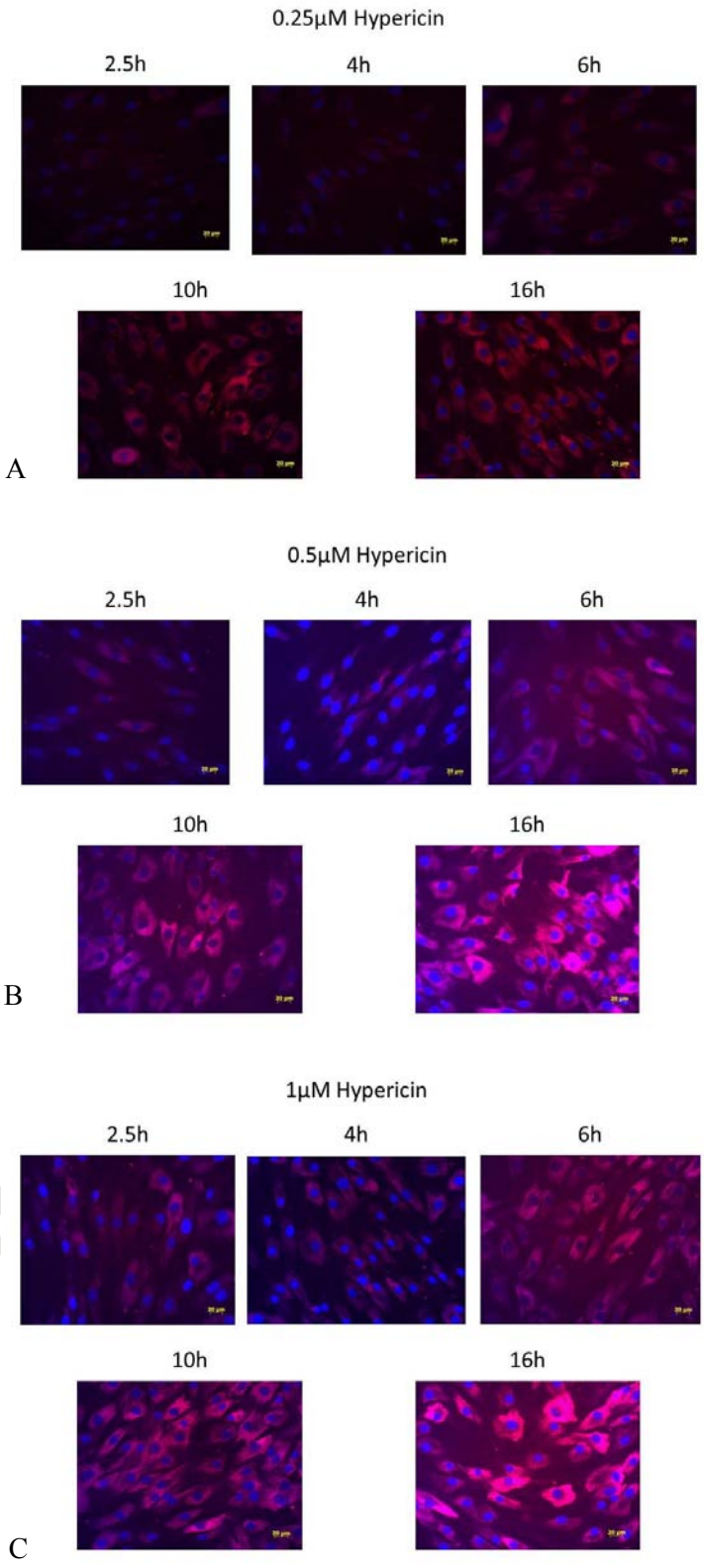

Figure A.8.1 Photographs indicating the increase in fluorescent intensity in primary human fibroblasts over time and with increasing hypericin concentrations (A) 0.25µM, (B) 0.5µM and (C) 1µM. The same exposure time was kept all for the images.

A.9. Maps of Plasmids Used in the Subcellular Localization Experiments

A.9.1. Yellow Fluorescent Plasmid – Endoplasmic Reticulum

The map below represents the plasmid used to visualise the ER. This plasmid was kindly donated by Georgia Schafer and Catherine Kaschula from the International Centre for Genetic Engineering and Biotechnology (ICGEB) and Department of Medical Biochemistry UCT. The plasmid design originated from Clontech (Catalog #6906, Clontech Laboratories, California, United States of America).

pEYFP-ER Vector Information PT3314-5

Catalog #6906-1

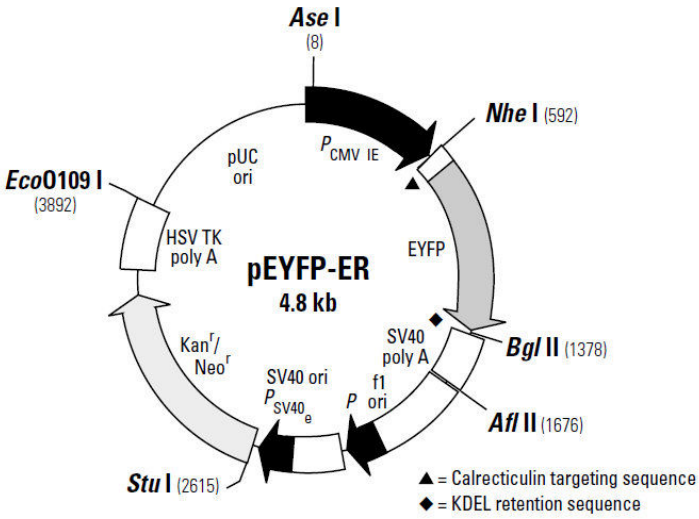

A.9.2. Green Fluorescent Protein - Golgi apparatus

The map below represents the plasmid used to visualize the Golgi apparatus. The plasmid was designed by Choudhory *et al* and can be acquired from Addgene with the reference number: Addgene plasmid 12605 (http://www.addgene.org/12605/) (Choudhury *et al.*, 2002).

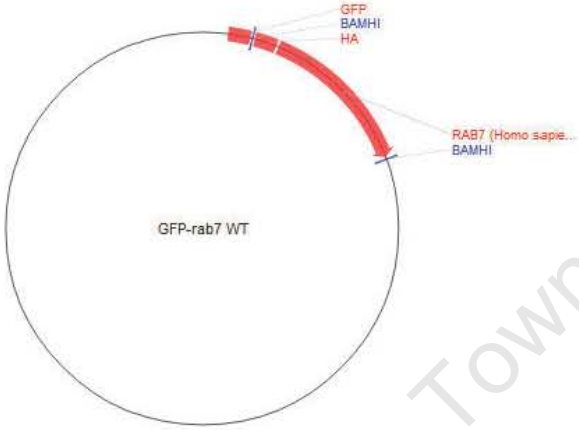

pEGFP-C1 Vector Information PT3028-5

GenBank Accession #: U55763 Catalog #6084-1

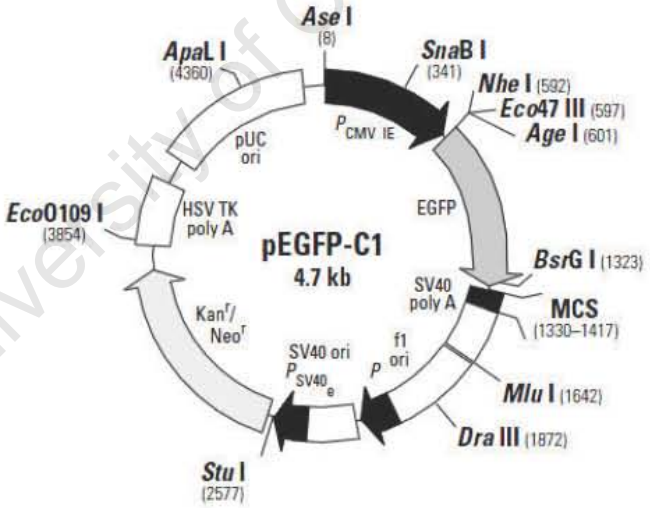

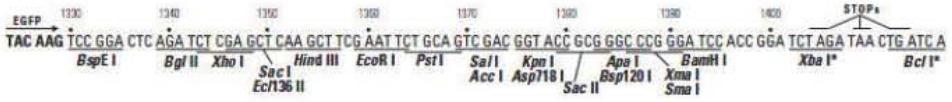

Restriction Map and Multiple Cloning Site (MCS) of pEGFP-C1. All restriction sites shown are unique. The *Xba* I and *Bcl* I sites (*) are methylated in the DNA provided by BD Biosciences Clontech. If you wish to digest the vector with these enzymes, you will need to transform the vector into a *dam*- host and make fresh DNA.

A.9.3. Green Fluorescent Protein – Mitochondria

This map represents the plasmid used to visualise the mitochondria. The ornithine tricarboxylase was inserted into the MCS (Davids, 2003). The plasmid was generated in our laboratory with the parent plasmid being pEGFP-N1 (Catalog #6085-1) (BD Biosciences Clontech, United States of America).

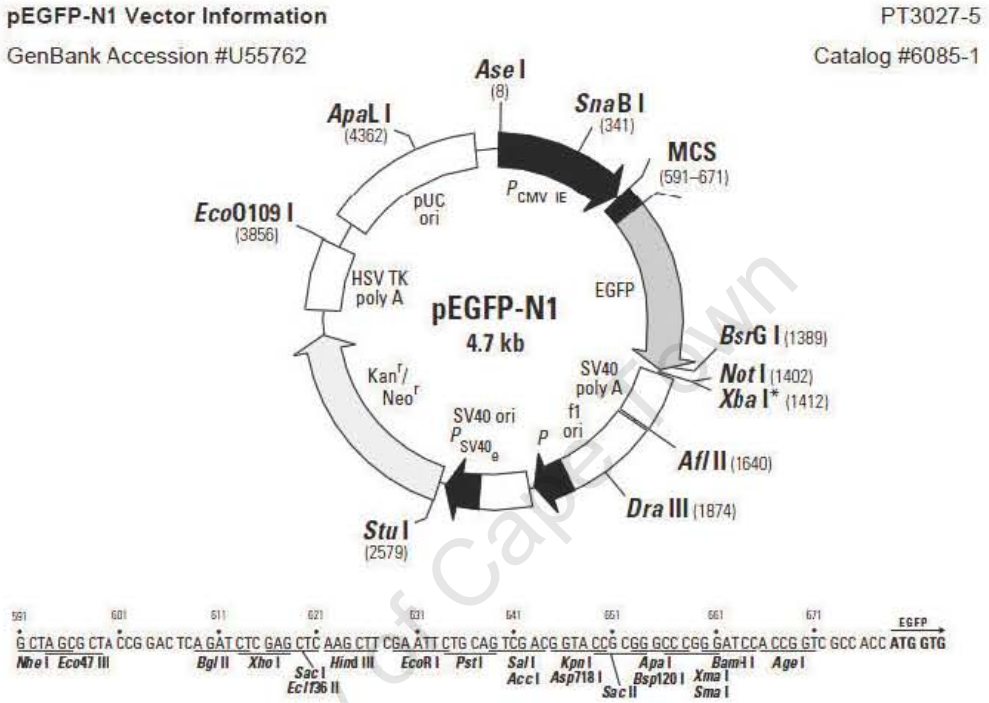

Restriction Map and Multiple Cloning Site (MCS) of pEGFP-N1 Vector. All restriction sites shown are unique. The *Not* I site follows the EGFP stop codon. The *Xba* I site (*) is methylated in the DNA provided by BD Biosciences Clontech. If you wish to digest the vector with this enzyme, you will need to transform the vector into a *dam*- and make fresh DNA.

A.10. Letter for Ethics Approval

UNIVERSITY OF CAPE TOWN

FACULTY OF HEALTH SCIENCES
Human Research Ethics Committee

Annual Progress Report

Date	
HREC REF Number	
Protocol number (if applicable) & Proposal title	
Principal Investigator	
Department / Office Internal Mail Address	

List of documentation

[Please see attached Letter.]

RESEARCH ETHICS COMMITTEE
2011 -09- 23
HEALTH SCIENCES FACULTY
UNIVERSITY OF CAPE TOWN

HREC office use only (FWA00001637, IRB00001938)

☑ Approved	This serves as notification of ethical approval, including all documentation described above
☐ Not approved	See attached comments
Type of review	☑ Expedited ☐ Full committee
Expiry date	28 June 2012
Signature Chairperson of the HREC	Date 21/6/2011

Department of Human Biology

Faculty of Health Sciences
University of Cape Town
Observatory Cape 7925
South Africa
Tel: + 27 21 406 6787
Fax: + 27 21 448 7226

June 2011

Attention : Professor Marc Blockman
Faculty of Health Sciences Research Ethics Committee
E52, Room 24
Old Main Building
Groote Schuur Hospital

Request to Extend Protocol : Registry of Skin Samples (REC REF : 493/2009)

Dear Prof Blockman and Committee Members

Permission for the above-mentioned protocol expired November 2010. The projects associated with the Skin Registry are however ongoing through 2011-12 and include a current Masters and PhD project under my supervision. I therefore request an extension of this protocol till the end of 2012.

If you and/or your committee feel that a progress report is necessary to further substantiate this request, I would gladly furnish you with one.

Looking forward to your response.

Regards.
Dr Lester M. Davids, Principal Investigator
Tel: 021-406 6787